

COMPLEX RESISTIVITY TO EVALUATE
THE BIOOXIDATION OF GOLD ORE

by

Kim C. Oshetski

A thesis submitted to the Faculty and the Board of Trustees of the Colorado School of Mines in partial fulfillment of the requirements for the degree of Master of Science (Geophysics).

Golden, Colorado

Date _____

Signed: _____
Kim C. Oshetski

Approved: _____
Dr. Gary R. Olhoeft
Thesis Advisor

Golden, Colorado

Date _____

Dr. Thomas L. Davis
Professor and Interim Head,
Department of Geophysics

ABSTRACT

Biooxidation is a pretreatment method that significantly increases gold recovery in refractory ores. In these ores, the gold is surrounded by sulfide minerals that must be removed to expose the gold for cyanide recovery. The use of biooxidation with large-scale heap operations has dramatically changed the efficiency and economics of gold recovery. The main problem for using this processing method has been the lack of a real-time monitoring technique to assess the progress of biooxidation and determine the optimal removal time of large-scale, heterogeneous heaps. I used complex resistivity to monitor the biooxidation of gold ores in columns at the Newmont Technical Facility in Englewood, CO, and compared the data with the diagnostic laboratory chemical analyses to identify the spectral response associated with biooxidation. The two mineralogically different ores examined had a direct correlation between the rate of sulfide oxidation and the phase spectra. These positive column results advocate the use of complex resistivity to monitor the heterogeneous biooxidation process and warrant further research in the laboratory and on experimental-scale heaps.

TABLE OF CONTENTS

	Page
ABSTRACT.....	iii
LIST OF FIGURES.....	vii
LIST OF TABLES.....	xv
ACKNOWLEDGMENTS.....	xvi
Chapter 1. INTRODUCTION.....	1
Chapter 2. BIOOXIDATION.....	5
2.1 Background.....	5
2.2 Sulfide Oxidation.....	8
2.3 Microorganisms.....	8
2.3.1 <i>Thiobacillus ferrooxidans</i>	9
2.3.2 Bacterial Attachment to Surfaces.....	11
2.3.3 Limiting Factors.....	13
2.4 Heap Biooxidation Method.....	15
2.4.1 Advantages.....	18
2.4.2 Disadvantages.....	18
2.4.3 Monitoring Requirements.....	19
2.5 Applicability of Complex Resistivity to Monitor Biooxidation.....	20
Chapter 3. COMPLEX RESISTIVITY.....	21

3.1 Historical Background.....	21
3.2 Theory.....	23
3.2.1 Electrical Properties.....	24
3.2.2 Charge Transport.....	25
3.2.3 Charge Storage.....	27
3.2.4 Nonlinearity.....	28
3.3 Complex Resistivity and Biooxidation.....	29
3.3.1 Pyrite Polarization.....	30
3.3.2 Oxidation/Reduction Reactions.....	33
3.3.3 Bacteria Effect.....	35
3.3.4 Advantages/Disadvantages.....	36
Chapter 4. EXPERIMENTAL SET-UP.....	38
4.1 Overview.....	38
4.2 Complex Resistivity System.....	38
4.2.1 Equipment Specifications.....	41
4.2.2 Laboratory vs. Column System.....	42
4.2.3 Calculations.....	42
4.2.4 Advantages / Disadvantages	49
4.3 Column Set-up.....	49
4.3.1 Ore Types Examined.....	50
4.3.2 Electrode Material.....	52
4.3.3 Column Specifications.....	53
4.3.4 Chemistry Analysis.....	58
4.4 Problems Encountered.....	59
4.5 Description of Typical Data Plots.....	61
Chapter 5. MEASUREMENT DATA.....	68
5.1 Overview.....	68
5.2 Tests of Electrode Material.....	68

5.3 Column Data	71
5.3.1 Chemical Analysis.....	74
5.3.2 Complex Resistivity	82
5.4 Data Quality.....	99
5.4.1 Chemistry Data Quality.....	102
5.4.2 Complex Resistivity Data Quality.....	103
5.4.3 EM Coupling.....	118
5.4.4 Electrode Corrosion.....	119
Chapter 6. DISCUSSION AND CONCLUSIONS.....	123
6.1 Data Correlation.....	123
6.1.1 High-Grade Ore.....	123
6.1.2 Low-Grade Ore.....	129
6.1.3 Control Ore.....	135
6.2 Recommendations For Future Work.....	138
6.3 Conclusions.....	141
REFERENCES.....	143
APPENDIX OUTLINE.....	148
Appendix A. Chemistry Data.....	CDROM
Appendix B. Laboratory Complex Resistivity Data.....	CDROM
Appendix C. Column Complex Resistivity Data.....	CDROM
Appendix D. Processing Programs.....	CDROM

LIST OF FIGURES

		Page
Figure 2.1.	The percent gold extraction as a function of percent sulfide oxidation for three refractory ores (courtesy of Jim Brierley, Newmont Metallurgical Services).....	7
Figure 2.2.	<i>Thiobacillus ferrooxidans</i> is a rod-shaped bacterium with a diameter of about ½ micron (photograph courtesy of Jim Brierley, Newmont Metallurgical Services).....	10
Figure 2.3.	Oxidation of ferrous iron by <i>T. ferrooxidans</i> (modified from Barrett et al, 1993). The half reaction (2.3) must take place in the outer regions of the bacteria envelope where the pH is lower (close to the surrounding environment), and the half reaction (2.4) occurs inside the cytoplasm.....	11
Figure 2.4.	The formation of a biofilm by <i>T. ferrooxidans</i> on a pyrite surface (after Crundwell, 1997).....	14
Figure 2.5.	The attachment of <i>T. ferrooxidans</i> to a surface with fibrils (after Crundwell, 1997).....	14
Figure 2.6.	Biooxidation heap construction using conveyors (photograph courtesy of Jim Brierley, Newmont Metallurgical Services).....	16
Figure 2.7.	Close-up of the side of biooxidation heap (photograph courtesy of Jim Brierley, Newmont Metallurgical Services).....	16
Figure 2.8.	Plastic pipes to transport air to the bottom of the heap for injection into the heap (photograph courtesy of Jim Brierley, Newmont Metallurgical Services).....	17
Figure 3.1.	Complex plane plot showing the relationship between the real (ρ') and imaginary (ρ'') resistivity and the phase (ϕ).....	26

Figure 3.2.	Sinusoidal waveforms for the input current (solid line) and output voltage potential (dotted line) in complex resistivity measurements. Where J_A is (J_o+J_s) and E_A is (E_o+E_s) , and the time delay is Δt	26
Figure 3.3.	a) An R-RC circuit can be used to describe the CR response of a solid-electrolyte mixture. b) Ion migration resulting when current is applied to a rock sample.....	31
Figure 3.4.	Amplitude (solid line and symbols) and phase (dashed line and open symbols) spectra measured for an R-RC circuit (as shown in Figure 3.3a).....	31
Figure 4.1.	Complex resistivity instrumentation for the column studies.....	42
Figure 4.2.	Complex resistivity instrumentation for the laboratory studies (from Jones, 1997).....	44
Figure 4.3.	Flow diagram of the data processing steps for the column studies.	48
Figure 4.4.	A flow diagram of the experiment design, set-up, and measurement process.....	54
Figure 4.5.	The set-up of columns and CR equipment at Newmont in Englewood, CO. This picture shows the test of all channels across decade resistor boxes, one for the potential channels and one for the current-sensing resistor.....	55
Figure 4.6.	Specifications for the columns (not to scale).....	56
Figure 4.7.	Pooling of approximately 1/3 inch of water on the top of the ore in Column 3 near the end of the experiment.....	60
Figure 4.8.	The electronic circuit (R-RC) used to test the accuracy of the amplitude and phase of each channel.....	60

Figure 4.9.	The phase of channels 1-15 for the R-RC circuit in Figure 4.6 before repairs of the system. Note that channels 3, 8, 11, and 14 have low phase peaks.....	62
Figure 4.10.	The phase of channels 1-15 for the R-RC circuit in Figure 4.6 after repairs to the system. Note that all the channels now match the calculated values (far left).....	63
Figure 4.11.	Typical data plot; the average of data from 3/1/99 for channels 1, 2, and 3.....	64
Figure 4.12.	Typical standard deviation and current density data plot; the average of data from 3/1/99 for channels 1, 2, and 3.....	66
Figure 5.1.	Teflon sample holder with platinum electrodes. The length of the holder is four inches and the width is one inch. The current is applied through the outer electrodes and the resulting potential is measured across the center electrodes.....	70
Figure 5.2.	Comparison of the resistivity (top), phase (middle), and %THD (bottom) for MP35N (diamonds) and Platinum (circles) for two splits of low-grade ore with biooxidant solution: Day 2.....	72
Figure 5.3.	Comparison of the resistivity (top), phase (middle) and %THD (bottom) for MP35N (triangles) and Platinum (circles) for two splits of low-grade ore with biooxidant solution: Day 10.....	73
Figure 5.4.	Plots of the pH vs. time (days) for high-grade ore vs. low-grade ore (top) and control ore (bottom).....	75
Figure 5.5.	Total iron (g/L)for high-grade ore vs. low-grade ore and control ore.....	76
Figure 5.6.	Photographs of the current electrode pairs for all five columns. The electrodes are in order from column 1 (left) to column 5 (right).....	80

Figure 5.7.	Resistivity (top section), negative phase (middle), and %THD (bottom), from 0.001 Hz to 50 Hz, for the <i>low grade ore with biooxidant</i> at day 13 (diamonds), day 62 (circles), and day 118 (triangles) for a total of 105 days.....	84
Figure 5.8.	CR phase data for critical days: Column 2, <i>low-grade ore with biooxidant</i>	85
Figure 5.9.	CR percent total harmonic distortion (%THD) data for critical days: Column 2, <i>low-grade ore with biooxidant</i>	86
Figure 5.10.	Resistivity (top section), negative phase (middle), and %THD (bottom), from 0.001 Hz to 50 Hz, for the <i>low grade ore with low pH water</i> at day 14 (diamonds), day 84 (circles), and day 112 (triangles) for a total of 98 days.....	88
Figure 5.11.	CR phase data for critical days: Column 4, <i>low-grade ore with low pH water and bacterial inhibitor</i>	89
Figure 5.12.	CR percent total harmonic distortion (%THD) data for critical days: Column 4, <i>low-grade ore with low pH water and bacterial inhibitor</i>	90
Figure 5.13.	Resistivity (top section), negative phase (middle), and %THD (bottom), from 0.001 Hz to 50 Hz, for the <i>high grade ore with biooxidant</i> at day 44 (diamonds), day 79 (circles), and day 132 (triangles) for a total span of 88 days.....	91
Figure 5.14.	CR phase data for critical days: Column 1, <i>high-grade ore with biooxidant</i>	93
Figure 5.15.	CR percent total harmonic distortion (%THD) data for critical days: Column 1, <i>high-grade ore with biooxidant</i>	94
Figure 5.16.	Resistivity (top section), negative phase (middle), and %THD (bottom), from 0.001 Hz to 50 Hz, for the <i>high grade ore with low pH water</i> at day 14 (diamonds), day 64 (circles), and day 112 (triangles) for a total of 98 days.....	95

Figure 5.17.	CR phase data for critical days: Column 5, <i>high-grade ore with low pH water and bacterial inhibitor</i>	96
Figure 5.18.	CR percent total harmonic distortion (%THD) data for critical days: Column 5, <i>high-grade ore with low pH water and bacterial inhibitor</i>	97
Figure 5.19.	Resistivity (top section), negative phase (middle), and %THD (bottom), from 0.001 Hz to 50 Hz, for the <i>control ore with tap water</i> at day 14 (diamonds), day 84 (circles), and day 112 (triangles) for a total of 98 days.....	98
Figure 5.20.	CR phase data for critical days: Column 3, <i>control ore with tap water</i>	100
Figure 5.21.	CR percent total harmonic distortion (%THD) data for critical days: Column 3, <i>control ore with tap water</i>	101
Figure 5.22.	Three CR measurements for channel two, the middle electrode pair for the <i>high-grade ore with biooxidant</i> . The first two measurements (diamonds and circles) are prior to implementation of the CR updates and the last measurement (triangles) is just after the updates.....	104
Figure 5.23.	CR measurements for all three potential electrode pairs in column 1, <i>the high-grade ore with biooxidant</i> . The first two channels (diamonds and circles) are good and channel 3 (triangles) is bad according to the R-RC test.....	106
Figure 5.24.	Percent resistivity standard deviation (top), phase standard deviation (middle), and current density in amperes/meter ² (bottom) for the two good potential electrode pairs in column 1. Channel 2 (circles) is the electrode pair chosen to represent the <i>high-grade ore with biooxidant</i>	107
Figure 5.25.	CR measurements for the potential electrode pairs in column 2 <i>the low-grade ore with biooxidant</i> . Channel 5 (diamonds) and channel 6 (circles) are both good according to the R-RC test. The resistivity is greater, the phase peak is less distinct, and the %THD is lower on channel 6.....	108

Figure 5.26.	Percent resistivity standard deviation (top), phase standard deviation (middle), and current density in amperes/meter ² (bottom) for the two good potential electrode pairs in column 2. Channel 5 (triangles) is the electrode pair chosen to represent the <i>low-grade ore with biooxidant</i>	109
Figure 5.27.	CR measurements for the potential electrode pairs in column 3 the <i>control ore with tap water</i> . Channel 8 (diamonds) is bad and channel 9 (circles) is good according to the R-RC test.....	110
Figure 5.28.	Percent resistivity standard deviation (top), phase standard deviation (middle), and current density in amperes/meter ² (bottom) for the two potential electrode pairs in column 3. Channel 9 (circles) is the electrode pair chosen to represent the control; <i>NAL composite ore with DI water</i>	111
Figure 5.29.	CR measurements for the potential electrode pairs in column 4 the <i>low-grade ore with low pH water</i> . Channel 11 (diamonds) is bad and channel 12 (circles) is good according to the R-RC test....	113
Figure 5.30.	Percent resistivity standard deviation (top), phase standard deviation (middle), and current density in amperes/meter ² (bottom) for the two potential electrode pairs in column 4. Channel 12 (circles) is the electrode pair chosen to represent the <i>low-grade ore with low pH water and bacteria inhibitor</i>	114
Figure 5.31.	CR measurements for the potential electrode pairs in column 4 the <i>high-grade ore with low pH water</i> . Channel 14 (diamonds) is bad and channel 15 (circles) is good according to the R-RC test....	115
Figure 5.32.	Percent resistivity standard deviation (top), phase standard deviation (middle), and current density in amperes/meter ² (bottom) for the two potential electrode pairs in column 5. Channel 15 (circles) is the electrode pair chosen to represent the <i>high-grade ore with low pH water and bacteria inhibitor</i>	116
Figure 5.33.	CR measurements on 3/3/99, day 90, for the <i>low-grade ore with biooxidant</i> . The average of four measurements before disturbing the columns (diamonds) are compared with after moving the ore to fill in gaps under the electrodes (circles).....	117

Figure 5.34.	One current electrode (left) and one potential electrode (middle) removed from column 1, the <i>high-grade ore with biooxidant</i> , on 3/3/99. The raw MP35N (right) looks identical to the potential electrode.....	120
Figure 5.35.	CR measurements for column 1, the <i>high-grade ore with biooxidant</i> , on 3/3/99, with the original electrodes (diamonds), after replacing the current electrodes (circles), and after replacing the potential electrodes (triangles).....	121
Figure 5.36.	Standard deviations and current densities for the CR measurements for column 1, the <i>high-grade ore with biooxidant</i> , on 3/3/99, with the original electrodes (diamonds), after replacing the current electrodes (circles), and after replacing the potential electrodes (triangles).....	122
Figure 6.1.	Comparison of total iron and phase at 2.0 and 0.01 Hz for the <i>high-grade ore with biooxidant</i> . Both the 2.0 and 0.01 Hz phase slopes increased dramatically near the end of the biooxidation period.....	125
Figure 6.2.	The total iron content and the difference between the 2.0 and 0.01 Hz phase for the <i>high-grade ore with biooxidant</i> both level off at the end.....	126
Figure 6.3.	Comparison of total iron and phase at 2.0 and 0.01 Hz for the <i>high-grade ore with low pH water and a bacteria inhibitor</i> . Additional bacteria inhibitor was added on days 43 and 99. The greatest separation between the two phases occurs when the slope of the iron curve is increasing.....	127
Figure 6.4.	The total iron content and the difference between the 2.0 and 0.01 Hz phase for the <i>high-grade ore with low pH water and a bacteria inhibitor</i>	128
Figure 6.5.	Comparison of total iron and phase at 2.0 and 0.01 Hz for the <i>low-grade ore with biooxidant</i> . The 2 Hz values increase and the 0.01 values decrease with a crossover when the ore was ready for removal.....	130

Figure 6.6.	The total iron content and the difference between the 2.0 and 0.01 Hz phase for the <i>low-grade ore with biooxidant</i> . The phase curve increases dramatically when the ore was ready for removal.....	131
Figure 6.7.	Comparison of total iron and phase at 2.0 and 0.01 Hz for the <i>low-grade ore with low pH water and a bacteria inhibitor</i> . Additional bacteria inhibitor was added on days 64 and 112. The phase becomes positive with the first addition because of reactions with the bacteria and ore.....	133
Figure 6.8.	The total iron content and the difference between the 2.0 and 0.01 Hz phase for the <i>low-grade ore with low pH water and a bacteria inhibitor</i>	134
Figure 6.9.	Comparison of total iron and phase at 2.0 and 0.01 Hz for the <i>control ore with tap water</i> . The total iron is plotted by the scale on the right and the phase according to scale on the left.....	136
Figure 6.10.	Comparison of the total iron and the difference between the 2.0 and 0.01 Hz phase for the <i>control ore with tap water</i>	137

LIST OF TABLES

		Page
Table 4.1.	X-ray diffraction (XRD) of the 3 ore types prior to oxidation expressed in weight percent (Brierley, 1999b).....	51
Table 4.2.	X-ray fluorescence (XRF) of the 3 ore types prior to oxidation expressed in weight percent (Brierley, 1999b).....	51
Table 4.3.	Sieve analysis for the 5 columns, performed after oxidation and removal of ore from columns (Brierley, 1999b). The numbers are percentages by weight; designation <i>in.</i> stands for inches and <i>m</i> stands for mesh size (refer to Table 4.4 for column specifications)...	52
Table 4.4.	Specifications for each column.....	57
Table 5.1.	The increase in electrolyte elements in g/L from ICP solution analysis (post - pre). The iron (Fe*) does not correlate with the weekly titration analysis in Figure 5.5 (Brierley, 1999b).....	78
Table 5.2.	Assay data before and after the column experiments. The percent recoverable gold (CN/FA) is expressed as the ratio of gold recoverable by cyanide assay (AUCN) over fire assay (AUFA) (Brierley, 1999b).....	81
Table 5.3.	Percentage sulfide oxidized for the high and low-grade ores (Brierley, 1999b).....	82
Table 5.4.	A comparison of the change in solution total iron content for the accurate titration method versus the questionable inductively coupled plasma (ICP) data.....	102

ACKNOWLEDGMENTS

I am extremely grateful to Newmont Mining Corporation for sponsoring this research and providing excellent technical support. I have enjoyed working with both the metallurgy and geophysics groups at the Newmont Technical Facility in Englewood, CO, and am thankful for the opportunity to learn from this exceptional group of scientists. I would like to thank James A. Brierley for his continual advice and enthusiasm on this project. His biooxidation expertise and generous use of resources have been a vital part of this research. I would also like to thank Jack Tryon for setting up, maintaining, and monitoring the chemistry of the column experiments. Bruno Nilsson and Eric Lauritsen provided valuable technical assistance and were always eager to share advice on instrumentation practicalities. I am thankful for their advice and discussions that have greatly accelerated my understanding of equipment design and testing.

I wish to thank Gary R. Olhoeft for his continual efforts to turn a geologist into a geophysicist. He has accomplished this and more by constantly challenging me to question everything, see a multitude of possible solutions to any problem, understand the assumptions, and search for knowledge. I thank my mother for always believing in me and encouraging me to strive for my goals. I sincerely thank my husband, Walter Oshetski, for helping me to find joy in learning and life.

Chapter 1

INTRODUCTION

Gold is sometimes found surrounded by or encapsulated in sulfides. These sulfides prevent conventional cyanide leach solutions from contacting and removing the gold. Biooxidation is a pretreatment method used to increase gold recovery in these refractory ores. The microorganisms expedite sulfide oxidation, releasing encapsulated gold for cyanide recovery. The use of biooxidation with large-scale heap operations has dramatically changed the efficiency and economics of gold recovery. The main problem in applying this processing method has been the lack of a monitoring technique to assess the progress of biooxidation and determine the optimal removal time for gold extraction and recovery of large-scale, heterogeneous heaps. It is important to allow an ore to oxidize long enough to release the encapsulated gold, without an ore spending unnecessary time on the heap pad. It is also important not to remove an ore too soon for cyanide leaching because prematurely ending the biooxidation process limits gold recovery by leaving too much encapsulating pyrite intact. This requires a method that can determine the rate of oxidation throughout the pile.

Complex resistivity addresses this with the ability to monitor oxidation/reduction reactions. Induced polarization, a simplified version of complex resistivity, is a common geophysical technique for sulfide mineral exploration from the earth's surface or in or

between boreholes (Sumner, 1976). Complex resistivity is a promising monitoring technique because it is a good indicator of the presence of sulfide minerals and sulfide oxidation, can be applied non-invasively from the bottom of the heap, and can evaluate different bulk volumes of the heterogeneous heap by varying the electrode spacing.

Complex resistivity measures any changes in the distribution or motion of charge within the sample. The presence of pyrite, the primary sulfide mineral in this study, is known to produce a measurable electrical response due to charge storage at the solution/metal interface (Klein and Shuey, 1978). Pyrite oxidation involves charge transfer and results in an increase in the number of iron ions in solution. Charge transfer is measured with complex resistivity (Olhoeft, 1985) and the change in solution chemistry is measured with iron titrations. Therefore, complex resistivity and iron titration measurements should correlate for bacteria-assisted pyrite oxidation.

Initial laboratory work that I performed from September to December 1997, established a positive correlation between the complex resistivity, pH, and first visible pyrite oxidation (Brenner, 1997) and forms the basis for the research in this thesis. The first signs of visible oxidation in two different gold ores, coupled with a decrease in the pH, corresponded to a low-frequency peak of 20% in the total harmonic distortion. This positive correlation between bacteria-assisted pyrite oxidation and complex resistivity justified further research.

The objective of this thesis is to evaluate whether or not the chemistry of biooxidation as determined in column studies at Newmont Technical Facility in

Englewood, CO, corresponds with a specific complex resistivity response. This is accomplished by measuring two ores that are typical targets of biooxidation with and without active biooxidation and a control ore containing minimal pyrite. All of the ore samples were from Gold Quarry, Nevada. The two target ores varied in gold and pyrite percentages and were monitored with biooxidation solution in one column and a solution of low pH water with sodium lauryl sulfate as a bacteria inhibitor in another column. The chemistry and mineralogy analyses were performed by Newmont Mining Corporation (Brierley, 1999b). The low-grade ore contained 0.022 ounces of gold per ton and 1.60% sulfide-sulfur (as pyrite) by weight. The high-grade ore contained 0.188 ounces of gold per ton and 1.77% sulfide-sulfur (as pyrite) by weight. The control ore was chosen because it contained minimal pyrite and tap water was used as the monitoring solution.

A 16-channel complex resistivity measurement system from the Colorado School of Mines was added to the standard procedures used at the Newmont Technical Facility for monitoring column biooxidation. Each ore/inoculum mixture was placed in an eight-inch diameter column with 1/4" rod MP35N electrodes run horizontally through the column for the complex resistivity measurements. The inoculum was dripped from a bucket at the top of each column, percolated through the ore, and collected for recirculation in a reservoir below each column. Air was circulated from the base of the column to expedite biooxidation. A weekly chemical analysis of the solution draining from the base of each column tracked the rate of biooxidation and forms the primary correlation for the continuous complex resistivity measurements.

Daily averages of the complex resistivity measurements on the dates of the weekly chemical analyses are compared with the total iron content in solution. The complex resistivity data quality is checked by measuring each channel with an R-RC circuit, examining raw data waveforms by eye, averaging data sets for a 24 hour period, computing the standard deviations of averaged data sets, and comparing good potential electrode pairs in each column for repeatability. Applicability for monitoring larger scale heap biooxidation and variations in measurements due to temperature and mineralogy differences are yet to be determined.

Chapter 2

BIOOXIDATION

2.1 Background

Biooxidation is a pretreatment method for sulfidic refractory ores and is useful as an integral part of a gold recovery program. This method exploits processes naturally occurring in acid mine drainage. Acid generation due to the breakdown of sulfides in mine waters was assumed to be due to exposure to air until Colmer and Hinkle (1947) showed that adding a bacteria inhibitor greatly decreased the oxidation of sulfides and generation of sulfuric acid. The same bacteria responsible for sulfide oxidation in mine waste are being utilized to increase gold recovery in refractory ores while decreasing the acid production potential of the waste material.

Sulfidic refractory ore is generally low-grade, finely disseminated ore occurring at depth of a larger, more economical deposit. Biooxidation exploits previously uneconomical zones by expediting the oxidation of sulfide minerals, preparing the ore for gold extraction by cyanide leaching. The reason cyanide leaching cannot be used directly on sulfidic refractory ores is that the gold is encapsulated by sulfide minerals, such as pyrite, which are impervious to cyanide. The mineral coating must be degraded by roasting, pressure autoclave, or biooxidation, exposing the gold for effective cyanide leaching (Barrett et al, 1993). Biooxidation is the least expensive and simplest method to

apply, yet results in lower recovery yields than the more expensive roasting or pressure autoclave methods. In high grade refractory ores, roasting is still more economical, since nearly 100 % of the gold can be recovered. With biooxidation, 90+ % can be recovered by concentrates in a stirred-tank-reactor, yet only 50 - 60 % is recovered in heap biooxidation (Brierley, 1999). Figure 2.1 shows the percent gold extraction for different percentages of sulfide oxidation for three different ores. The percent gold extraction is the percentage of the total gold, determined by fire assay, recoverable by cyanide leaching. The lower the initial percent gold extraction, the more refractory the ore is and the more useful biooxidation is.

Newmont Gold Company has patented an improvement to the heap biooxidation method (Brierley and Hill, 1993), which improves the economics of biooxidation by expediting and facilitating the biooxidation of larger volumes of lower-grade ore. Unfortunately, inefficient monitoring inhibits optimization of operation and removal time of the biooxidation heaps. The faster an ore oxidizes, the sooner it can be removed from the heap, neutralized, and cyanide leached. The mineralogy, pH, temperature, bacteria activity, oxygen content, and particle size affect the rate of oxidation, decreasing the predictability of optimal oxidation time for each heap. Heterogeneity within a heap means that there will be different rates of oxidation throughout an individual heap, requiring monitoring of different volumes in a heap. If the ore is removed too soon, less gold will be recovered because some of the gold will still be encapsulated by pyrite. If

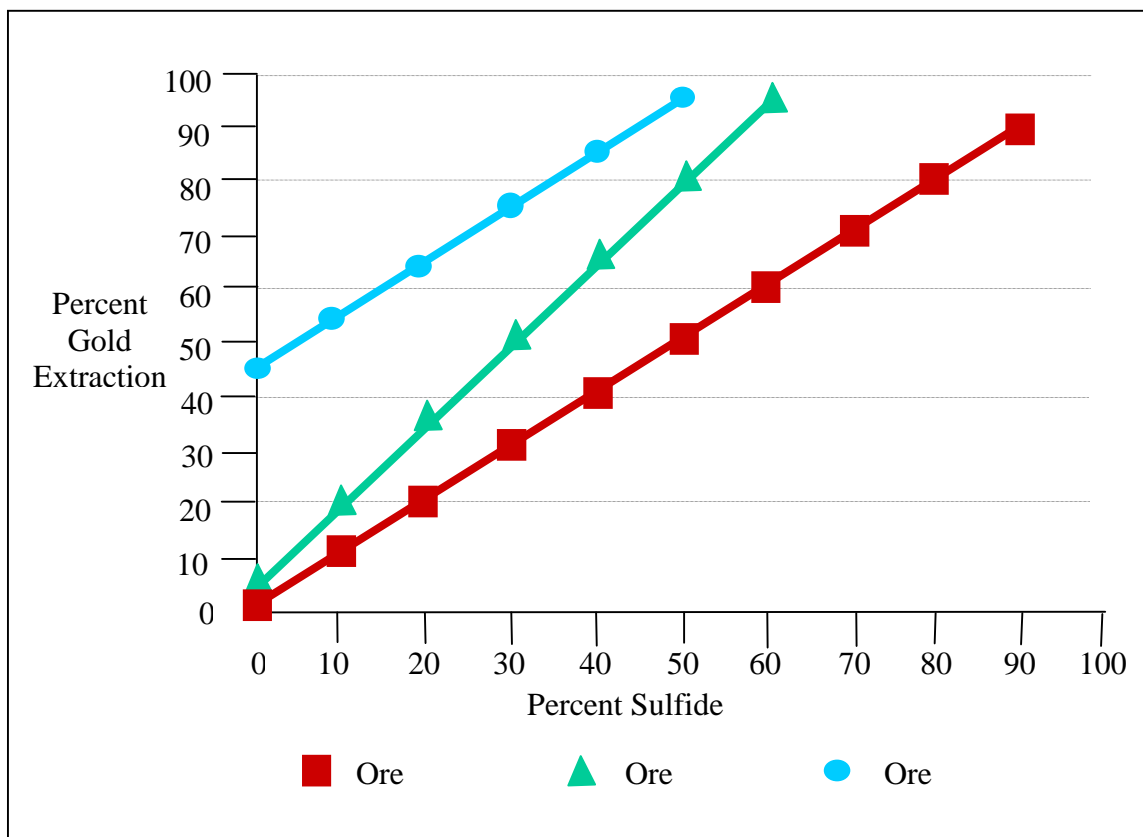
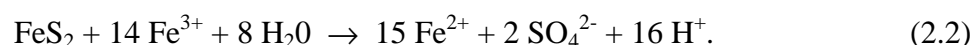
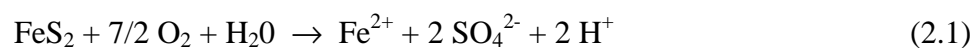


Figure 2.1. The percent gold extraction as a function of percent sulfide oxidation for three refractory ores (courtesy of Jim Brierley, Newmont Metallurgical Services).

the ore is left on the heap much longer than necessary, the processing cost per ounce of gold increases and less ore can be processed on a given pad. Therefore, in order to increase the efficiency and economics of gold recovery, determination of the optimal removal time from the biooxidation pre-treatment process is necessary.

2.2 Sulfide Oxidation

Pyrite is the predominant sulfide mineral encapsulating gold in sulfidic refractory ores. The two primary chemical reactions for pyrite oxidation are (Ritchie, 1997):



Reaction (2.1) requires oxygen and water, and is relatively slow. Reaction (2.2) can be much faster than reaction (2.1), depending on the availability of Fe^{3+} , and more hydrogen ions are produced, dramatically decreasing the pH of the solution. The rate-limiting step in pyrite oxidation is the formation of Fe^{3+} required for reaction (2.2). Therefore, the total amount of these ferric-iron ions in solution is related to the kinetics of pyrite oxidation. Biooxidation expedites pyrite oxidation by increasing the amount of Fe^{3+} available in solution and the increasing acidity creates optimal conditions for the bacteria.

2.3 Microorganisms

The primary function of the microorganisms used in biooxidation is to create optimal conditions for pyrite oxidation. The bacteria oxidize ferrous ions (Fe^{2+}) to ferric

ions (Fe^{3+}), increasing the amount of Fe^{3+} available in solution for fast pyrite oxidation. *Thiobacillus ferrooxidans* (Brierley, 1997) is among the primary bacteria utilized in biooxidation. Since the discovery of *T. ferrooxidans* in 1947 for its role in acid mine drainage (Colmer and Hinkle, 1947), metallurgists and microbiologists have studied this bacterium extensively and have proven its effectiveness in mineral oxidation. An understanding of the bacterial processes and factors impacting their productivity are important to optimize conditions and develop better monitoring techniques.

2.3.1 *Thiobacillus ferrooxidans*

T. ferrooxidans (see Figure 2.2) is naturally occurring in sulfide mine waters and is known to accelerate the production of acid mine drainage by increasing the rate of pyrite oxidation (Huswit and Sykes, 1994; Borner et al, 1993; Braddock et al, 1984; Gray, 1997; Smith, 1994). *T. ferrooxidans* exist in a pH range between 1.0 and 6.0 and at temperatures below 45° C. Maximum activity occurs at pH less than 2.5 and at temperatures between 25 and 35° C. This aerobic microorganism obtains energy from the exothermic oxidation of ferrous to ferric iron and may directly oxidize sulfides (Bartlett, 1992 and Evangelou, 1995). The oxidation of ferrous iron to ferric iron is the most significant activity and is the proposed energy source for metabolism and carbon dioxide fixation. Redox proteins spanning the cytoplasmic membrane catalyze iron oxidation according to the reaction (Barrett et al, 1993):

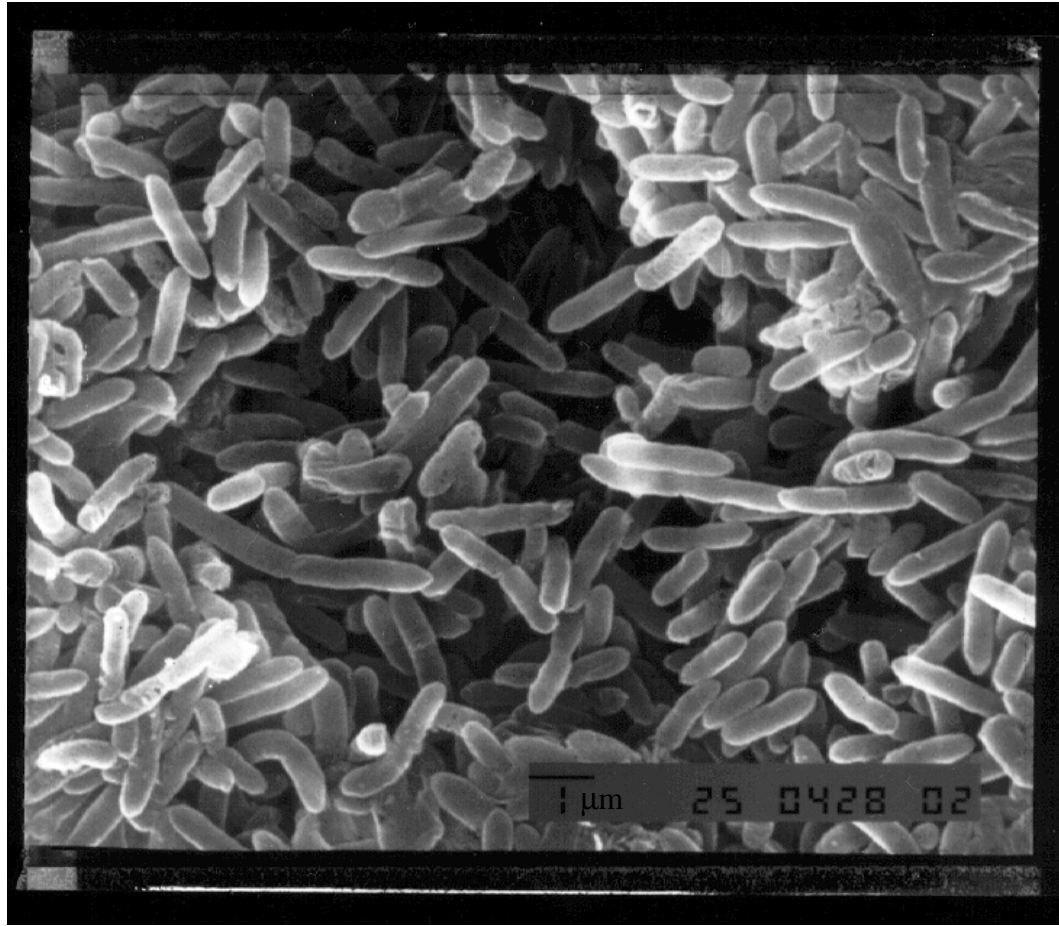


Figure 2.2. *Thiobacillus ferrooxidans* is a rod-shaped bacterium with a diameter of about $\frac{1}{2}$ micron (photograph courtesy of Jim Brierley, Newmont Metallurgical Services).

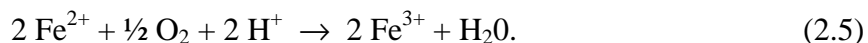
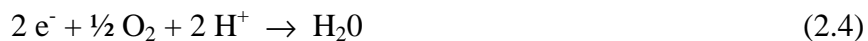
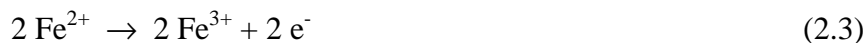


Figure 2.3 demonstrates that the half reaction (2.3) occurs in the outer part of the microorganism, and the half reaction (2.4) occurs inside the microorganism. The outermost protein is the most tolerant of acidic environments and is the initial acceptor of electrons. Electrons are then transferred to the other proteins and cytochromes through the cytoplasmic membrane. The resulting electrochemical gradient supplies the energy for vital functions of the microorganism (Rossi, 1990). As the electrons enter the cytoplasm, they react with hydrogen and oxygen to form water, thereby maintaining the pH in the cytoplasm to around 6.0 and allowing the organism to survive in very acidic environments. Bartlett (1992) proposes that the ferrous ions actually diffuse through the cell wall and oxidation occurs at the cytoplasmic membrane.

2.3.2 Bacterial Attachment to Surfaces

Bacteria are known to adhere readily to many types of surfaces (Crundwell, 1997). The direct oxidation of sulfides by bacteria is indicated by the preferential attachment of *T. ferrooxidans* to hydrophobic sulfide minerals, such as pyrite. This often results in the formation of a biofilm on pyrite and other minerals, which forms a protective coating on the surface. Crundwell (1996) reported that a biofilm completely

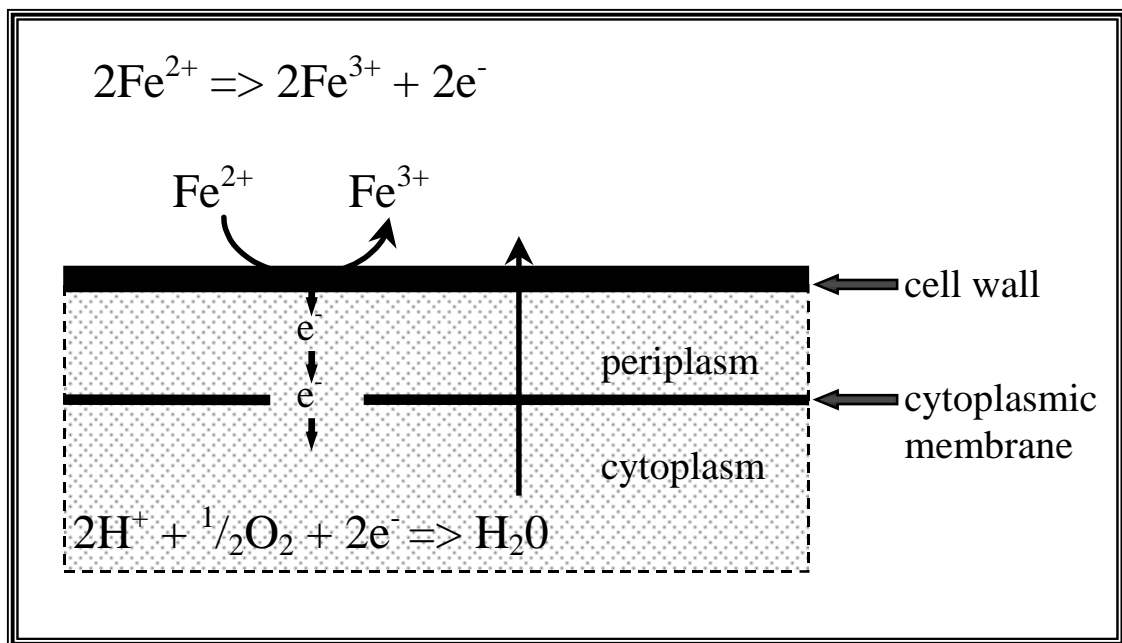


Figure 2.3. Oxidation of ferrous iron by *T. ferrooxidans* (modified from Barrett et al, 1993). The half reaction (2.3) must take place in the outer regions of the bacteria envelope where the pH is lower (close to the surrounding environment), and the half reaction (2.4) occurs inside the cytoplasm.

covered a polished pyrite section within 13 days, with a thick layer of ferric hydroxide forming between the pyrite and biofilm (Figure 2.4). The bacteria did not require direct attachment to the pyrite because the biofilm matrix between the bacteria and pyrite can cycle the iron. The biofilm contains high concentrations of ions and nutrients that allow the bacteria to flourish. This biofilm has been observed to form on almost any surface, and may form on the metal electrode surfaces. Direct attachment of the bacteria usually involves the growth of fibrils between the bacteria and the surface (Figure 2.5).

2.3.3 Limiting Factors

The solution temperature, pH, oxygen, and Fe^{2+} concentration directly limit the productivity of bacteria. Particle size and sulfide content indirectly influence productivity. The reactions for pyrite oxidation are exothermic, causing the temperature in the heap to increase over time. Thermophilic bacteria (like *Sulfolobus*, *Acidianus*, and *Metallosphaera*), which operate at higher temperatures, are used to ensure that iron oxidation continues as the temperature rises (Brierley, 1999). The pH of the solution is usually sufficiently low, since pyrite oxidation produces H^+ and sulfuric acid. In ores with a sufficient amount of carbonate material to buffer the pH, acid must be added to decrease the pH to optimal levels. Pumping air from the base of an ore heap increases the oxygen availability. The amount of total iron in solution increases as pyrite oxidizes. In equation (2.2), for fast pyrite oxidation, 14 moles of Fe^{3+} are consumed and 15 moles of Fe^{2+} are produced for every mole of pyrite oxidized. The Fe^{2+} is in turn oxidized to Fe^{3+}

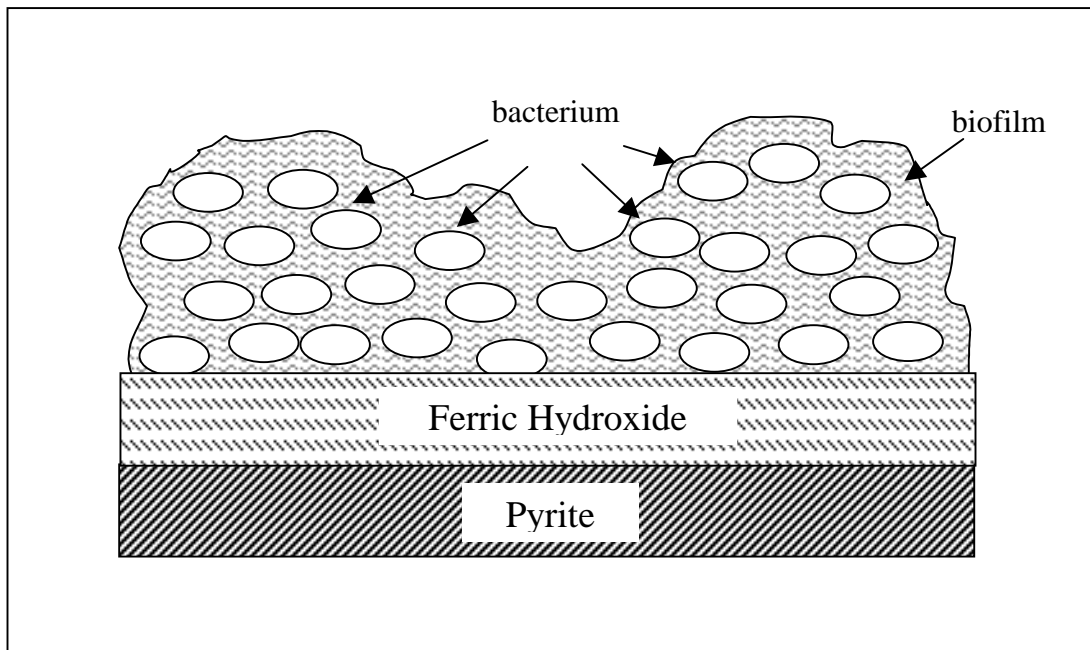


Figure 2.4. The formation of a biofilm by *T. ferrooxidans* on a pyrite surface (after Crundwell, 1997).

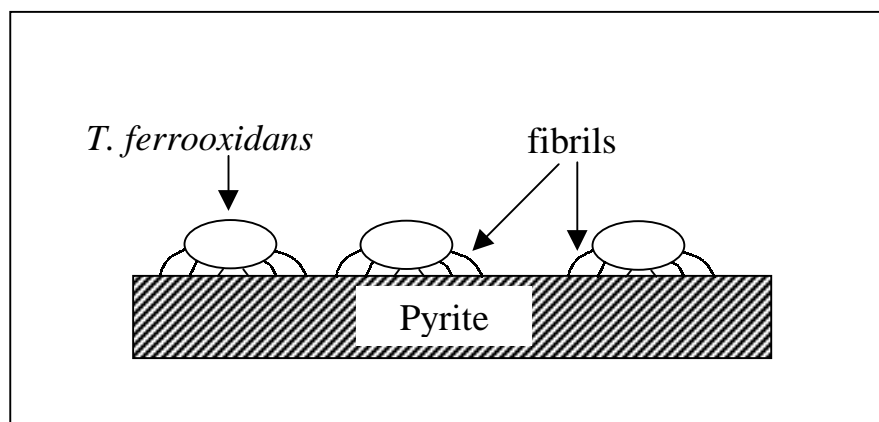


Figure 2.5. The attachment of *T. ferrooxidans* to a surface with fibrils (after Crundwell, 1997).

by the bacteria, with one extra iron ion being available each time one mole of pyrite is oxidized. Therefore, the conductivity of the solution increases as pyrite oxidizes, due to increases in the number of total iron and sulfate ions. Smaller particle sizes have more surface area for faster oxidation, but clay size particles can inhibit fluid and air circulation, indirectly interfering with bacteria productivity. If there is mineralogical clay the chemistry may change and interfere with biooxidation (Brierley, 1999) due to the cation exchange capacity of clays.

2.4 Heap Biooxidation Method

Heap biooxidation proves economical for gold recovery from low-grade ores. Ore is crushed to a nominal half-inch and placed with a stacker onto a lined heap pad to a height of up to 10 meters (see Figures 2.6 and 2.7). The ore must not be compacted, therefore trucks should not be used to construct the heap. The biooxidation solution is applied with sprinklers or drippers to the top of the heap. Low pressure fans transfer air to the base of the heap via a network of plastic pipes (see Figure 2.8), providing the oxygen and carbon dioxide necessary for the microorganisms. In tests of this technology, pilot heaps ranged in size from a few hundred tons to about 708,000 tons (Shutey-McCann et al, 1997). Typically, 50% of the sulfide minerals must be oxidized to sufficiently increase gold recovery. The time required for 50% sulfide oxidation can range from 100 to 300 days, depending on the ore and optimization of operating conditions.



Figure 2.6. Biooxidation heap construction using conveyors (photograph courtesy of Jim Brierley, Newmont Metallurgical Services).



Figure 2.7. Close-up of the side of biooxidation heap (photograph courtesy of Jim Brierley, Newmont Metallurgical Services).



Figure 2.8. Plastic pipes to transport air to the bottom of the heap for injection into the heap (photograph courtesy of Jim Brierley, Newmont Metallurgical Services).

2.4.1 Advantages

The advantages of heap biooxidation over other pretreatment methods are the low cost, simple application, and reduction in sulfidic mine wastes. The cost is approximately ten times less than roasting (Brierley, 1999), allowing for economic processing of low-grade ores which would normally be waste. The method only requires a lined pad with pipes for air circulation, crushed ore, bacteria-rich solution, a method for building the heap without compaction, a sprinkler system to distribute biooxidizing solution, and a collection system for run-off. Since approximately 50% of the sulfidic minerals are normally oxidized during the biooxidation process, the sulfide content in the waste rock is reduced by 50%. In addition, the acid generated during oxidation is neutralized prior to cyanide leaching, thereby greatly reducing acid mine drainage.

2.4.2 Disadvantages

The main disadvantages of heap biooxidation are that the process is time-intensive, gold recovery can be less than other methods, it is difficult to monitor, and the ore must be neutralized prior to cyanide leaching. Neutralization can be easily applied by adding carbonate material, such as lime, to the ore to increase the pH. The time required for heap biooxidation can range from 100 to 300 days, depending on the ore and conditions within the heap. The process can be expedited by maintaining optimal conditions for pyrite oxidation. Since gold recovery is only 50-60%, heap biooxidation is

only economical for low-grade ores that cannot be economically processed by more expensive processes. Monitoring the rate of oxidation is a challenging issue.

2.4.3 Monitoring Requirements

Accurate monitoring is necessary to determine when a sufficient amount of pyrite oxidation has occurred. Knowing when oxidation is complete could greatly enhance recovery without spending unnecessary time on the heap pad. Factors influencing an ore's performance are ore mineralogy (including pyrite, clay, and carbonate content), oxygen, temperature, bacteria viability, and solution pH. Heterogeneity within a heap causes different sections to oxidize at different rates, which means the bulk oxidation over different volumes is necessary to accurately assess a heap. Directly monitoring bulk pyrite oxidation would be much more effective than attempting to monitor all the individual factors affecting biooxidation.

An optimal monitoring method would determine the optimal removal time and diagnose the performance throughout the heap in order to pinpoint problem areas. The primary monitoring method has been chemical sampling of the solution draining from the base of the heap. This is inefficient because the solution originates from unknown sections of the heap and may not be indicative of overall oxidation in the heterogeneous heap. Coring through the heap would result in unwanted compaction, especially if done from the top, and would only give discrete samples that would not represent the performance of a heterogeneous heap. The cost of installing sensors or sampling

mechanisms throughout the heap far exceeds economic feasibility. The ideal monitoring method would be placed under the heap and non-invasively measure the pyrite oxidation throughout the heap.

2.5 Applicability of Complex Resistivity to Monitor Biooxidation

The presence of pyrite is known to produce a CR response due to charge storage (Klein and Shuey, 1978) at the solution/metal interface (discussed in Section 3.3.1) and the resulting discharge when the signal input is turned off. As pyrite oxidizes, the solution/metal interface is disrupted and the charge storage capabilities decrease. Oxidation/reduction reactions involve the transfer and redistribution of charge in solution and across interfaces (discussed in Section 3.3.2), influencing CR measurements. The oxidation of pyrite described in Section 2.2 involves charge transfer and increases the number of ions in solution. Microorganism activity, as described in Section 2.3, also involves charge transfer when Fe^{2+} is oxidized to Fe^{3+} . The presence of pyrite as well as the oxidation of pyrite and iron in the sample should be observable with CR. The bacteria may have a direct effect on the measurements because of their negative charge and the formation of biofilms.

The purpose of this thesis is to evaluate the applicability of complex resistivity to monitor the biooxidation process, based on the observed correlation of CR and the chemistry of pyrite oxidation in laboratory research.

Chapter 3

COMPLEX RESISTIVITY

3.1 Historical Background

Complex resistivity (CR), or spectral induced polarization (SIP), in geophysics is also known as complex impedance in electrical engineering and impedance spectroscopy in electrochemistry. These are generally frequency domain measurements over a wide frequency band from as low as 10^{-5} Hz to as high as 10^6 Hz and are used to characterize the frequency dependent electrical behavior of a system. The system might be electronic circuits in electrical engineering, electrochemical and corrosion systems in electrochemistry (Macdonald, 1987; Macdonald et al, 1998), or the earth or rock/soils samples in geophysics (Sumner, 1976; Bertin and Loeb, 1976; Olhoeft, 1985). The input to the system is current, the output from the system is electric potential, and the transfer function that relates the two is the complex electrical impedance. A brief summary of some of the important research with induced polarization and complex resistivity establishes a basis of the utility of the technique and applicability to this research.

Induced polarization (IP), a simplified case of CR with only one or two frequencies, has been used primarily for mineral discrimination and specifically for sulfide exploration, both in the time and frequency domains. Conrad Schlumberger made the first IP measurements in 1912 (Sumner, 1976). In 1946, Newmont Mining

Corporation began research to develop IP for sulfide mineral exploration. The landmark monograph by Wait (1959) contains a collection of papers based primarily on work by Newmont Mining Corporation between 1946 and 1958. In this monograph, time and frequency domain IP measurements are discussed and the application to pyrite identification is shown. Marshall and Madden (1959) showed the utility of low frequency electrical properties for the detection of metallic or semi-conducting minerals.

Zonge and Wynn (1975) proposed that complex resistivity was advantageous for (1) complete coupling removal, (2) identification of the host rock response, and (3) mineral discrimination. Pelton et al (1978) used in-situ CR measurements of 26 mineral deposits to show that mineral texture was a main factor in the differences in spectral responses and approximate corrections for inductive coupling were possible. Laboratory frequency domain IP measurements, by Klein and Shuey (1978), at 0.002 Hz distinguished between pyrite and chalcopyrite.

Wong (1979) developed an electrochemical theory for the frequency dependent IP of disseminated sulfide ores, concluding that:

- (1) electrochemical reactions must occur to transfer charge from the solution to the metallic mineral,
- (2) it is difficult to separate the effects of electrochemistry from mineral habit and texture,
- (3) there is a frequency-dependent dispersion related to the metallic particle size and due to the diffusion-limited nature of chemical reactions,

- (4) the metal-electrolyte interface acts like a leaky capacitor (as an insulator at low frequencies and a conductor at high frequencies), and
- (5) if very large reaction rates occur, then the metal-electrolyte interface becomes almost perfectly non-polarizable (decreasing the IP response).

Even though his model contained spherical metallic particles in a simple electrolyte, the results can be applied to disseminated sulfide ores.

Olhoeft (1979a, 1979b, and 1985) performed CR measurements over a wide frequency range to investigate the nonlinear electrical impedance of minerals, clay-organic reactions, oxidation-reduction reactions, permafrost, and organic matter. Some experiments examined the affects of temperature and saturation. The equipment and methods developed in Dr. Olhoeft's research form the basis of the techniques used here.

3.2 Theory

The frequency dependence of electrical properties can be determined by using a wide range of measurement frequencies. The input to the sample is current and the output from the sample is electric potential, whose amplitude, phase, and harmonic content may vary from the input. The ratio of the output to the input is the transfer function of the system, which in this case is the complex electrical impedance of the sample.

Olhoeft (1979a) used Ohm's Law to derive the electrical properties of a linear system as related to the input, output, and transfer function of CR. Frequency dependent

electrical properties of a sample are related to the conduction (charge transport) and polarization (charge storage) in response to a stimulus current. The nonlinear electrical properties of the system are a result of chemical reactions and can be characterized by the Hilbert distortion and total harmonic distortion of the complex electrical impedance, as discussed in Section 3.2.4.

3.2.1 Electrical Properties

Electrical resistivity (ρ) can be described by the generalized Ohm's Law as:

$$E = \rho J, \quad (3.3)$$

where E is the electric field strength (volt/meter), J is the current density (amp/m²), and ρ is in ohm-m. The fundamental equations for the linear case, derived by Olhoeft (1979a), are:

$$E(\omega) = E_s + E_o \sin(\omega t + \phi_e) \quad (3.4)$$

$$\text{and } J(\omega) = J_s + J_o \sin(\omega t + \phi_j), \quad (3.5)$$

where E_s = spontaneous polarization

E_o = amplitude of the potential voltage

ω = angular frequency (radians/sec) = $2\pi f$ (f is the frequency in Hz)

t = time (sec)

ϕ_e = phase of the voltage

J_s = DC offset (or initial) current, typically of zero value

J_o = amplitude of the current

and ϕ_j = phase of the current.

If an arbitrary time zero is chosen for the measurement, both the current and voltage waveforms may have a phase value and the desired CR phase angle is the difference between them.

The complex resistivity and phase for one frequency are calculated by:

$$\rho' - i\rho'' = \text{complex resistivity} \quad (3.6)$$

$$\rho' = (E_o / J_o) \cos \phi = \text{real resistivity} \quad (3.7)$$

$$\rho'' = (E_o / J_o) \sin \phi = \text{imaginary resistivity} \quad (3.8)$$

$$|\rho| = (\rho'^2 + \rho''^2)^{1/2} = E_o / J_o = \text{resistivity magnitude} \quad (3.9)$$

and $\phi = \tan^{-1} (\rho'' / \rho') = \phi_e - \phi_j = \text{phase angle (radians)}. \quad (3.10)$

Figure 3.1 shows the representation between the resistivity and phase in the complex plane. The relationship between the input and output waveforms is illustrated in figure 3.2.

3.2.2 Charge Transport

In an aqueous electrolytic solution, ionic conduction is the method of charge transport and oppositely charged ions migrate when an external electrical field is applied. The ability of a solution to facilitate charge transport is related to the ionic concentration and ion mobility. In metallic minerals (such as copper), electronic conduction is the

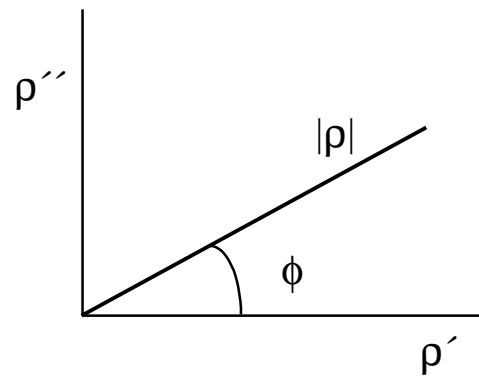


Figure 3.1. Complex plane plot showing the relationship between the real (ρ') and imaginary (ρ'') resistivity and the phase (ϕ).

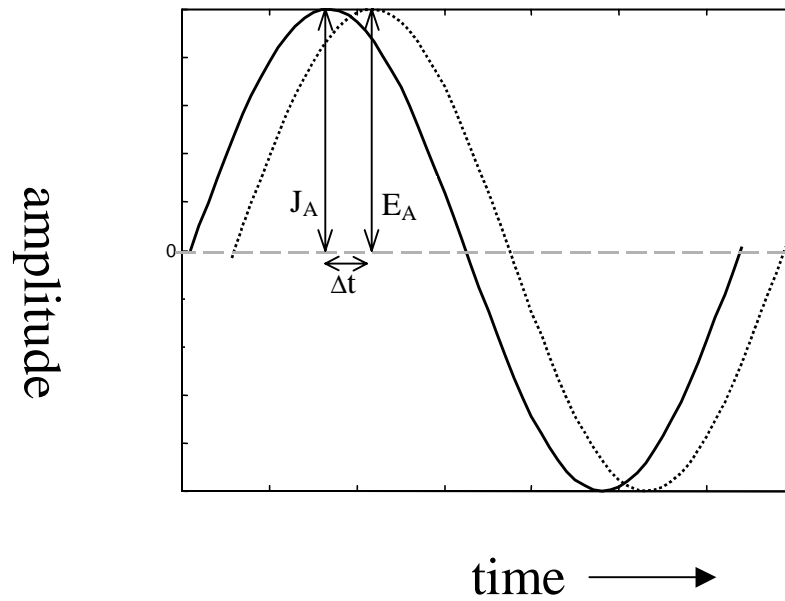


Figure 3.2. Sinusoidal waveforms for the input current (solid line) and output voltage potential (dotted line) in complex resistivity measurements. Where J_A is (J_o+J_s) and E_A is (E_o+E_s) , and the time delay is Δt .

method of charge transport. Non-metallic minerals (such as quartz) have few mobile charge carriers and charge transport is minimal. In an electrolyte-solid mixture, both ionic and electronic conduction may occur, with the interface producing complex frequency-dependent impedance as a result of the polarization of the interface.

3.2.3 Charge Storage

Polarization is the spatial separation of charges. When an electric field is applied to an electrolyte-solid mixture, charge migration produces a current, and a polarization occurs if there is a separation and/or redistribution of charge. Interfaces where the electrical properties of the sample change, such as the interfaces between metallic minerals and electrolyte are energy barriers. Charge is stored at the interface (i.e. the interface is polarized) until there is a high enough potential to overcome the energy barrier and transfer electron(s) across the interface.

Oxidation/reduction reactions transfer charge between the ions in solution and electrons in the metal. In these electrochemical reactions, the amount of energy necessary to overcome the energy barrier is the reaction potential for the specific metal and ions interacting. The polarization response will change when the state of the solid, electrolyte, or interaction between the two changes, as occurs in the biooxidation of pyrite. The complex impedance of electrochemical reactions cannot be represented by only combinations of fixed resistors and capacitors, and is described by the Warburg

impedance (Grahame, 1952). Warburg impedance varies as a square root of the frequency and represents the complex, frequency dependent, and non-linear, diffusion-limited electrochemical reactions (Olhoeft, 1985; Macdonald, 1987; Sluyters-Rehback and Sluyters, 1970).

3.2.4 Nonlinearity

According to Olhoeft (1979b), nonlinear electrical properties of naturally occurring materials are due primarily to oxidation/reduction or ion-exchange processes and can be used to remotely measure chemistry. In biooxidation, the dominant cause of nonlinearity is assumed to be the oxidation/reduction reactions occurring at the pyrite interface. The magnitude of the input current will influence the response of a nonlinear system. According to Klein and Shuey (1978), too large of a current (greater than 10 milliamps/cm²) will cause nonlinear electrode corrosion, which may interfere with the determination of nonlinear sample chemistry. If too low a current density is used, the system becomes linear (Olhoeft, 1979b).

The input current density and output potential field are proportional for a linear system and the complex impedance is independent of the current density. If the energy barriers are much smaller than the driving force (current density), then an increase in the driving force results in a linearly proportionate amount of charge movement across the barriers (Jones, 1997). If the current density is too high, the system may become nonlinear (Olhoeft, 1979b) because of the occurrence of chemical reactions.

There are two primary mathematical representations of nonlinearity that have been used by Olhoeft (1979a and 1985); Kramers-Kronig (KK) transforms (or Hilbert Transform) and total harmonic distortion (THD). The Kramers-Kronig transforms are a mathematical relation between the real and imaginary parts of the transfer function and assume a causal, linear, and stable system with continuous, finite values (Macdonald, 1987). All natural systems are causal, which means they cannot predict the future.

There may be a potential difference prior to the input of the current density due to streaming potentials or other spurious currents, such as electron transfer during oxidation/reduction or the percolation of charge-carrying solution. The system may be nonlinear due to high current densities, electrochemical reactions, or to ion exchange as occurs in clay minerals (Olhoeft, 1979b).

Total harmonic distortion is a mathematical description of the difference between the harmonics of the input and the output. If the input is a pure sinusoidal waveform, any harmonics in the output are due to nonlinearity of the system. The THD is expressed as a percent, which is the ratio of the deconvolved harmonics of the output and input. Oxidation-reduction reactions often exhibit peaks in the THD because nonlinear electrochemical reactions result in new harmonic content, which may be significant.

3.3 Complex Resistivity and Biooxidation

Complex resistivity may prove to be a useful monitoring tool for biooxidation because of the non-linear, frequency dependent behavior of oxidation/reduction reactions

and the polarization response associated with pyrite. CR measures charge transfer, which occurs in oxidation/reduction reactions. Biooxidation relies on the bacteria-assisted oxidation of ferrous to ferric ions to facilitate the oxidation of pyrite. CR has been used by electrochemists to determine the corrosion of metals (Macdonald and McKubre, 1987), as occurs when pyrite corrodes during biooxidation. The primary exploration method for sulfide ores has been induced polarization, a simplified form of CR, because of the polarization response of pyrite (Marshall and Madden, 1959; Wait, 1959; Van Voorhis et al, 1973; Sumner, 1976; Ward, 1990). The fact that CR can detect pyrite and oxidation is augmented by the non-invasive nature of the technique to make this a promising monitoring method for biooxidation.

3.3.1 Pyrite Polarization

The polarization phenomena at the interface between pyrite and the electrolyte has been used in the exploration for massive and disseminated sulfidic ore bodies (Wait, 1959; Anderson and Keller, 1964; Sumner, 1976; Bertin and Loeb, 1976; Klein and Shuey, 1978; Pelton et al, 1978). According to Sumner (1976), current-induced transfer of electrons between electrolyte ions and metallic minerals are the main cause of polarization.

The model for polarization, as outlined by Marshall and Madden (1959) and Sumner (1976) is shown in Figure 3.3. The equivalent circuit in Figure 3.3a represents the geologic kinetics model for the geologic model in Figure 3.3b. Figure 3.4 shows the

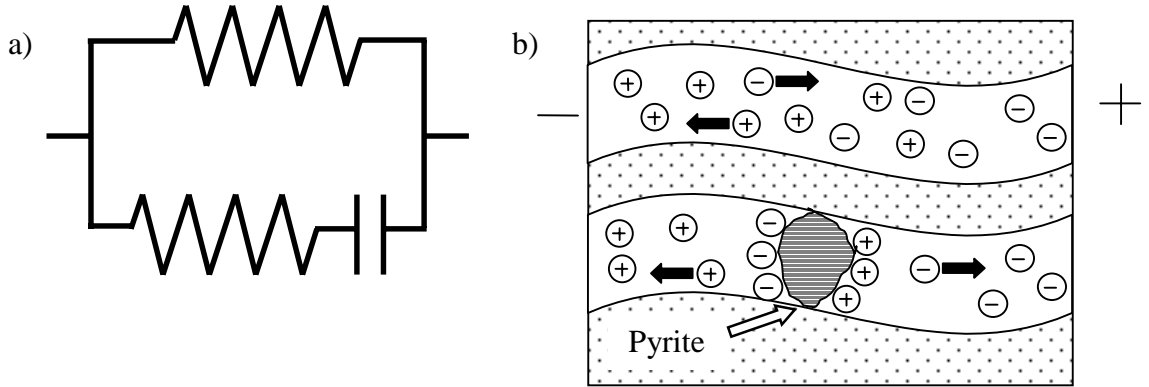


Figure 3.3 a) An R-RC circuit can be used to describe the CR response of a solid-electrolyte mixture. b) Ion migration resulting when current is applied to a rock sample.

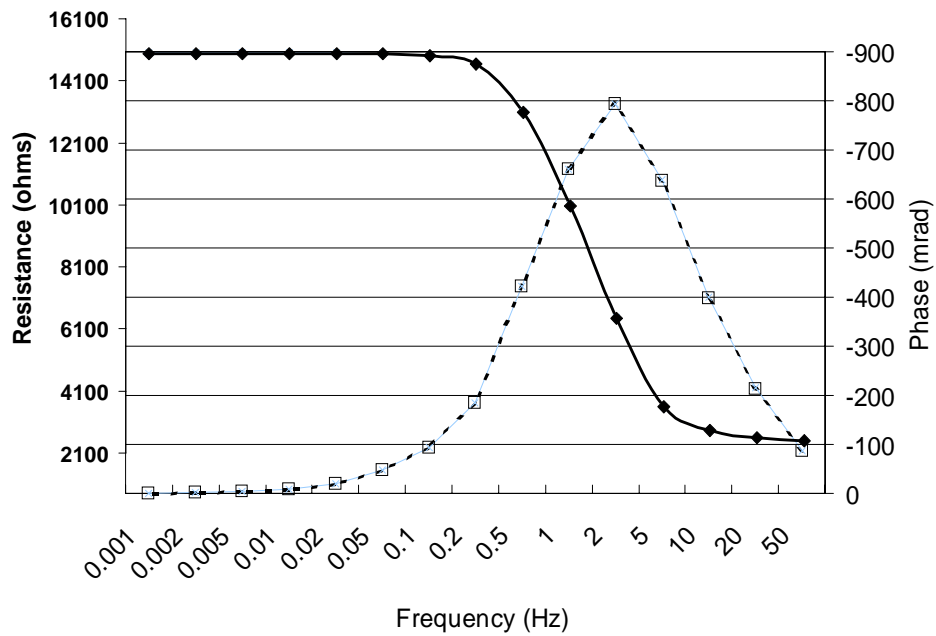


Figure 3.4 Amplitude (solid line and symbols) and phase (dashed line and open symbols) spectra measured for an R-RC circuit (as shown in Figure 3.3a).

amplitude and phase spectra for the circuit in Figure 3.3a. The geologic model in Figure 3.3b shows two passageways; one open and one blocked by a pyrite grain. A resistor is the equivalent electronic component for the CR response of the ionic conduction of an electrolyte in an unimpeded path (as occurs in the upper fluid-filled pore in the model), with the resistance being equal to the inverse of the conductance of solution. A resistor in series with a capacitor is the electronic equivalent for the kinetics model of an electrolyte-filled pore blocked by a pyrite grain. In the diffusion model, Warburg impedance would replace the capacitor.

These models require that the pyrite grain completely blocks the pathway of the migrating ions. In a sample where there are continuous paths for fluid flow it is obvious that not all pores are blocked, which means there is a combination of both pathways. The contrast in electrical properties between the pyrite and pore-fluid. Metallic mineral grains distort the electrical current flow, causing more current to flow near and through the highly conductive mineral grain (Olhoeft, 1985). In biooxidation, iron ions migrate toward pyrite grains and possibly to bacteria that may coat the pyrite.

Klein and Shuey (1978) measured the nonlinear electrical impedance of pyrite to determine if it was feasible to discriminate between minerals based on their electrical properties. They concluded that the polarization response for a mineral depends on the waveform used, mineral composition, polarization history of the electrode, and the chemical composition of reactants in secondary reactions. The response also varied as a function of current density. At current densities up to 1 mA/cm^2 , primary mineral

dissolution reactions occurred and secondary reactions (which involve the products of previous reactions) were observed at lower current densities. For the dissolution of pyrite (measured at 1 mA/cm²), they identified important secondary reactions to be H⁺ and O₂ reduction, the Fe²⁺-Fe³⁺ redox couple (measured at 0.1 mA/cm²), reduction of an unidentified iron oxide, and iron-hydroxide oxidation. Their findings are important to this study because they show that the total electrical response is nonlinear and depends on the chemistry of pyrite and oxidation products in addition to the amplitude of the input current density. In order to identify temporal changes in a sample, similar amplitude of current density are required to sense the same chemical reactions and their nonlinear behavior over time.

With biooxidation, the pyrite content decreases over time due to oxidation, resulting in a resistivity decrease (due to increasing ionic concentration) and a phase decrease (due to a reduction in the number of pyrite-blocked pores). As the rate of pyrite oxidation increases, the polarization response may decrease because there is less pyrite and fewer pyrite-blocked pores.

3.3.2 Oxidation/Reduction Reactions

The primary oxidation-reduction reactions occurring during biooxidation are the oxidation of pyrite (Equation 2.2) and the oxidation of ferrous to ferric ions (Equation 2.3). Pyrite oxidation produces ferrous ions, sulfate ions, and hydrogen ions. The hydrogen and sulfate ions generally react to produce sulfuric acid (Ritchie, 1997). These

reactions readily occur in the sample whether or not current is applied and involve the transfer of charge across the pyrite-electrolyte interface. This section will investigate what effect these reactions have on the nonlinear complex electrical impedance.

Oxidation-reduction transfers charge from the ions in solution to the electrons in a metal (as described in Section 3.2.3). Most reactions are not spontaneous and there is an energy barrier (i.e. reaction potential) that must be overcome for oxidation-reduction to occur. Oxidation-reduction at the pyrite surface is more likely to be kinetics limited in biooxidation because there are plenty of iron ions in the biofilm on the surface of the pyrite and it is the speed of pyrite oxidation that is the rate-limiting chemical reaction (Ritchie, 1997). The re-distribution of charge due to oxidation/reduction will appear as an increase in polarization if charge separation occurs and as an increased conductivity if the number of ions in solution increases.

According to Klein and Shuey (1978) the amplitude of the current density will determine which chemical reactions (primary or secondary) affect the nonlinear impedance measured by CR. Pyrite oxidation, the primary reaction during biooxidation, should be the primary contributor to the nonlinear impedance at high current densities (but less than 10 mA/cm^2). The bacteria-assisted oxidation of ferrous to ferric ions, the reduction of H^+ and O_2 , and the formation of iron oxides are secondary reactions (because they involve products of pyrite oxidation) and should contribute more to the nonlinear impedance at lower current densities. Distinguishing between primary and

secondary reactions on the basis of current density is mentioned to stress the importance of maintaining current density over time and is not discussed further.

3.3.3 Bacteria Effect

The purpose of this section is to propose possible bacteria effects on CR measurements. Bacteria may have both indirect and direct effects on complex resistivity measurements. Indirect effects are due to changes in sample chemistry resulting from bacteria activity and include the affect of biofilms. Direct effects are due to the presence of charged bacteria and their interaction with current flow. Since bacteria readily attach themselves to surfaces (see Section 2.3.2), their presence may change the natural pyrite response by interfering with the natural diffusion of ions and with the migration of ions in response to an electric field. The formation of biofilms increases the iron ion concentration near the pyrite surface and may decrease the diffusion limitations of chemical reactions because of the high availability of ions for oxidation/reduction reactions.

A biofilm rich with iron forms on the pyrite and the bacteria cycle iron ions to and from the pyrite surface. If there was no biofilm and the pyrite was in contact with the pore fluid, current flow would move charged particles (such as iron and water) to and from the pyrite surface. When there is a biofilm, a pyrite-electrolyte interface is replaced by the pyrite-biofilm and biofilm-electrolyte interfaces. Charged particles move in the solution to the biofilm where they may accumulate at the interface, or move through the

biofilm to the pyrite surface. The accumulation of charge at the biofilm-pyrite interface produces a polarization and may result in the transfer of charge between the solution and pyrite through oxidation-reduction reactions.

Small electric currents are believed to stimulate bacteria (Natarajan, 1992), and it is possible that they act as a receptor for electrons. Bacteria have a negative charge (Crundwell, 1997) and as a result may initially behave as anions and migrate through solution during a CR measurement. Bacteria are more complicated than negatively charged particles because bacteria may attach to surfaces with fibrils, or may be bound by a biofilm, as explained in section 2.3.2. If strongly attached to pyrite, the bacteria may be perturbed from their equilibrium position, resulting in a polarization. The biofilm contains ions and nutrients in addition to negatively charged bacteria and may exhibit polarization of its own. A layer of ferric hydroxide may form between the bacteria and pyrite, facilitating the transfer of charge to the pyrite. These possible bacteria influences are beyond the objective of this thesis and are left for future investigation.

3.3.4 Advantages/Disadvantages

The previously discussed advantages of complex resistivity are that it is:

- 1) a good pyrite indicator,
 - 2) sensitive to charge transfer as occurs in redox,
 - 3) an indicator of the presence of clay minerals,
- and
- 4) a non-invasive measure of the bulk response of a sample.

CR has the potential to become the optimal monitoring method for biooxidation because the effectiveness of biooxidation could be determined through a network of electrodes alongside the existing plastic air pipes under the heap described in Section 2.4.

The disadvantages are related to the difficulty of interpretation of the data. Many factors contribute to how the electrical properties of a sample interact with a current density and it is often difficult to identify individual factors. The object of this research is to correlate measurements of oxidizing ore with the chemical analysis used to monitor biooxidation in the laboratory, to determine if the CR response varies as a function of pyrite oxidation and changes in chemistry.

Chapter 4

EXPERIMENT SET-UP

4.1 Overview

The complicated chemical and biological processes occurring during biooxidation are very difficult to completely understand, even in a laboratory. However, there is a direct correlation between the measurable solution iron content and the oxidation of pyrite. The total iron in solution increases rapidly during biooxidation, and stabilizes when biooxidation slows. This research investigated two siliceous sulfidic refractory ores and a control rock in columns at Newmont Technical Facility in Englewood, Colorado, from October 1998, to April 1999. This evaluation lasted over 100 days for each sample and included chemical analysis of the solution in each sample to track the iron content throughout the biooxidation cycle. Ore mineralogy was determined with x-ray diffraction (XRD) and x-ray fluorescence (XRF). The ore chemistry was determined by assay analysis of elements including gold, sulfur, arsenic, and iron. A sieve analysis was performed when the ore was removed from the columns at the end.

4.2 Complex Resistivity System

The geophysical method of complex resistivity applies an electrical field to a sample, which produces current when charged particles move. The resulting potential

voltage and geometry are used to calculate the magnitude of the resistivity and the phase angle (time delay) for multiple frequencies. There are numerous possibilities for equipment to perform CR both in the time and frequency domains. The frequency domain is preferable because the chemistry of the sample is frequency dependent and time domain measurements must rely on problematic algorithms that require linear systems to determine the frequency dependence. Time domain measurements are faster because step function input contains a broad frequency range and save time. However, the speed of measurements is not a factor in this case because the process being monitored takes over 100 days to complete and changes in chemistry are tracked on a weekly basis.

The input waveform and frequency range are important variables in frequency domain measurements. The input waveform is normally a square wave or sinusoid. A square wave is easier to generate because it has two parts, positive singular voltage for half the cycle and an equal and opposite voltage for half the cycle. However, commercial function generators that produce extremely accurate sinusoids for a wide range of frequencies are readily available. The advantage of using a sinusoidal waveform is that harmonic distortions in the sinusoid shape occur due to the charge build-up at interfaces and overcoming the energy barrier of the interface when sufficient voltage has been applied in the sinusoid. If the full sinusoid waveform is recorded for both the input and output, the harmonic content from the equipment can be separated from the harmonic content due to sample chemistry. The frequency band may range from as low as 10^{-5} Hz

to as high as 10^6 Hz. The time to perform one cycle is the inverse of the frequency of the input waveform. This means that the cycle takes 10^{-6} seconds at 10^6 Hz and 10^5 seconds (27.8 hours) at 10^{-5} Hz. At low frequencies, the measurement time increases and the repeatability of the measurements decreases because the sample will most likely not remain at equilibrium for 27.8 hours and may be significantly different for consecutive measurements. In practice, the low-frequency limit is generally 10^{-3} Hz due to time and repeatability issues. Low frequency information is useful because most chemical reactions appear at low frequencies (inverse of the time constant for the reaction). High frequency data are dominated by dielectric properties of the sample and the polarization response of water molecules. The high frequency limit often depends on capabilities of the function generators and the rate of digitization necessary to accurately record the waveforms. The number of channels in the system dictates the number of electrode pairs that can be simultaneously measured.

The complex resistivity system used in this research records the full waveforms for the system input and output in the frequency domain for a total of 16 channels. The input is a sinusoidal waveform at frequencies from 10^{-3} Hz to 10^6 Hz (10^3 Hz in the column studies) and the output is the resulting potential difference between two electrodes in the sample. Full waveform analysis of frequency domain measurements is necessary to obtain precise measurements and calculate the nonlinearity of the sample. Differences in the complex resistivity system used in the laboratory studies are discussed in Section 4.2.2.

4.2.1 Equipment Specifications

The specifications for the 16-channel frequency domain CR system used in the column studies are also important in designing a field system. Measurements of frequencies from 10^3 to 10^{-3} Hz take approximately 35 minutes. The system was designed for continuous operation with no user input as a stand-alone monitoring device. The control program performs continuous data acquisition and will automatically restart when the computer is re-booted, in case of a long power failure. An un-interruptible power supply was used to prevent temporary outages from interfering with measurements.

A schematic of the measurement system is shown in Figure 4.1. Two Stanford Research Systems 30 MHz synthesized function generators (model DS45) are phase-locked together, with one generating a single cycle of the current waveform and the other acting as the clock to trigger the digitizing boards. The current goes to the Crown amplifier (model DC-300A) (a constant voltage source), which amplifies the signal with minimal harmonic distortion. The amplifier output is a voltage, which passes through the sample and a precision resistor in series with the sample. The potential difference across the resistor is used to calculate the current through the sample, according to Ohm's Law. The voltage drop across this current-sensing resistor and between the potential electrodes are simultaneously sampled by two Analogic 8-channel sample-and-hold boards (model SSH-8) and are then digitized at 1024 points per cycle with a 16-bit

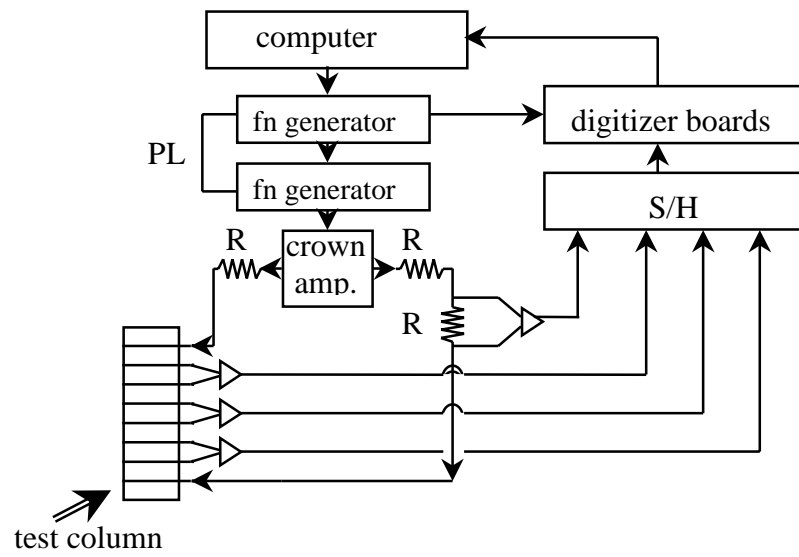


Figure 4.1. Complex resistivity instrumentation for the column studies.

Analogic A/D converter (model Fast 16-1-1). These digitized waveforms are stored as a series of bits for all 16 channels so that full-waveform processing can be performed.

4.2.2 Laboratory vs. Column System

The main difference between the laboratory and column systems is the frequency range of measurements. The laboratory system (see Figure 4.2) measures frequencies from 10^6 to 10^{-3} Hz for two channels. The signals at 20 Hz and above are generated by a HP4284A LCR meter and the low frequencies are generated with a HP3325A function synthesizer. A second HP3325A function synthesizer serves as the A/D clock to trigger the digitizer, as in the column system. The laboratory system is set-up as a 2-channel system to measure one sample at a time.

The column system has an amplifier to increase the current magnitude in the field so that the current densities in the laboratory can be matched in the field. Two 500 ohm resistors are used in the current loop for each column to increase the input impedance. This ensures that when columns of different resistances are in parallel, the same amount of current goes to each column. These resistors also prevent feedback into the system.

4.2.3 Calculations

The full waveform digital data from the column studies are processed and plotted with the program *nldr_nm.c*, written in ANSI-C. Parts of the program *nldr_lab.c* (Jones, 1997) were used. The processing algorithm was written by Olhoeft (1979a) and relies on

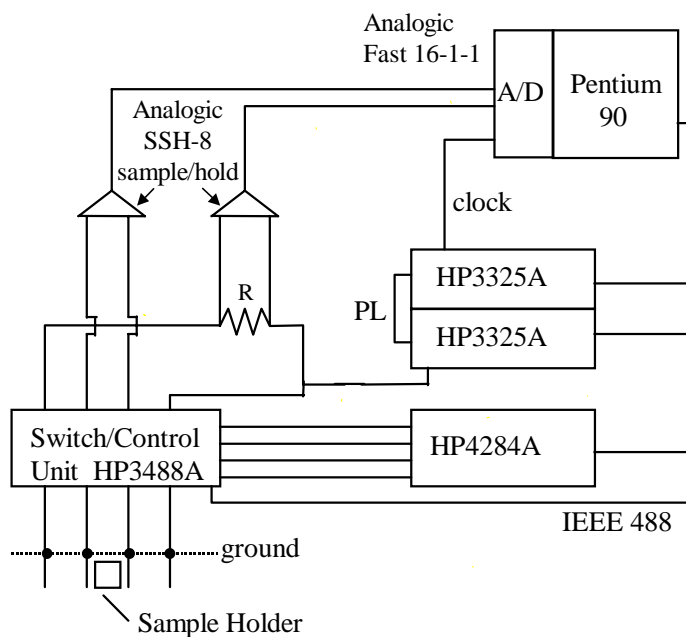


Figure 4.2. Complex resistivity instrumentation for the laboratory studies (from Jones, 1997).

linear inversion to obtain the resistivity and phase data, according to equations 3.3 and 3.4. Two channels are processed at a time, one potential and the corresponding current channel. The current and potential waveforms at each frequency are processed for the resistivity, phase, Hilbert transform, total harmonic distortion, SP (spontaneous potential), and current density.

The 1024 data points at time (t) for each frequency are stored as a series of bits (with each bit representing some fraction of a volt determined by the digitizers) for the potential channel and the current channel. The current channel voltage is divided by the magnitude of the current-sensing resistor to obtain the current (I). The current is converted to the current density (J) by dividing by the sample area. The potential is converted to the electric field (E) by dividing by the sample thickness. The resulting electric fields and current densities are:

$$E_1, E_2, E_3, \dots, E_{1024} \text{ and}$$

$$J_1, J_2, J_3, \dots, J_{1024} \text{ at times } t_1, t_2, t_3, \dots, t_{1024}.$$

The measured data are arranged in the 2 by 1024 matrix (\mathbf{X}) such that

$$\mathbf{X} = \mathbf{T} \mathbf{A} \tag{4.1}$$

where the \mathbf{X} , \mathbf{T} , and \mathbf{A} matrices are:

$$\mathbf{X} = \begin{vmatrix} E(t_1) & J(t_1) \\ \cdot & \cdot \\ \cdot & \cdot \\ \cdot & \cdot \\ E(t_{1024}) & J(t_{1024}) \end{vmatrix}$$

$$\mathbf{T} = \begin{vmatrix} 1 & \sin(\hat{u} t_1) & \cos(\hat{u} t_1) \\ \cdot & \cdot & \cdot \\ \cdot & \cdot & \cdot \\ \cdot & \cdot & \cdot \\ 1 & \sin(\hat{u} t_{1024}) & \cos(\hat{u} t_{1024}) \end{vmatrix} \quad \text{and} \quad \mathbf{A} = \begin{vmatrix} E_s & J_s \\ E_0 \cos \phi_e & J_0 \cos \phi_j \\ E_0 \sin \phi_e & J_0 \sin \phi_j \end{vmatrix}.$$

The \mathbf{T} matrix is calculated and the \mathbf{A} matrix is solved for according to:

$$\mathbf{A} = (\mathbf{T}^T \mathbf{T})^{-1} \mathbf{T}^T \mathbf{X}. \quad (4.2)$$

The spontaneous polarization is the value A_{11} times a bit-to-volt conversion factor. The value of A_{21} is the in-phase voltage, which is the real part. The value of A_{31} is the out-of-phase voltage, which is the imaginary part of the complex voltage. The in-phase and out-of-phase voltages for the current-sensing resistor are A_{22} and A_{32} , respectively. The voltage amplitude (E_o) and current amplitude (J_o) are calculated according to:

$$E_o = (A_{21}^2 + A_{31}^2)^{1/2} \quad (4.3)$$

$$\text{and} \quad J_o = (A_{22}^2 + A_{32}^2)^{1/2}, \quad (4.4)$$

and the resistance (R) and phase (ϕ) values are calculated by:

$$|R| = E_o / J_o, \quad (4.5)$$

$$\phi_e = \tan^{-1} (A_{31} / A_{21}), \quad (4.6)$$

$$\phi_j = \tan^{-1} (A_{32} / A_{22}), \quad (4.7)$$

$$\text{and} \quad \phi = \phi_e - \phi_j. \quad (4.8)$$

The resistivity (ohm-meters), an intrinsic electrical property of the material, must be calculated by multiplying the resistance by a scaling factor to account for the

measurement geometry. In the case of a cylindrical conductor, the resistivity (ρ) is calculated by:

$$\rho = R (A/L), \quad (4.9)$$

where A is the cross-sectional area and L is the length of the cylinder. The Hilbert transform (Kramers-Kronig relations) calculations are described in the appendix of Olhoeft (1985). The total harmonic distortion (THD) is the root-mean-square difference between the deconvolved harmonic content of the current and voltage (Olhoeft, 1979a). Deconvolving the input and output result in a THD value that is independent of equipment effects (such as harmonics introduced by the amplifier).

The processing steps used are outlined in Figure 4.3. The data in the column studies are truncated at 50 Hz in the program *nocr_nm.c* for the calculations and display. At frequencies at 50 Hz and below the acquisition program simultaneously records all sixteen channels. However, at 100 Hz and above only one current and one potential channel are recorded at a time and the program used channel zero as the current channel for all potential channels. This means the high frequency data is only valid for the first column where channel zero was the current channel. The output from this program is resistivity, phase, Hilbert distortion, total harmonic distortion, spontaneous polarization, and current density. The program *cr_ave*.c* uses the resulting data files to compute the averaged data spectra and standard deviation.

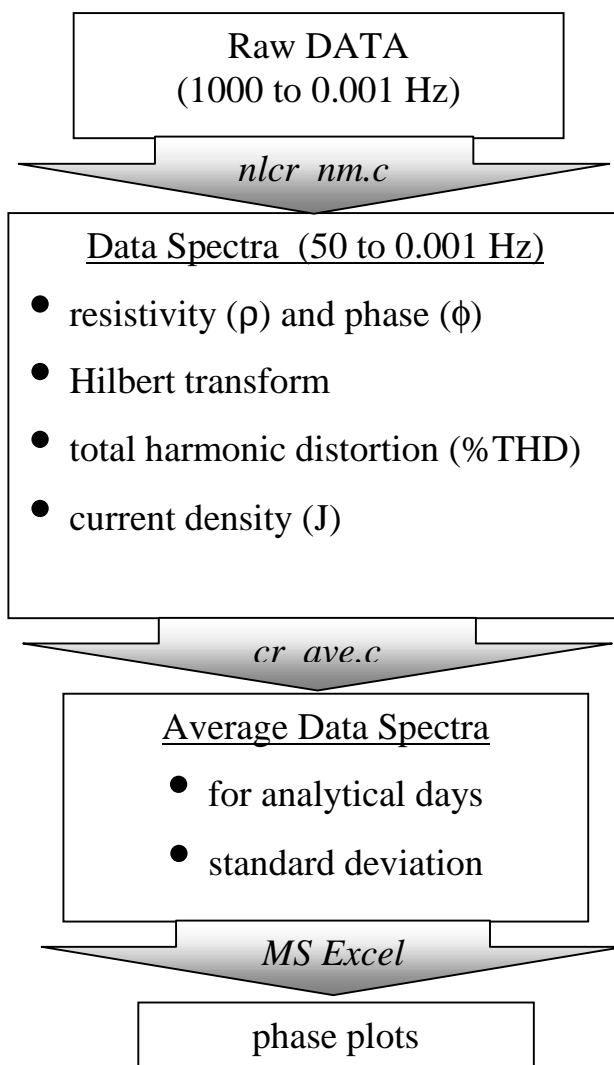


Figure 4.3. Flow diagram of the data processing steps for the column studies.

4.2.4 Advantages / Disadvantages

The advantages of this complex resistivity system are that measurements are in the frequency domain, a wide frequency range can be used, a sinusoidal waveform is input, 16 channels can be simultaneously measured, and the full waveform for both the input and output are saved. The measurements are extremely accurate and continuous data acquisition is possible.

The disadvantages are that the system is fairly bulky, a complete measurement cycle takes 35 minutes, and the resulting data files are 1.2 MB. The equipment remained in one location for the entire experiment, so portability was not an issue. The time for each measurement was not important because continuous data acquisition eliminated the need for a person to monitor each measurement and the time for noticeable chemistry changes is on the day to week scale. The size of the data files was the major disadvantage because of the immense amount of data generated over 100 days (at 42 measurements/day). However, data storage is fairly inexpensive and well worth storing the full waveform data.

4.3 Column Set-up

The column set-up was designed to monitor the CR and chemistry for five samples is to distinguish between the CR response for slow (no bacteria) and fast (with bacteria) pyrite oxidation and be sure that temporal changes in the electrical measurements correspond to chemistry changes. The column experiment included five

columns and three different ores. In addition to the continuous complex resistivity measurements, weekly chemical analysis included the pH, Eh, and iron content of the solution sampled from the bottom of each column. These are the standard chemical analyses used by Newmont to assess the oxidation of ores in column experiments and were performed by Jack Tryon at the Newmont Technical Facility. Ore mineralogy was determined before the experiments using x-ray diffraction and x-ray fluorescence. Assays and ICP solution analysis were also performed before and after. A sieve analysis after removal of the ores determined the particle sizes in each column.

4.3.1 Ore Types Examined

There were two siliceous sulfidic refractory (SSR) ores and one control composite with minimal pyrite, all from Carlin, Nevada. SSR is the designation given to the higher grade ore (0.144 oz/ton) and P5SSR (standing for pad 5 SSR) is the lower grade ore (0.022 oz/ton). The SSR ores were examined with and without bacteria so that the response of bacteria-assisted pyrite oxidation could be distinguished from un-assisted pyrite oxidation. The NAL composite was chosen as a low-pyrite (< 1%) oxide control to verify that the complex resistivity measurements do not have the same features as the sulfidic gold ores. This control was measured with tap water. Each ore had a different mineralogical composition (see Tables 4.1 and 4.2) and particle size (see Table 4.3).

XRD	High-grade SSR ore	Low-Grade P5SSR ore	Control NAL composite
quartz	62	80	74
illite	20	8	11
kaolin	6	4	5
apatite	1	0	0
barite	4	1	1
alunite	2	0	4
pyrite	3	4	1
rutile	0	0	1
iron oxides	1	0	3

Table 4.1. X-ray diffraction (XRD) of the 3 ore types prior to oxidation expressed in weight percent (Brierley, 1999b).

XRF	High-grade SSR ore	Low-Grade P5SSR ore	Control NAL composite
silica	68.17	79.14	72.52
alumina	9.55	6.37	8.51
iron	2.28	1.85	2.40
magnesium oxide	0.43	0.49	0.83
calcium oxide	0.57	0.62	2.48
sodium oxide	0.12	0.01	0.12
potassium oxide	1.71	0.97	1.43
titanium oxide	0.49	0.39	0.53
phosphate	0.22	0.14	0.12
sulfur	1.98	1.35	0.35
manganese oxide	0.02	0.01	0.06
barium	2.17	0.76	0.33
copper	0.01	0.00	0.01
lead	0.02	0.00	0.00
zinc	0.08	0.02	0.02
arsenic	0.13	0.18	0.13

Table 4.2. X-ray fluorescence (XRF) of the 3 ore types prior to oxidation expressed in weight percent (Brierley, 1999b).

Column	3/4 to 1/2 in.	1/2 to 1/4 in.	1/4 in. to 48m	48m to 100m	<100m
High-Grade	32.7	22.4	30.7	3.8	10.4
Low-Grade	0.0	10.8	70.1	4.0	15.2
Control	0.0	13.1	71.7	5.0	10.2
Low-Grade/ no bacteria	0.0	10.1	70.1	3.6	16.1
High-Grade/ no bacteria	29.7	26.0	30.8	3.9	9.6

Table 4.3. Sieve analysis for the 5 columns, performed after oxidation and removal of ore from columns (Brierley, 1999b). The numbers are percentages by weight; designation *in.* stands for inches and *m* stands for mesh size (refer to Table 4.4 for column specification).

4.3.2 Electrode material

The low pH, high iron content, and bacteria activity create a highly corrosive environment. An appropriate corrosion resistant metal is necessary to minimize effects of potential electrode corrosion on the CR measurements. Platinum mesh is used in the laboratory, but the expense is not justifiable on larger scales. Several less expensive metals were tested in the laboratory by placing them in contact with biooxidation solution and sulfidic ore for 10 days. CR measurements were also made to determine repeatability of measurements and correlation with platinum electrodes. The results from these measurements are shown in Section 5.2.2. The only satisfactory metal was MP35N, an alloy with 35% nickel, 35% cobalt, 20% chromium, and 10% molybdenum.

MP35N is used in the medical and dental industries because it does not react with biological cells. It has also been used by the petroleum industry for logging cable in high

temperature and sulfur environments. Electrodes for the columns are 1/4 inch diameter rod cut to protrude from the column by 1/2 to 1 inch on one end for connecting wires.

4.3.3 Column Specifications

The column experiments were conducted at the Newmont Technical Facility in Englewood, CO. An outline of the procedures is in Figure 4.4. Figure 4.5 shows a picture of the rack with columns and equipment during operation of the experiments. Five columns were used to allow for simultaneous testing of each sample. The columns are 8 inch diameter polystyrene clear plastic with plastic connectors in the bottom to connect hoses. Quarter inch holes were drilled horizontally through the columns, 4 inches apart starting 4 inches from the bottom (see Figure 4.6). MP35N electrodes were placed in these holes with 1/2 to 1 inch excess on one side to attach wires, for a total of eight electrodes per column. The holes were sealed with silicone aqua-sealing compound to prevent leaks around the electrodes.

A container at the base of each column held approximately 5 liters of solution. The solution percolating through the column drained into this container and was then recirculated through the column. A pump on the rack above the column brought solution from the container to a perforated plastic bucket (functioning as a solution distributor) in the top of the column. The solution dripped through the holes in the bucket and percolated down through the ore. An aquarium pump forced air through a tube on the outside of the column to one of the holes at the base to circulate air, increasing the

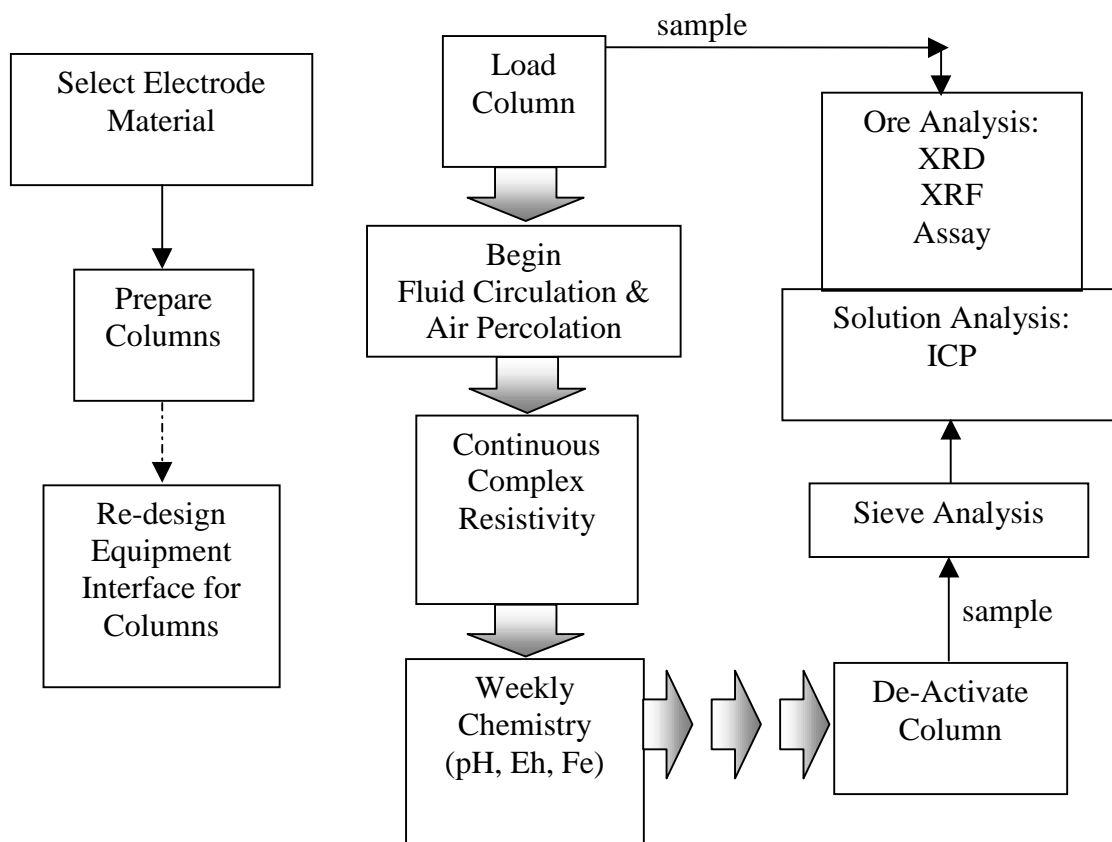


Figure 4.4. A flow diagram of the experiment design, set-up, and measurement process.



Figure 4.5. The set-up of columns and CR equipment at Newmont in Englewood, CO. This picture shows the test of all channels across decade resistor boxes, one for the potential channels and one for the current-sensing resistor.

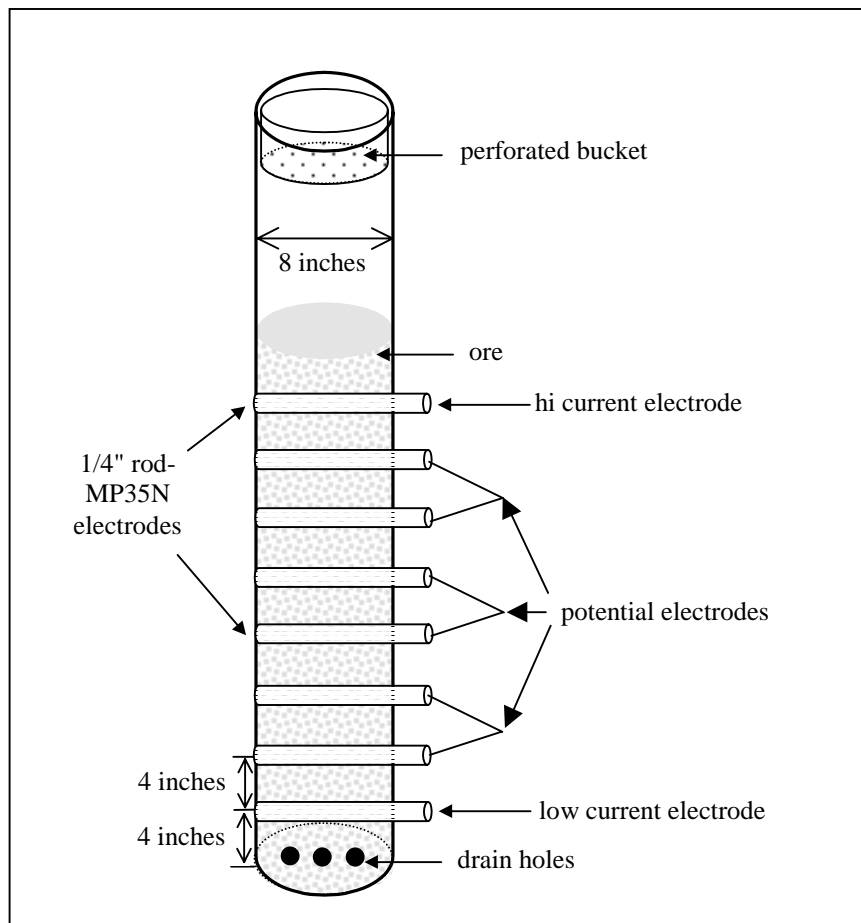


Figure 4.6. Specifications for the columns (not to scale).

availability of oxygen and carbon dioxide to bacteria while clearing pathways for solution percolation. The drip and air percolation rates were the same for all columns. However, the column with the control ore had difficulties with the tubes plugging and at one point the solution was pooling on the top of the ore, probably due to higher amount of fine particles.

A summary of the channels in the 16-channel CR system used for each electrode pair is in Table 4.4. Column 1 contained the high-grade siliceous sulfidic refractory ore (SSR) with biooxidation solution. Column 2 contained the low-grade siliceous sulfidic refractory ore (P5SSR) with biooxidation solution. Column 3 contained the control ore with tap water. Column 4 contained the low-grade ore with low pH water and a bacteria

Column Number	Current Channel	Potential Channels	Grade	Bacteria	Acid	Operational Days
1	0	1,2,3	high	yes	yes	140
2	4	5,6	low	yes	yes	133
3	7	8,9	control	no	no	127
4	10	11,12	low	no	yes	127
5	13	14,15	high	no	yes	127

Table 4.4. Specifications for each column.

inhibitor (sodium lauryl sulfate). Column 5 contained the high-grade ore with low pH water and a bacteria inhibitor. The low pH water was a mixture of sulfuric acid and tap water.

Each column had 8 electrodes, four inches apart. The current was applied to the top and bottom electrodes, 28 inches apart, and the potential voltage was measured across a pair of adjacent electrodes (4 inches apart). Column 1 had 3 potential electrode pairs; the second and third electrodes from the top, the fourth and fifth electrodes, and the sixth and seventh electrodes. Columns 2 through 5 had 2 potential electrode pairs; the third and fourth electrodes from the top, and the fifth and sixth electrodes, with the second and seventh electrodes unused.

4.3.4 Chemistry Analysis

Chemical analysis was performed on a weekly basis for all five columns to track the rate of oxidation. The solution for analysis was collected from the base of the columns to ensure the sample was indicative of processes occurring in the column and not in the holding container. The pH and Eh were measured using a meter and the total iron was titrated with ceric sulfate/phenanthroline, according to standardized procedures normally used by Newmont (Kothoff and Belcher, 1957). These data are in Appendix A. A complete solution ICP (inductively coupled plasma) solution analysis was performed at the beginning and end of the experiment. These data are shown in Section 5.2.1.

4.4 Problems Encountered

The purpose of this section is to outline the possible errors in the data due to problems with the columns and the equipment. There were initial problems with the equipment that were fixed before the 2nd-5th columns were activated. Column 1 was set-up first to test the complex resistivity equipment. The data for the first 40 days of column 1 are not usable due to problems with the equipment. The equipment set-up, as described in Section 4.1, was not in use until part way into the experiment because the front end had to be re-designed to accommodate continual data collection. Intermittent pre-amplifier boxes were removed and an isolation amplifier box was replaced with a straight connection from the electrodes to the sample and hold boards. Also, a board had to be wired to send current to all five columns in parallel. Since the chemical analysis showed that biooxidation was occurring and had not yet reached a critical point, this column was not re- started.

Column 3, which contained the control ore, had problems with the circulation of fluid due to plugging of the hoses and a malfunctioning pump. At one point solution had pooled on the surface of the ore as shown in Figure 4.7.

Four of the sixteen channels in the complex resistivity system had problems due to a bad cable, two broken connectors, and a bad solder joint in the box that replaced the isolation amplifier box. These problems were identified late in the experiment when the electronic circuit shown in Figure 4.8 was measured. In order to accurately test the linearity, phase, and frequency dependence of the system, a circuit that exhibits phase and



Figure 4.7. Pooling of approximately 1/3 inch of water on the top of the ore in Column 3 near the end of the experiment.

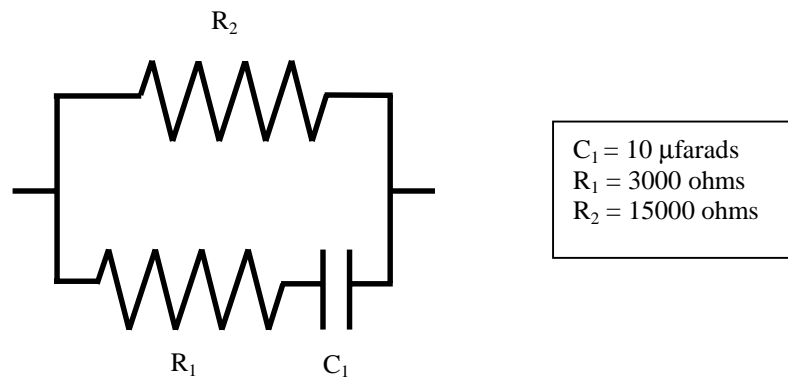


Figure 4.8. The electronic circuit (R-RC) used to test the accuracy of the amplitude and phase of each channel.

frequency dependence is necessary. If the measurement of a linear circuit shows nonlinearity, it is likely due to equipment contributions. The bad channels in the box were fixed and the system was re-measured across the same circuit, this time yielding good results. Figure 4.9 shows the phase before the repairs to the system. Figure 4.10 shows the phase after the channels were repaired. These measurements of an R-RC circuit have proven very useful in identifying problems with the equipment. The electrodes in columns 4 and 5 were not initially sealed with silicone and they began to leak. The electrodes were cleaned and silicone was applied to stop the leaking. Data were continuously collected for a total of 42 measurements on most days except for several disruptions to system tests and installation of an additional hard-drive.

4.5 Description of Typical Data Plots

The results from calculations described in Section 4.2.3 are displayed in a hpgl (Hewlett Packard Graphics Language) plot file. These plot files were produced using a protected mode C extended graphics library (Olhoeft, 1993) and are described in this section. All of the data sets from one day were averaged together to produce time-averaged data plots. The days chosen correspond to when chemical analyses were performed.

Figure 4.11 is a plot of the average of the CR measurements on 3/1/99 for channels 1, 2, and 3. The averaged data filenames used to produce the plot are listed to

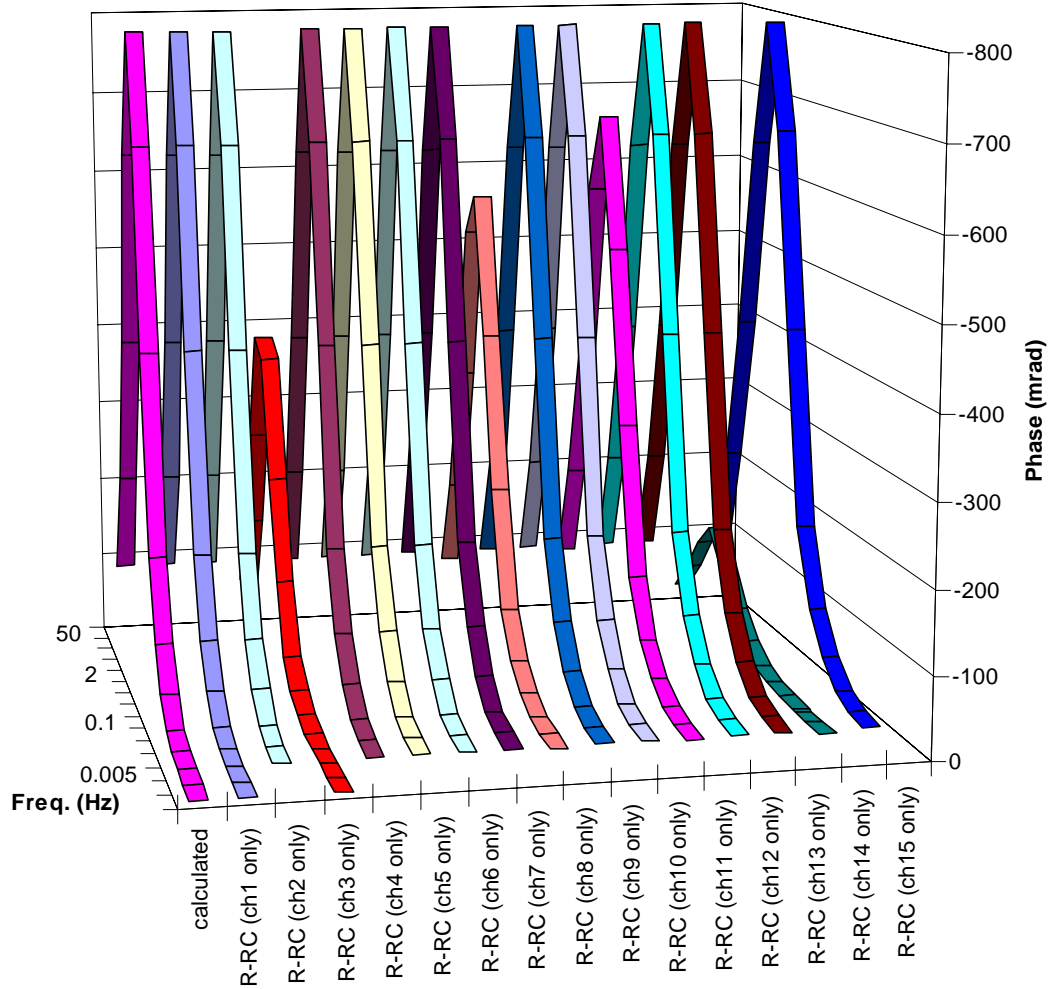


Figure 4.9. The phase of channels 1-15 for the R-RC circuit in Figure 4.7 before repairs of the system. Note that channels 3, 8, 11, and 14 have low phase peaks.

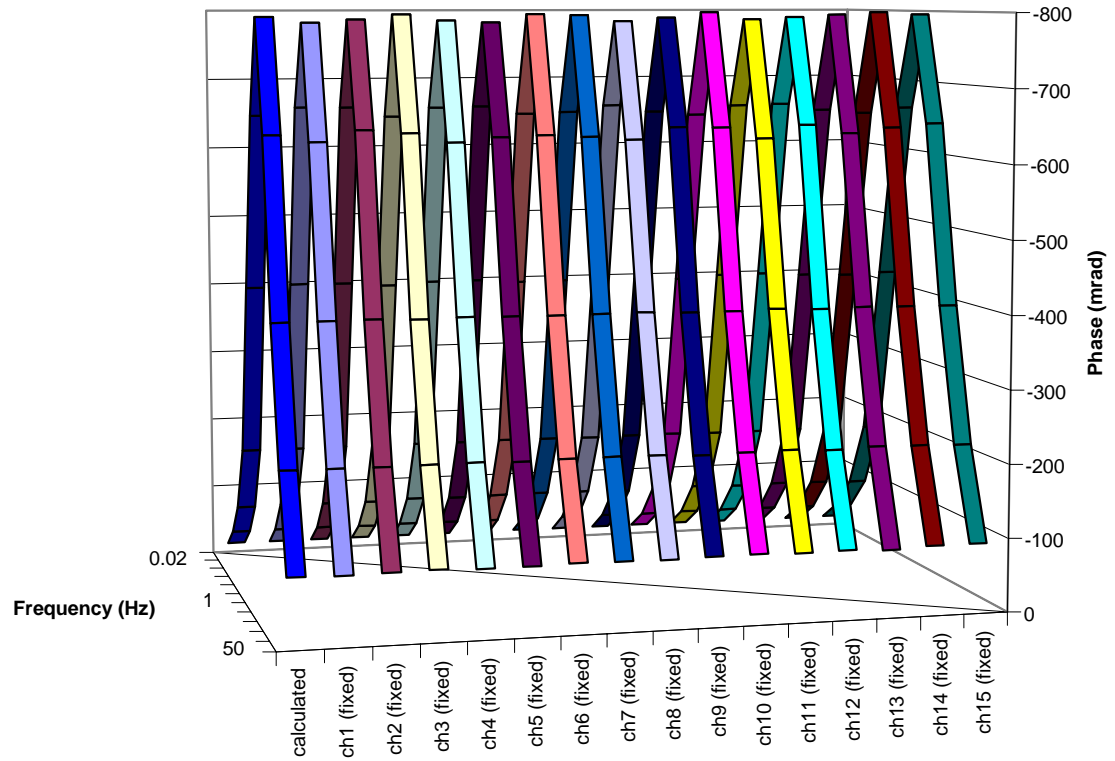


Figure 4.10. The phase of channels 1-15 for the R-RC circuit in Figure 4.7 after repairs to the system. Note that all the channels now match the calculated values (far left).

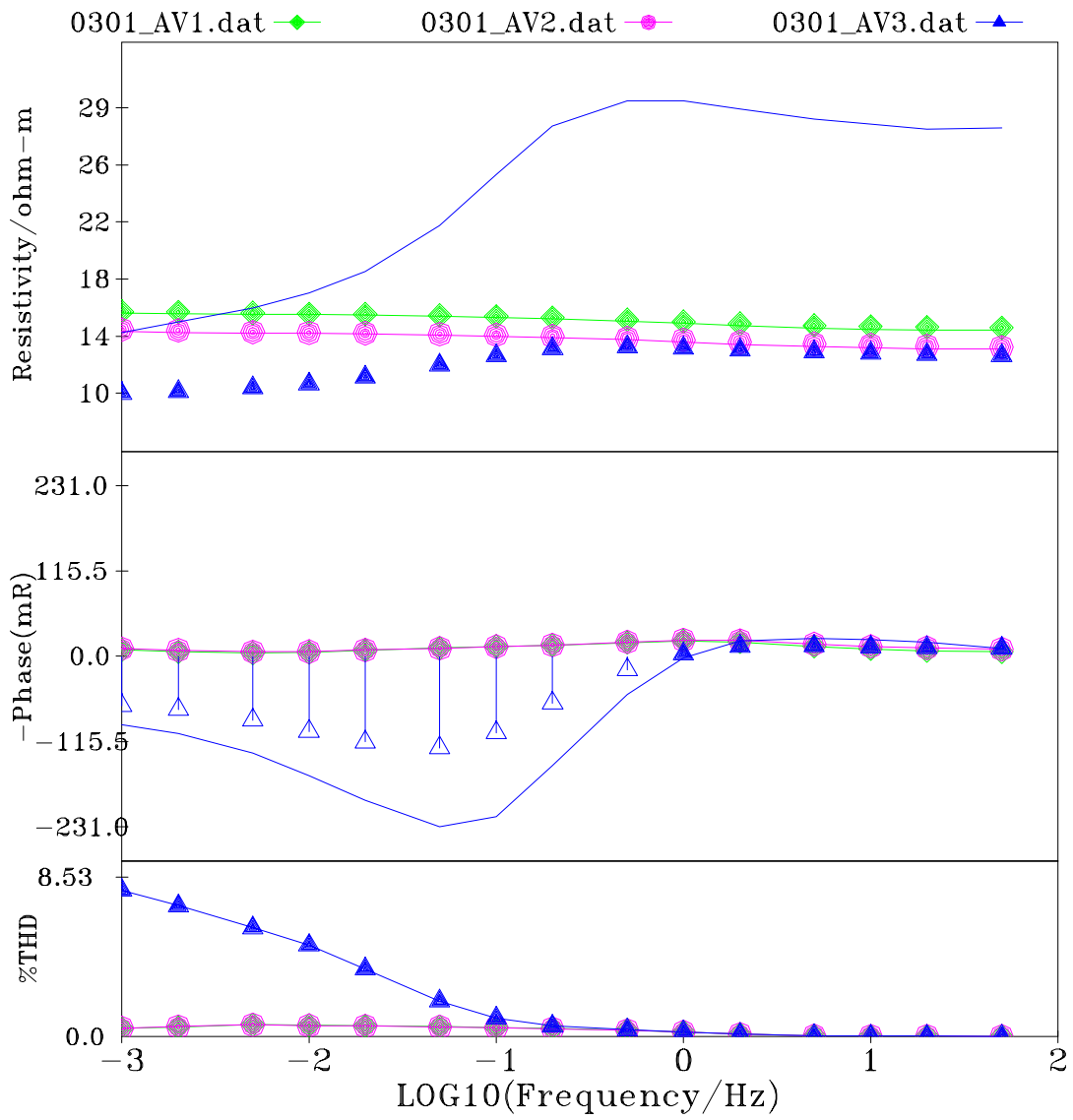


Figure 4.11 Typical data plot; the average of data from 3/1/99 for channels 1, 2, and 3.

the left of each plotting symbol across the top of the plot. These filenames contain the month and day of the measurements and the channel number. For example, 0301_av2.dat is the filename of the data from 3/1/99 for channel 2. The plot is broken into three sections; the top, middle, and bottom.

The top shows the resistivity data for all three channels, the middle shows the phase data, and the bottom displays the total harmonic distortion data. The horizontal scale on the bottom of the plot is log frequency, which is from -3 to 2 (0.001 to 50 Hz) in the column studies and from -3 to 6 (0.001 to 100,000 Hz) in the laboratory studies. The data in the column studies were collected from 0.001 to 1000 Hz, yet are truncated to 50 Hz as described in 4.2.3. The solid lines through the resistivity and phase data points are the calculated Hilbert values. The close fit for channels one and two indicates a low amount of Hilbert distortion, or nonlinearity. The vertical bars through the symbols are the measurement errors from the variance and covariance calculated from the measured waveforms using linear regression analysis as described by Jones (1997) and Olhoeft (1986).

Figure 4.12 is a plot of the standard deviations of the averaged resistivity and phase as well as the current density for the time-averaged data. The filenames are again along the top of the plot with the plotting symbols. The top section contains the standard deviation of the measurement spectra used to compute the averaged resistivity, expressed as a percent of deviation. The middle section contains the standard deviation of the

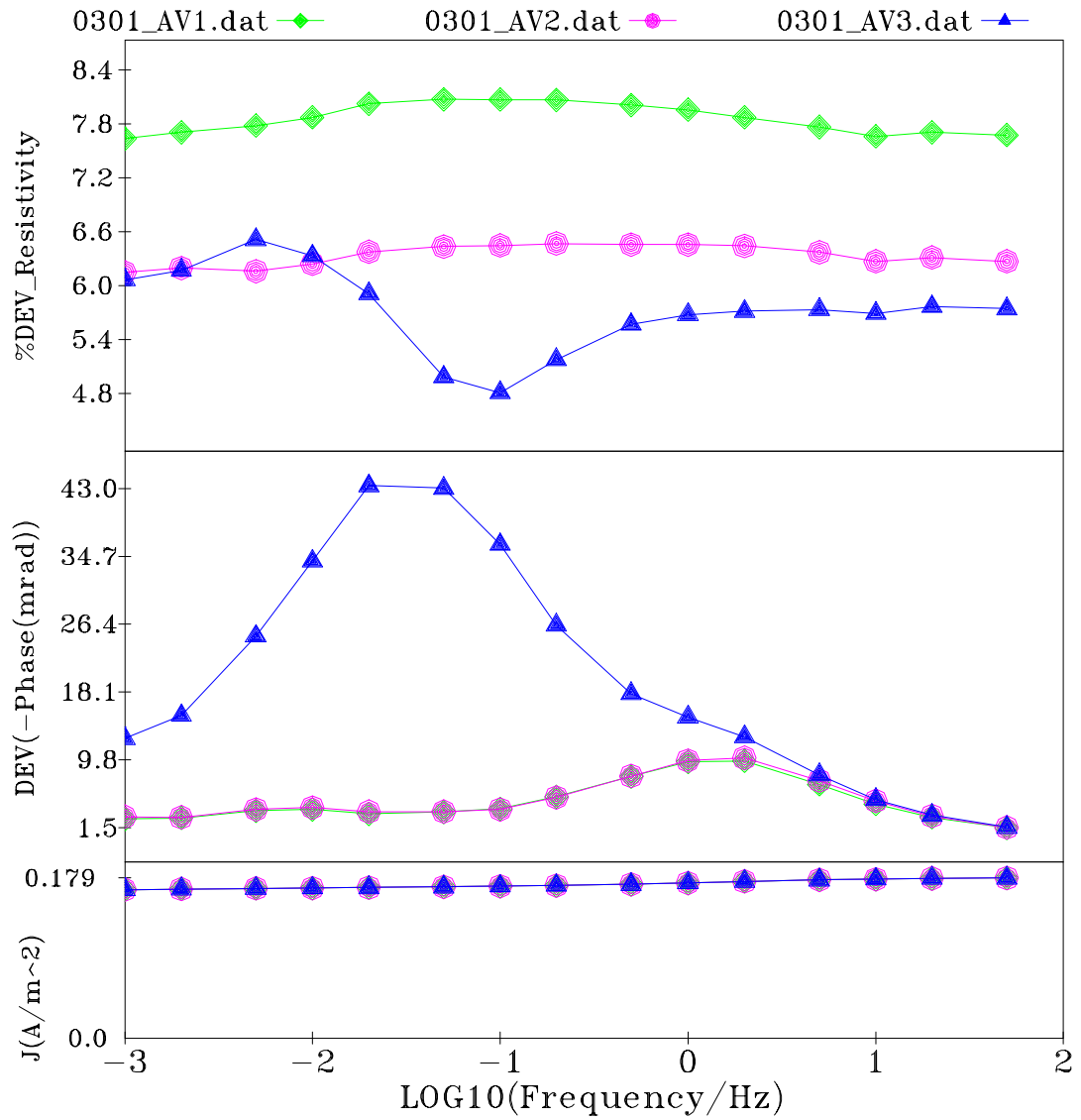


Figure 4.12. Typical standard deviation and current density data plot; the average of data from 3/1/99 for channels 1, 2, and 3.

phases, expressed in milliradians. The bottom section displays the current density in A/m². The standard deviation (s) was calculated according to:

$$s = \sqrt{\frac{\sum_{n=1}^N (X_n - X_a)^2}{N}} \quad (4.10)$$

where X_n is either the resistivity or phase data value, X_a is the average value, and N is the total number of averaged files.

Chapter 5

MEASUREMENT DATA

5.1 Overview

The purpose of this chapter is to present the complex resistivity and chemistry measurement data for the tests of electrode materials and the column experiments. Prior to beginning column studies, it was necessary to choose an economic electrode material that gave repeatable CR results and was resistant to the highly corrosive biooxidation environment. The column biooxidation experiments were then performed according to standard procedures used by Newmont Metallurgical Services to test biooxidation and were analyzed with continuous CR measurements to determine any correlation with chemical changes over time. The CR measurements are presented along with the chemical and mineralogical data.

5.2. Tests of Electrode Material

Platinum is the electrode material used in the laboratory because it is non-polarizable and non-reactive in nature, and gives repeatable measurements. The use of platinum is not economical on a larger scale. In normal field CR measurements where the contact media is unsaturated ground, lead electrodes are adequate as potential electrodes and any metal can be used as current electrodes. This project requires

electrodes that are stable to low pH values (less than 2.0), will not be oxidized by iron, sulfides, sulfuric acid, or bacteria, and show little to no frequency dependence.

Laboratory tests of lead, stainless steel #304, titanium, a titanium-niobium alloy, Ultimet, and MP35N led to the selection of MP35N as the electrode material for column studies.

With the exception of lead, which was chosen for its low cost, all materials were chosen due to their corrosion resistance. The electrode material MP35N is a corrosion resistant metal used in the medical and dental industries and by the petroleum industry for logging cable in highly corrosive environments. Data to test electrodes were measured in the petrophysics laboratory at the Colorado School of Mines, using the equipment shown in Figure 4.2, for a frequency range of 10^{-3} to 10^6 . The samples were measured with teflon sample holders, as shown in Figure 5.1.

The tests showed that lead was easily corroded and extremely time-variant, therefore inappropriate as electrode material in this environment. Of the remaining materials, only MP35N gave results that were comparable with platinum. A sample of low-grade ore with biooxidant was split into two samples: one with MP35N electrodes and one with platinum mesh electrodes. The MP35N electrodes were 1/4" rods, cut into 7/8 inch lengths with stainless steel wire as electrode leads in 1/8" holes drilled in the top of the rods. The samples were measured for ten days and were retained in sealed jars between measurements. The test data for all electrodes are on the accompanying CD-ROM in the *lab_data* directory.

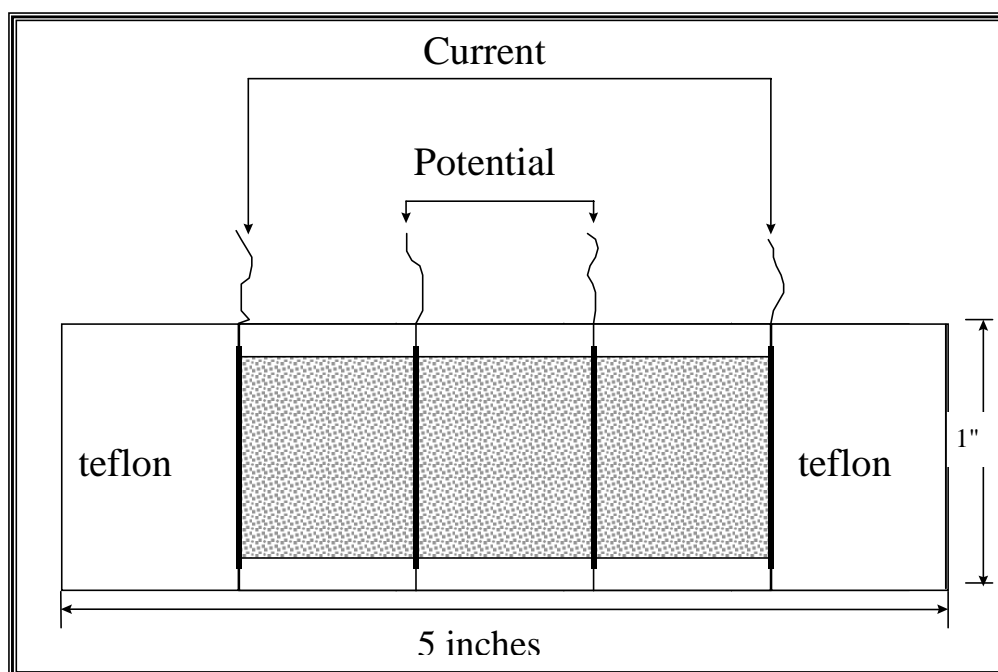


Figure 5.1. Teflon sample holder with platinum electrodes. The length of the holder is five inches and the width is one inch. The current is applied through the outer electrodes and the resulting potential is measured across the center electrodes.

Plots comparing MP35N and platinum are in Figure 5.2 for day 2 and Figure 5.3 for day 10. The discrepancy between resistivity values for MP35N and platinum is due to the rod-shaped electrodes, which do not establish as uniform a current pattern through the sample as the platinum mesh electrodes. On day 2 the %THD was much higher for the MP35N electrodes and may be related to electrode stabilization because it was greatly reduced by day 10. The vertical error bars on the day 10 phase measurement are greater in the MP35N sample and are most likely due to corrosion of the stainless steel wire leads. Despite these discrepancies, MP35N was chosen as the electrode material for the column studies because of its corrosion resistance, similarity to platinum measurements, and availability in relatively inexpensive 1/4" rods.

5.3 Column Data

This section will present the chemistry, mineralogy, and complex resistivity data for the column studies at Newmont Metallurgical Services. First the chemistry and mineralogy data are presented for the solution and ore in each column. Then the CR data for each column is shown. Correlations between the different columns or types of data are presented in Chapter 6.

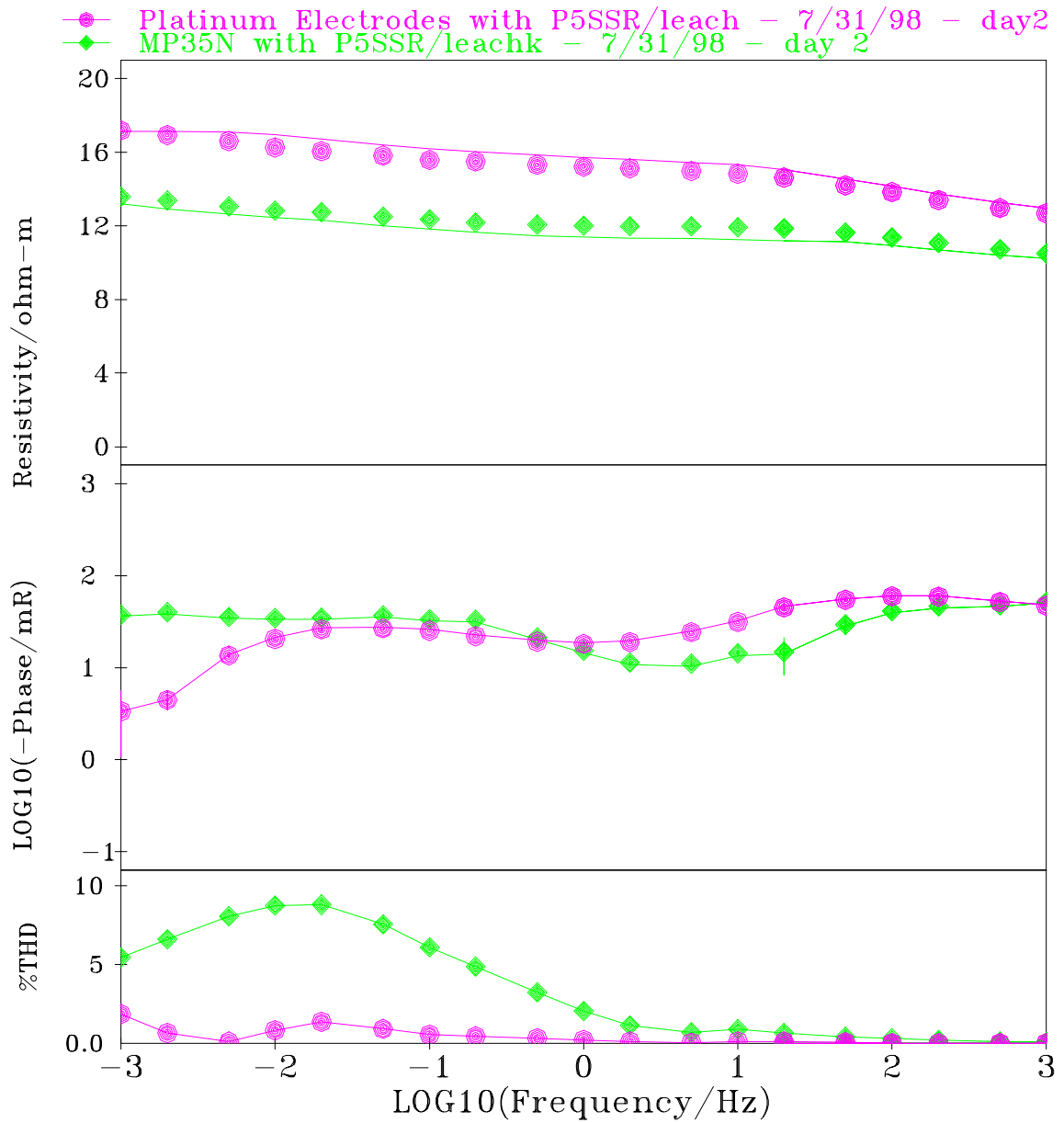


Figure 5.2. Comparison of the resistivity (top), phase (middle), and %THD (bottom) for MP35N (diamonds) and platinum (circles) for two splits of low-grade ore with biooxidant solution: Day 2.

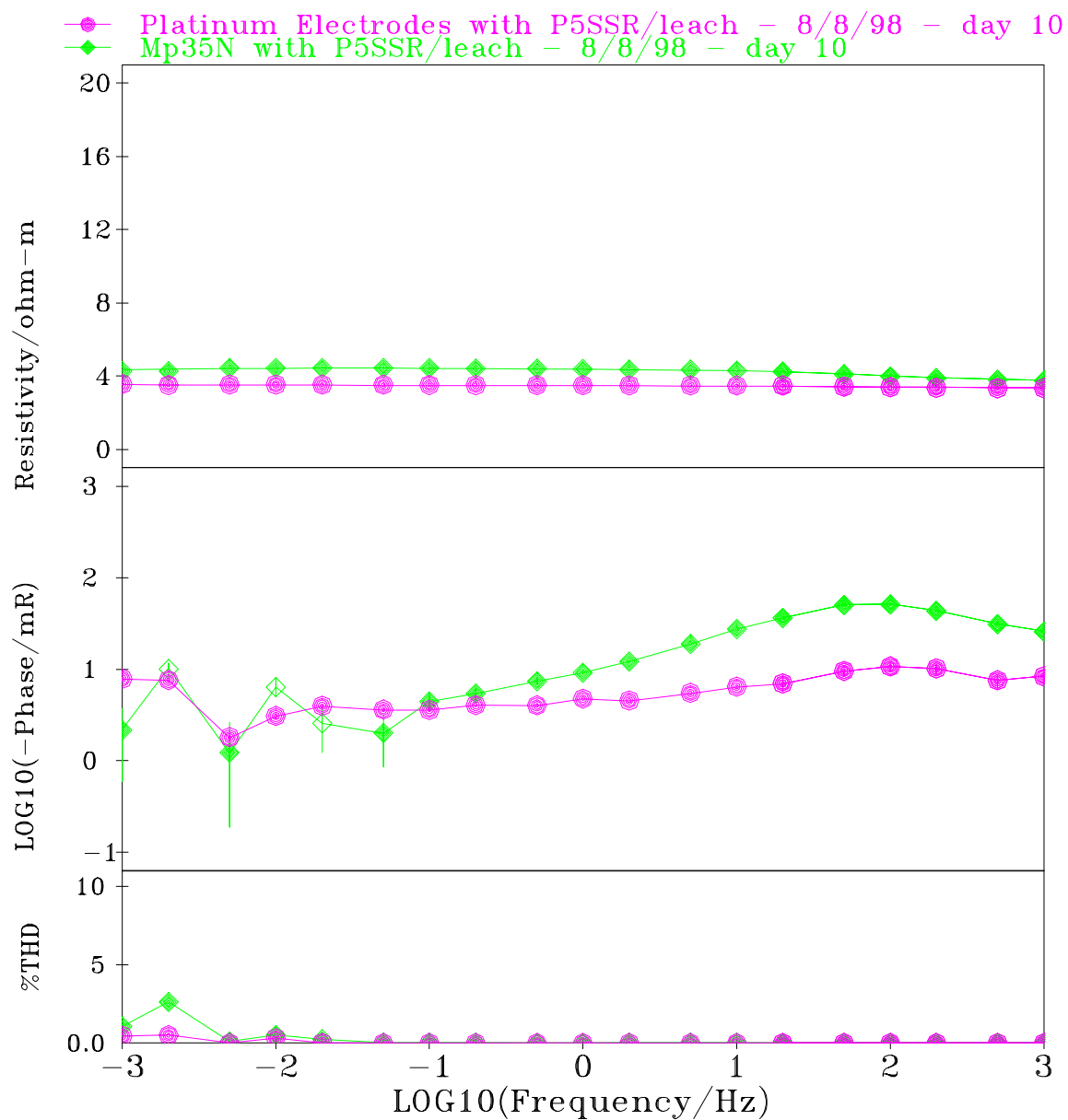


Figure 5.3. Comparison of the resistivity (top), phase (middle) and %THD (bottom) for MP35N (triangles) and platinum (circles) for two splits of low-grade ore with biooxidant solution: Day 10.

5.3.1 Chemical Analysis

The chemical data were measured by personnel at the Newmont Technical Facility, Englewood, CO. The original data sheets for all chemical analysis are in Appendix A. This includes the X-Ray Diffraction (XRD) and X-Ray Fluorescence (XRF), Inductively Coupled Plasma (ICP) solution analysis, fire and cyanide gold assays (AUFA & AUCN), iron content by atomic absorption (AA), sulfur by the Leco Carbon-Sulfur Analyzer, sieve analysis, and weekly pH, Eh, and iron solution content data for each column. The data are summarized in this section in tabular and/or graphical format.

Prior to beginning the column studies, the mineralogy of each ore was determined using XRD and XRF. These results are shown in Tables 4.1 and 4.2, respectively. The gold content was determined using fire assay (which determines total gold) and cyanide assay (which determines the amount of gold recoverable with cyanide). An ICP solution analysis was performed on the solution at initial activation for each column to determine the concentration of elements in parts per million (ppm). Initial activation refers to the time when a column was loaded with ore and electrodes, and the pumps turned on to circulate solution and air. At this time, a weekly analysis of the solution chemistry was begun. This analysis included the pH, Eh (with a silver calomel electrode), and iron ion content in the solution draining from the base of the columns. The pH plots are in Figure 5.4 and plots of the total iron in solution are in Figure 5.5. After each column was shut down, a sieve analysis was performed for each column and post ICP solution analysis, gold assay, and iron and sulfide contents measured.

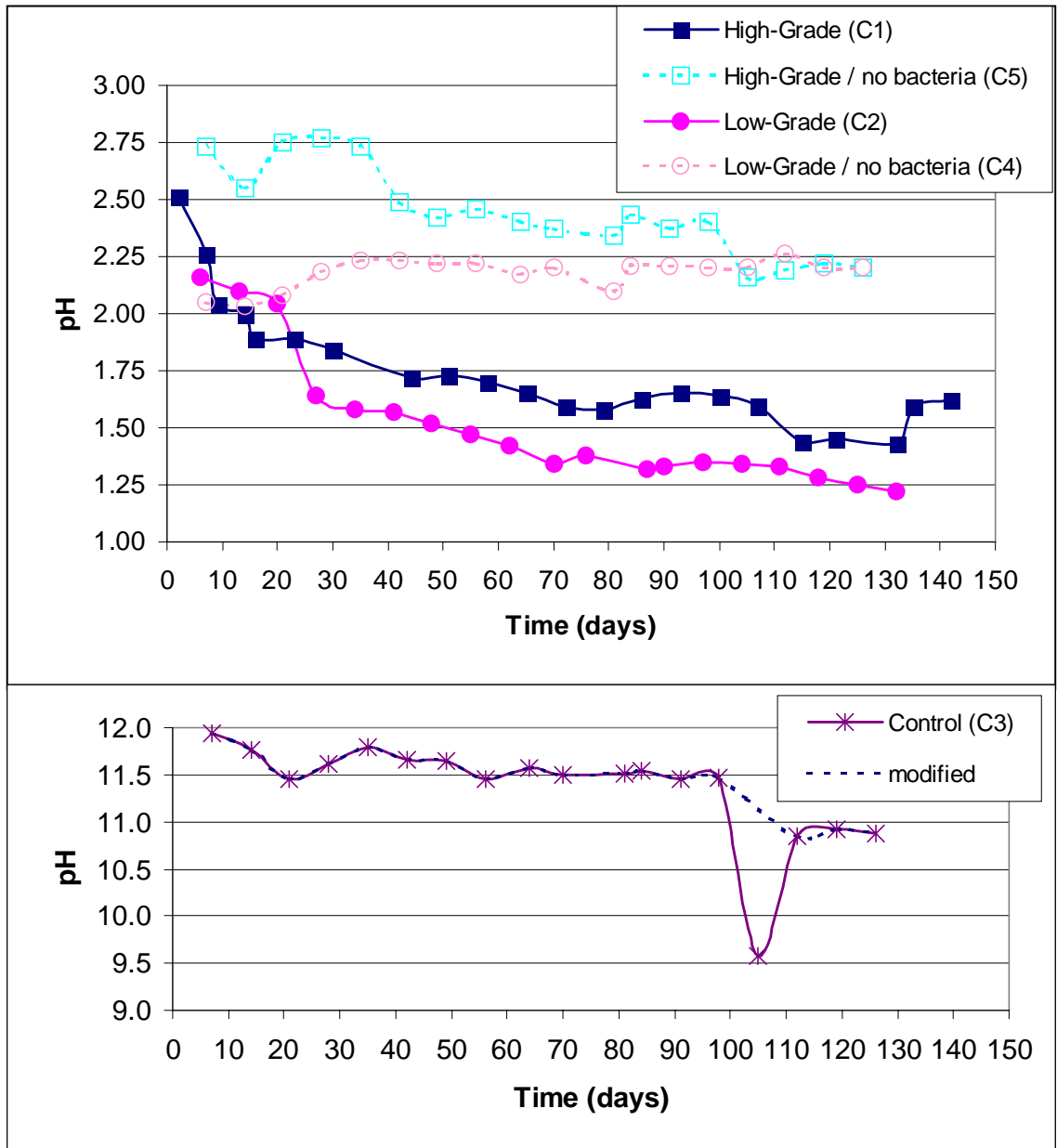


Figure 5.4. Plots of the pH vs. time (days) for high-grade ore vs. low-grade ore (top) and control ore (bottom).

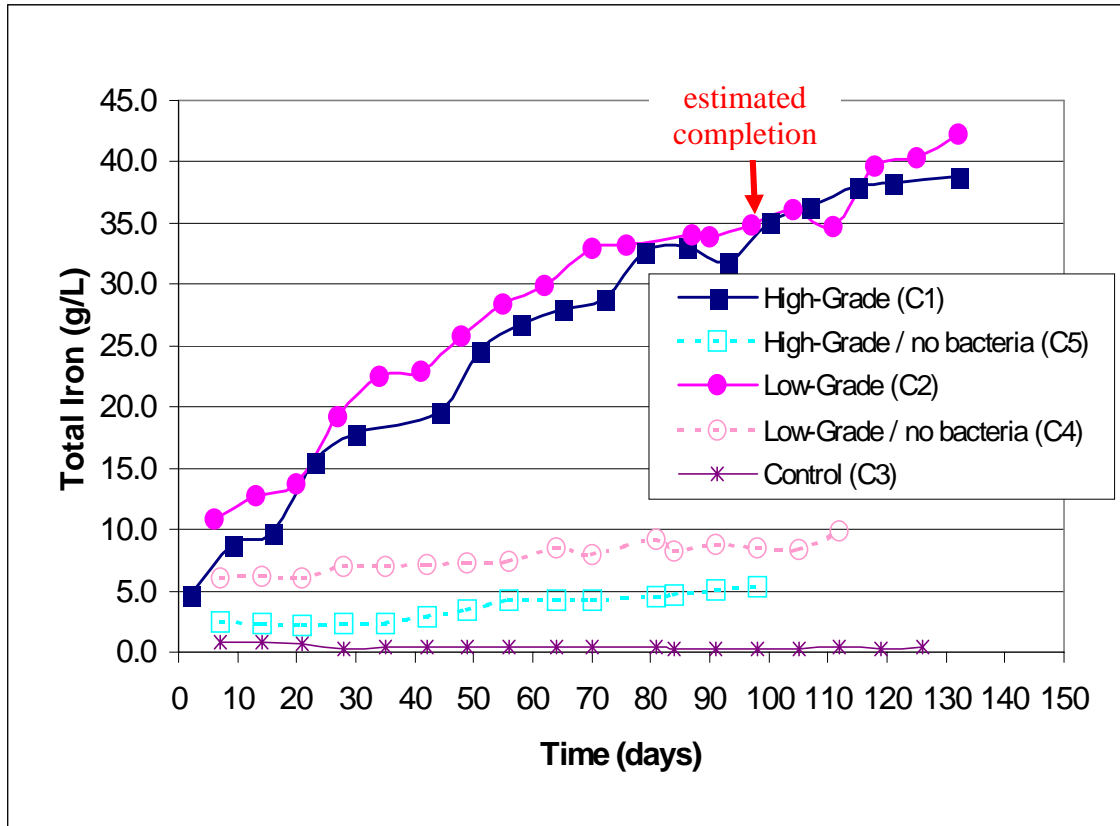


Figure 5.5. Total iron (g/L) for high-grade ore vs. low-grade ore and control ore.

The oxidation of sulfide minerals decreases the pH of solution, due to the release of hydrogen ions, and keeps the solution in an optimal pH range (< 2.5) for the bacteria to flourish. Biooxidation is generally highest below a pH of 2.0 and jarosite ($\text{KFe}_3(\text{SO}_4)_2(\text{OH})_6$) begins to precipitate between a pH of 2.0 and 3.0, depending on the temperature and Eh (Dutrizac, 1983). The high-grade and low-grade ores under active biooxidation have similar trends in the pH. An initial pH of about 2.5 quickly decreased to below 2.0 and remained low. The high-grade and low-grade ores with a bacteria inhibitor (sodium lauryl sulfate) have pH's above 2.0. Each ore had the inhibitor added three times to keep the bacteria inactive and prevent the pH from lowering. The pH was significantly higher in the control ore due to the lack of sulfide minerals and the use of tap water, instead of a low pH solution.

As sulfide minerals oxidize, iron is released into solution. When the rate of oxidation of sulfides is fast, there is a rapid increase in the total iron in solution. The rate of increase in the total iron in solution reaches a plateau when oxidation slows and can be used to determine when an ore has been sufficiently oxidized in the biooxidation process. Figure 5.5 shows that the high-grade and low-grade ores have a similar increase in the total iron in solution over time, with an estimated completion time for biooxidation marked. This indicates that sulfides were oxidizing, releasing a similar amount of iron into solution for the two ores. In the same ores with a bacteria inhibitor, the total iron content did not exceed 10 g/L, indicating that minimal sulfide oxidation occurred. The

control ore remained below 1 g/L due to fewer sulfide minerals and the high pH, which would encourage the precipitation of iron in the form of iron hydroxides, such as jarosite.

The difference between the pre and post ICP solution analysis are shown in Table 5.1 for the significant elements for all five samples. A zero value indicates that there was no change, or that it was below the sensitivity of the analysis. The increase in arsenic (As) is due to the oxidation of arsenopyrite (FeAsS). The increases in iron (Fe) and sulfur (S) are due to the oxidation of pyrite (FeS_2) and/or arsenopyrite. The values for iron do not correspond to the more accurate weekly titration results and are most likely invalid. Therefore, the ICP iron data will be ignored and the titration results used as an indicator of the total iron content in solution. The high-grade sample under active biooxidation had the highest increases in As, Fe, and S, indicating that more sulfides oxidized in column one than any other column. The high-grade sample with a bacteria inhibitor increased an order of magnitude less for arsenic and sulfur, indicating that much

ELEMENT	HIGH-GRADE	HIGH-GRADE, NO BACTERIA	LOW-GRADE	LOW-GRADE, NO BACTERIA	CONTROL
As	4.7	0.5	1.9	0.7	0
Fe*	7.0*	4.1*	1.2*	3.6*	0
S	27.9	7.8	23.0	7.3	0
Ni	0.3	0.3	0.3	0.4	0
Co	0.5	0.2	0.2	0.3	0

Table 5.1. The increase in electrolyte elements in g/L from ICP solution analysis (post - pre). The iron (Fe*) does not correlate with the weekly titration analysis in Figure 5.5 (Brierley, 1999b).

less sulfide oxidation occurred. The low-grade sample under active biooxidation increased less in key elements than the high-grade sample, yet increased about 3 times more than the low-grade sample with a bacteria inhibitor. This indicates that the low-grade sample oxidized fewer sulfides than the high-grade sample. The minimal changes in the control sample are due to the lack of sulfide minerals to be oxidized.

The elements nickel (Ni) and cobalt (Co) are the two primary constituents of the electrode material, MP35N. A large increase of these elements may be due to the corrosion of the current electrodes. The current electrode pairs oxidized in all five columns and are shown in a photograph in Figure 5.6. The control column electrodes (the middle pair) oxidized significantly less, which can explain why the ICP analysis did not show a significant increase in the primary electrode elements.

The gold content from assay analysis is important to determine whether or not a sample was effectively oxidized. Fire assay (FA) determines the total gold content in a sample. Cyanide assay (CN) determines the amount of gold that can be recovered with cyanide leaching, which is the primary method for gold recovery. For 100% recovery, the total gold content would equal the recoverable gold content. The reason an ore is targeted for biooxidation is because 60% or less CN recovery would result due to the presence of sulfide minerals around the gold. Biooxidation exposes more gold for the cyanide to react with and thereby increases recovery. Table 5.2 shows the percentage of recoverable gold (CN/FA), before and after oxidation, for all five columns. The high-grade ore with biooxidant had the largest increase in recoverable gold (24.5 to 61.3%).



Figure 5.6 Photographs of the current electrode pairs for all five columns. The electrodes are in order from column 1 (left) to column 5 (right).

Sample	Solution	PRE			POST		
		AUFA (opt)	AUCN (opt)	CN/FA (%)	AUFA (opt)	AUCN (opt)	CN/FA (%)
High-Grade (C1)	biooxidant	0.188	0.046	24.5	0.199	0.122	61.3
High-Grade (C5)	low pH water	0.188	0.046	24.5	0.192	0.100	52.1
Low-Grade (C2)	biooxidant	0.022	0.011	50.0	0.019	0.008	42.1
Low-Grade (C4)	low pH water	0.022	0.011	50.0	0.020	0.009	45.0
Control (C3)	tap water	0.028	0.020	71.4	0.024	0.021	87.5

Table 5.2. Assay data before and after the column experiments. The percent recoverable gold (CN/FA) is expressed as the ratio of gold recoverable by cyanide assay (AUCN) over fire assay (AUFA) (Brierley, 1999b).

The same ore with a low pH water solution (little to no bacteria) had an increase from 24.5 to 52.1%. The low-grade ore had much higher initial recovery (50%) and showed a decrease in recoverable gold. This is most likely due to the extremely low concentrations of gold and the detection limits for cyanide leaching. The control ore also had a very low gold concentration, yet had high initial recovery (71.4%) and showed a slight increase over time.

The weight percent of sulfide material, determined by the Leco Carbon-Sulfur Analyzer, is in Table 5.3 for the low-grade and high-grade ores. In the low-grade ore, only 27.5% sulfide oxidized in the active column and 5.6% in the control. The percent of sulfide oxidized in the high-grade ore is 42.4% sulfide in the active column and 18.1% in the control, indicating this ore was significantly more productive than the low-grade ore.

Sample	Column	Condition	Sulfide-S, %		S-Oxidation
			Head	Residue	%
Carlin low grade SSR	C2	Biooxidized	1.60	1.16	27.5
	C4	Control	1.60	1.51	5.6
Carlin high grade SSR	C1	Biooxidized	1.77	1.02	42.4
	C5	Control	1.77	1.45	18.1

Table 5.3. Percentage sulfide oxidized for the high and low-grade ores (Brierley, 1999b).

Some sulfide oxidation and improved gold extraction occurred in the high-grade ore control because the bactericide did not 100% control bacteria activity.

According to this chemistry data, the high-grade ore was oxidized most effectively and had the highest increase in recoverable gold. This is evidenced by the low pH, increase in solution iron, arsenic, and sulfur content over time, the 42.4% sulfide oxidation, and increased from 24.5% to 61.3% recoverable gold. Therefore, any correlation between the chemistry and complex resistivity data should be strongest in column 1, the high-grade ore with biooxidant, and second highest in column 2, the low-grade ore with biooxidant.

5.3.2 Complex Resistivity

An immense amount of data has resulted from the continuous CR data collection. The raw, digital data are on the CD-ROM accompanying this thesis. The purpose of this

section is to show the major changes in the CR data over time for analytical days. The analytical days are those corresponding to the weekly chemical analysis because this will be the basis for correlating the CR and chemistry in Chapter 6. The 42 raw data measurements for each analytical day were processed and the arithmetic average computed. The standard deviation of the time-averaged spectra were computed and are presented here for the resistivity and phase. These data plots (described in Section 4.5) are presented for one electrode pair in each column at the beginning, middle, and end of the study. 3D phase plots show the general trends of the phase on the analytical days for each column.

The resistivity, phase, and percent total harmonic distortion (%THD) for the low-grade ore (P5SSR) with biooxidant solution is plotted in Figure 5.7 for days 13, 62, and 118. This plot represents 105 days of the 132 days column number 2 was in operation. The resistivity decreased 50% between days 13 and 62, and remains fairly constant through day 118. This decrease may be due to a combination of increasing ionic strength of solution and wetting of the ore. Initially, there is a slight phase peak at 2 Hz, which decreased by day 62 and disappeared by the end of the experiment. The phase between 0.05 and 0.002 Hz increased slightly. This indicates that the processes causing the 2 Hz phase peak significantly diminished by day 118. The phase magnitudes flattened over time, which is apparent in the plot of phases for analytical days in Figure 5.8. The total harmonic distortion (% THD) at 0.001 Hz decreased by about 75% between day 13 and day 118. The %THD for analytical days in Figure 5.9 shows the decreasing trend.

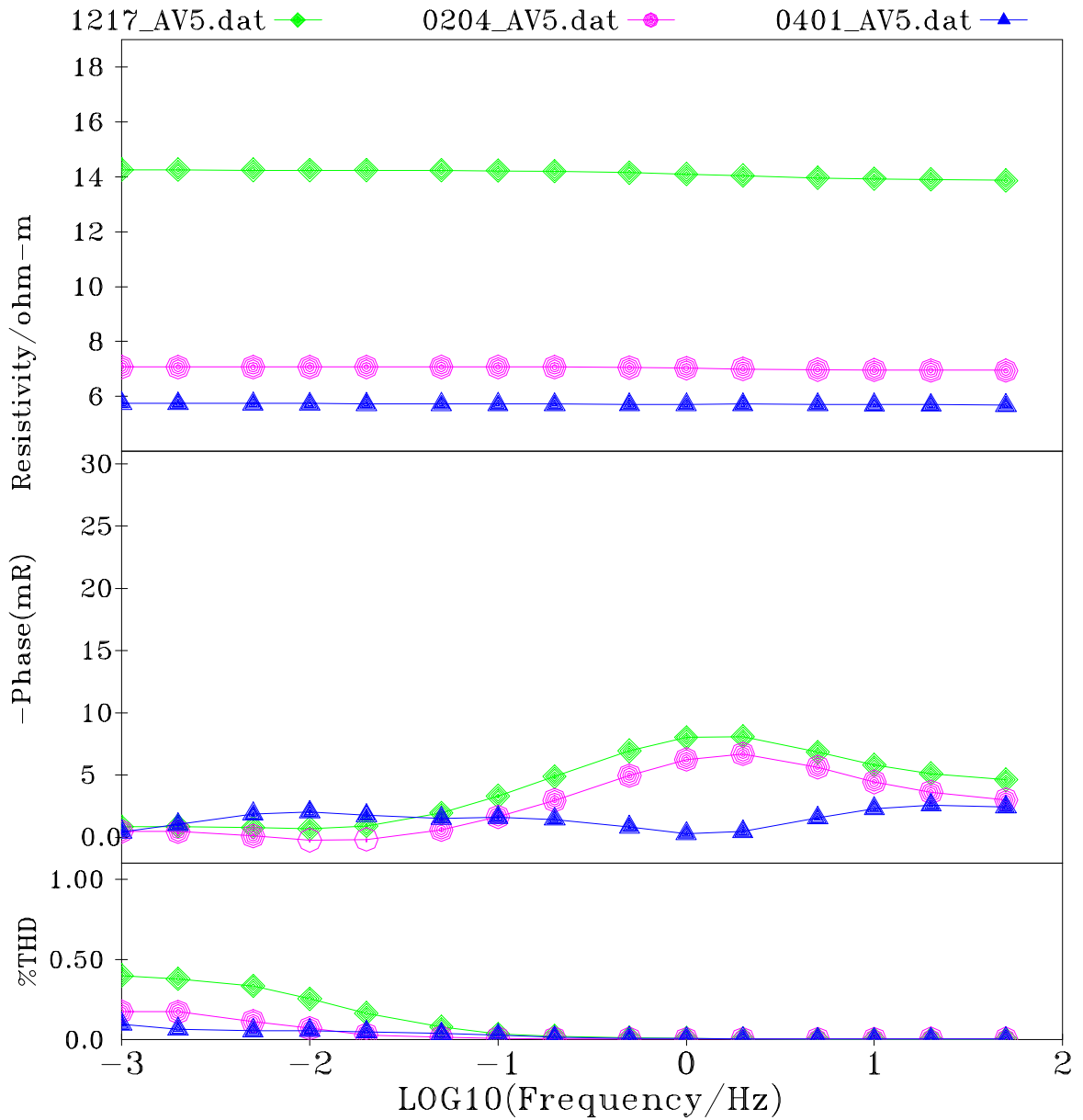


Figure 5.7. Resistivity (top section), negative phase (middle), and %THD (bottom), from 0.001 Hz to 50 Hz, for the *low grade ore with biooxidant* at day 13 (diamonds), day 62 (circles), and day 118 (triangles) for a total of 105 days.

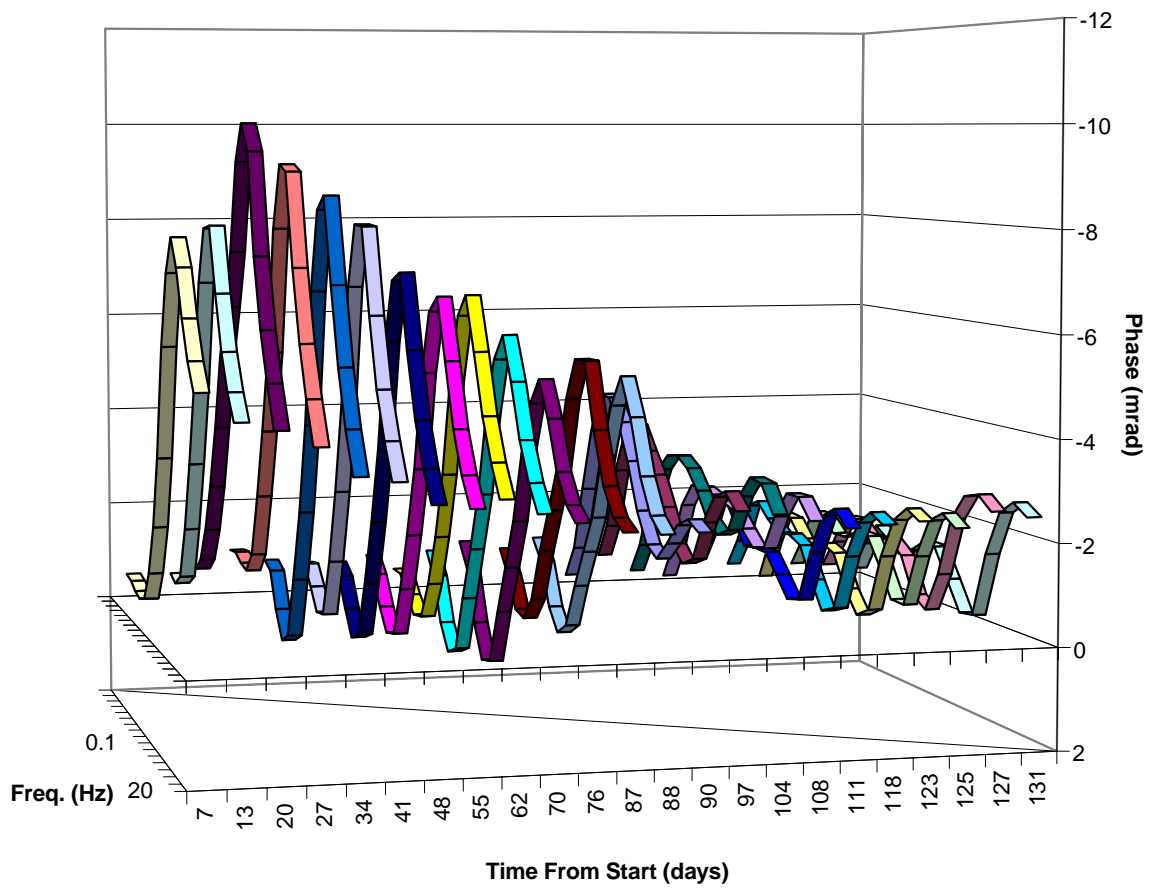


Figure 5.8. CR phase data for analytical days: Column 2, *low-grade ore with biooxidant*.

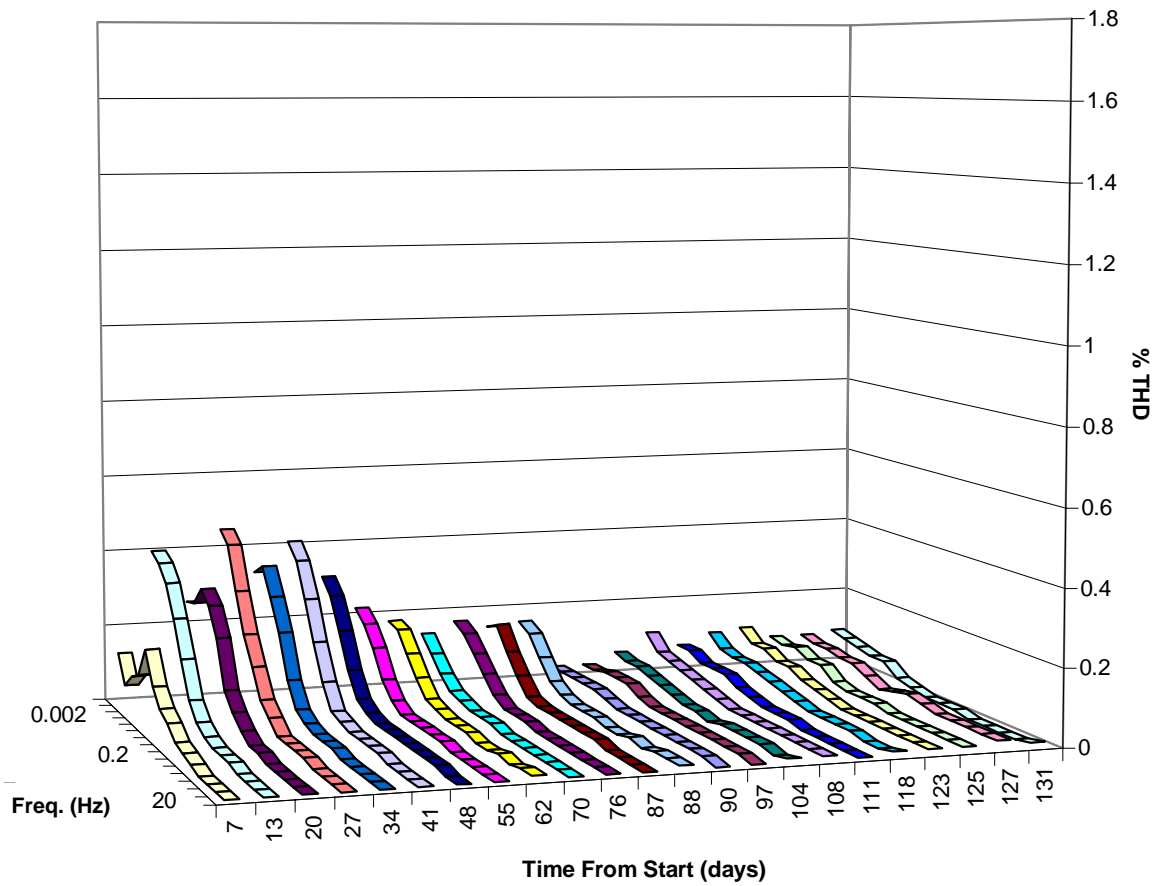


Figure 5.9. CR percent total harmonic distortion (%THD) data for analytical days:
 Column 2, *low-grade ore with biooxidant*.

The low-grade ore with low pH solution and a bacteria inhibitor is shown in Figure 5.10 for days 14, 84, and 112. This plot represents 98 of the 127 days column number 4 was in operation and is scaled identical to the low-grade ore with biooxidant. The resistivity initially decreased and then remained about the same, with less change than the ore with biooxidant. The phase had an initial peak of 6.0 milliradians at 1 Hz, which dropped by 50% and shifted to lower frequencies over time. The phase also became positive (plotted as open symbols on the negative phase scale) at high and low frequencies. The plot of phases for analytical days in Figure 5.11 shows there were some large positive phases, which corresponded to when additional sodium lauryl sulfate (the bacteria inhibitor) was added to the column. Positive phase angles occur when the current waveform is received after the measured potential. It is likely that the reaction between the sodium lauryl sulfate and the bacteria and/or ore are responsible for the unusual phases. The total harmonic distortion for analytical days is in Figure 5.12. It initially increased and then decreased by the end of the experiment. This increase in nonlinearity is over the same days when the bacteria inhibitor was added and is indicative of active chemistry.

The high-grade ore (SSR) with biooxidant is plotted in Figure 5.13 for days 44, 79, and 132. This plot is scaled the same as the plots of the low-grade ore measurements and represents 88 of the 142 days column 1 was in operation. As mentioned in Section 4.4, the complex resistivity system configuration was not completely operational until day 44 of the first column and earlier data is not presented due to inconsistencies and

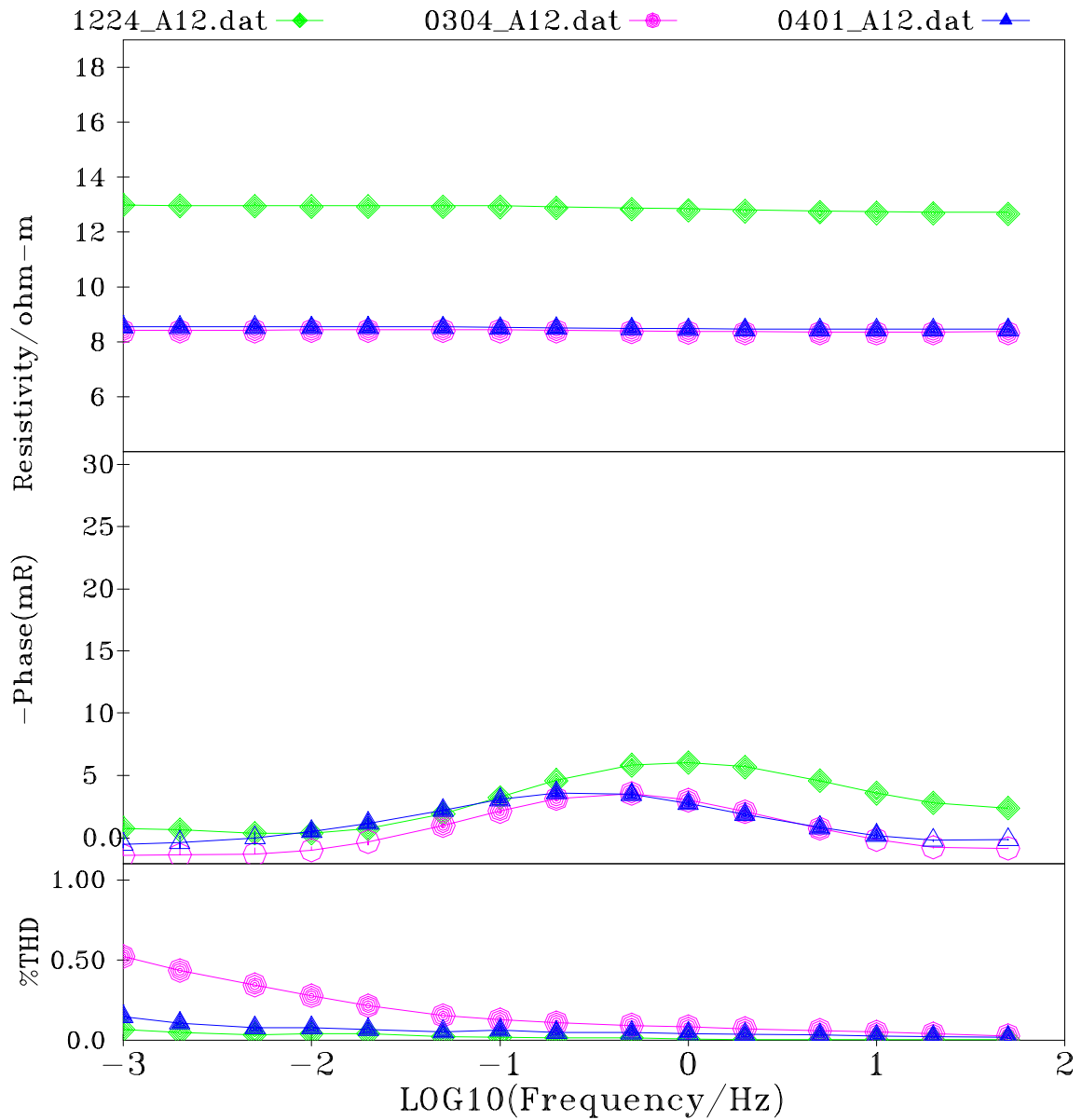


Figure 5.10. Resistivity (top section), negative phase (middle), and %THD (bottom), from 0.001 Hz to 50 Hz, for the *low grade ore with low pH water* at day 14 (diamonds), day 84 (circles), and day 112 (triangles) for a total of 98 days.

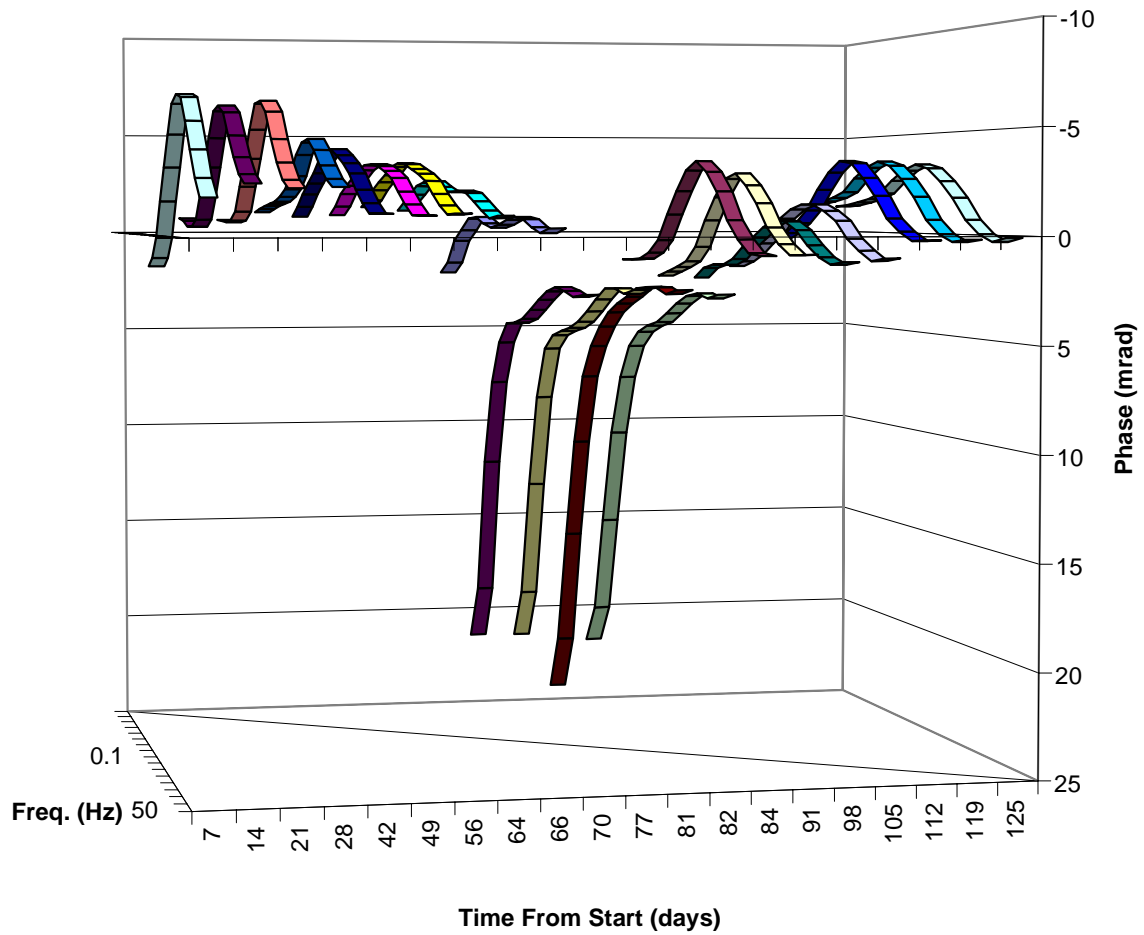


Figure 5.11. CR phase data for analytical days: Column 4, *low-grade ore with low pH water and bacterial inhibitor*.

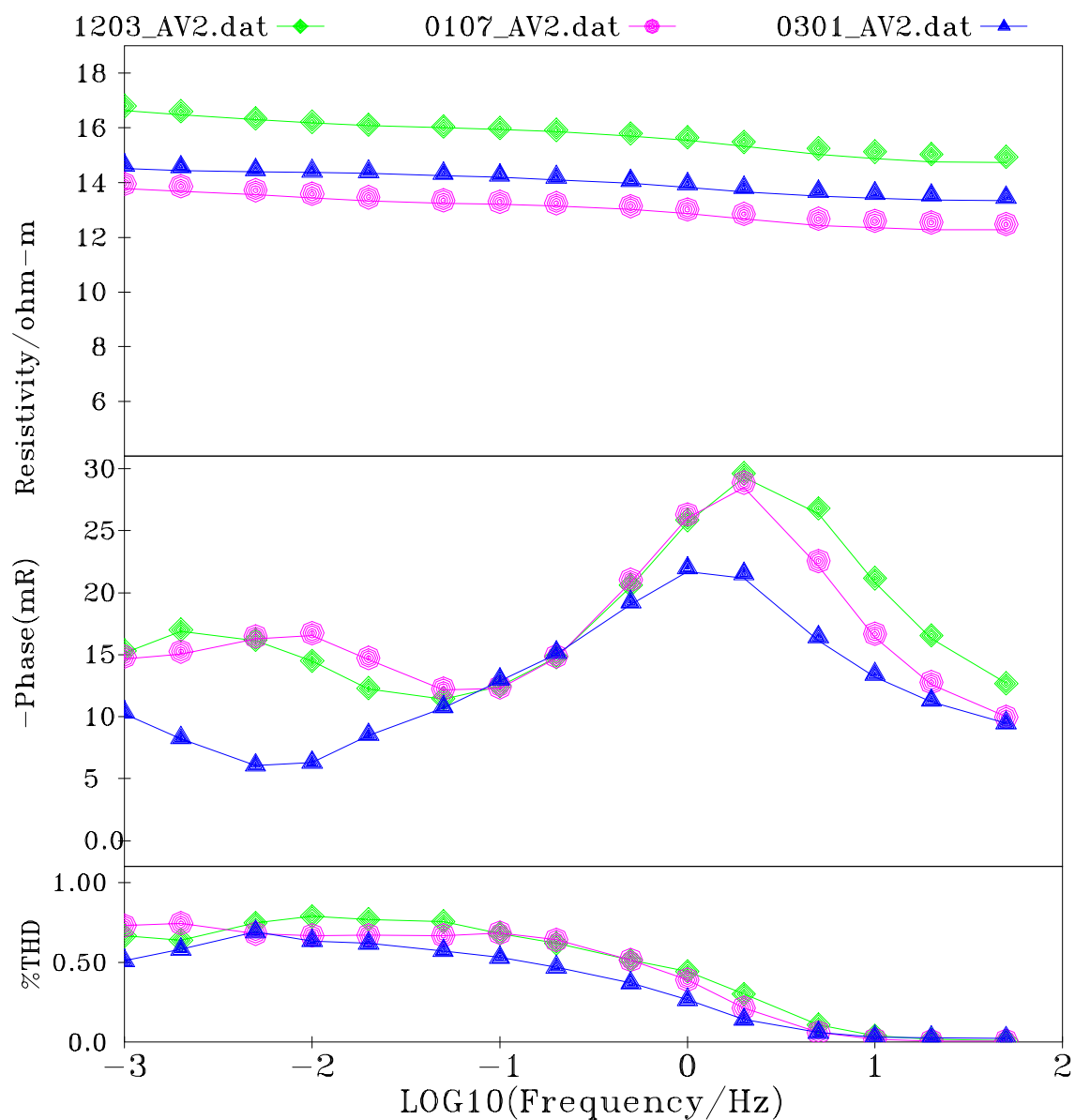


Figure 5.13. Resistivity (top section), negative phase (middle), and %THD (bottom), from 0.001 Hz to 50 Hz, for the *high grade ore with biooxidant* at day 44 (diamonds), day 79 (circles), and day 132 (triangles) for a total span of 88 days.

noise. The resistivity decreased initially and then increased slightly near the end. The initial phase peak at 2 Hz is much more prominent than the 2 Hz peak in the low-grade ore. This 2 Hz peak narrowed slightly between day 44 and 79 and decreased 30% by day 132. The phase below 0.05 Hz also decreased even more dramatically. The %THD decreased slightly and is similar in shape for the experiment. The phase angles for all analytical days are plotted in Figure 5.14 and the %THD plots are in Figure 5.15. The downward trend in the 2 Hz phase peak after day 100 and the associated %THD decreases may be important indicators of the slowing of pyrite oxidation.

Figure 5.16 shows the CR measurements for the high-grade ore with low pH solution and a bacteria inhibitor for days 14, 64, and 112. This plot represents 98 of the 127 days column 5 was in operation. The resistivity is much higher than the sample with biooxidant (Figure 5.13) because the solution had lower ionic strength, yet showed a similar pattern of initial decrease and slight increase near the end. The phase decreased over time and lacked any significant peaks. The phase is distinctly different in character from the high-grade ore with biooxidant, indicating that the phase may be a good indicator of whether or not this SSR ore is oxidizing. The %THD is less than the high-grade ore with biooxidant. Figure 5.17 shows the phase angles and Figure 5.18 shows the %THD for analytical days.

The CR measurements for the NAL Oxide Composite with tap water, the control ore with essentially no pyrite, for days 14, 64, and 112 are plotted in Figure 5.19. The resistivity increased by about 150% during the experiment, the opposite of the ores

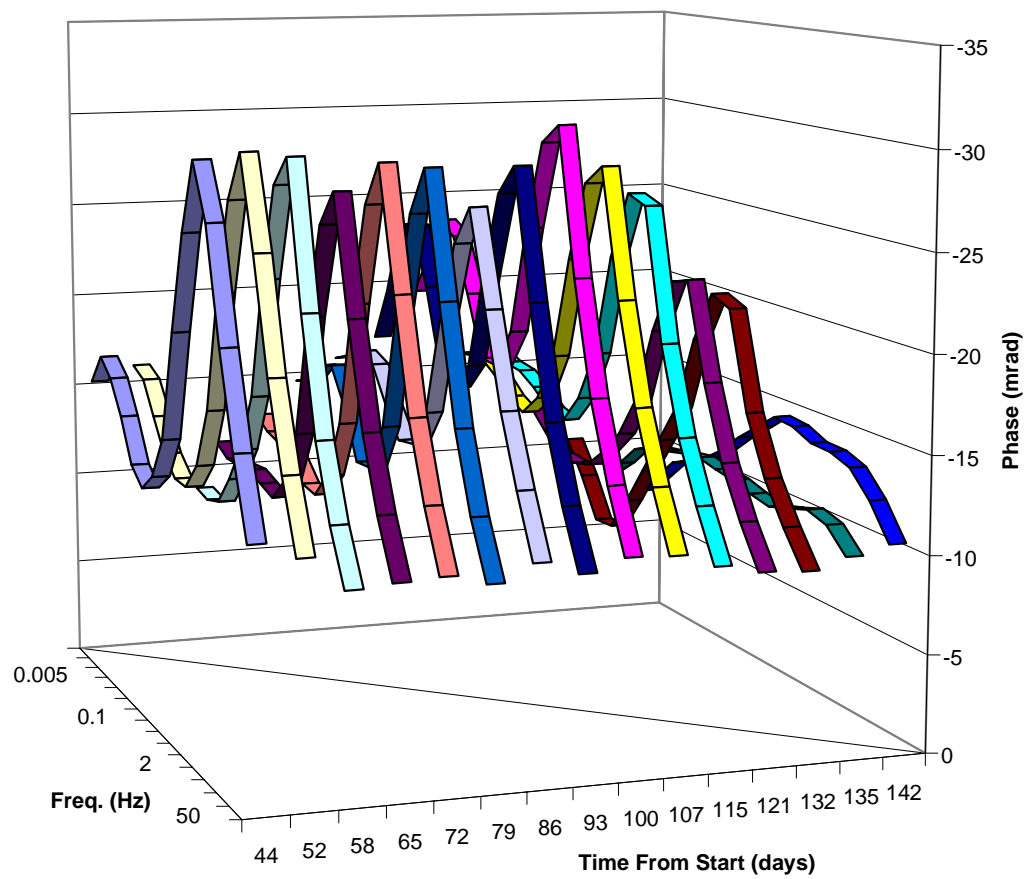


Figure 5.14. CR phase data for analytical days: Column 1, *high-grade ore with biooxidant*.

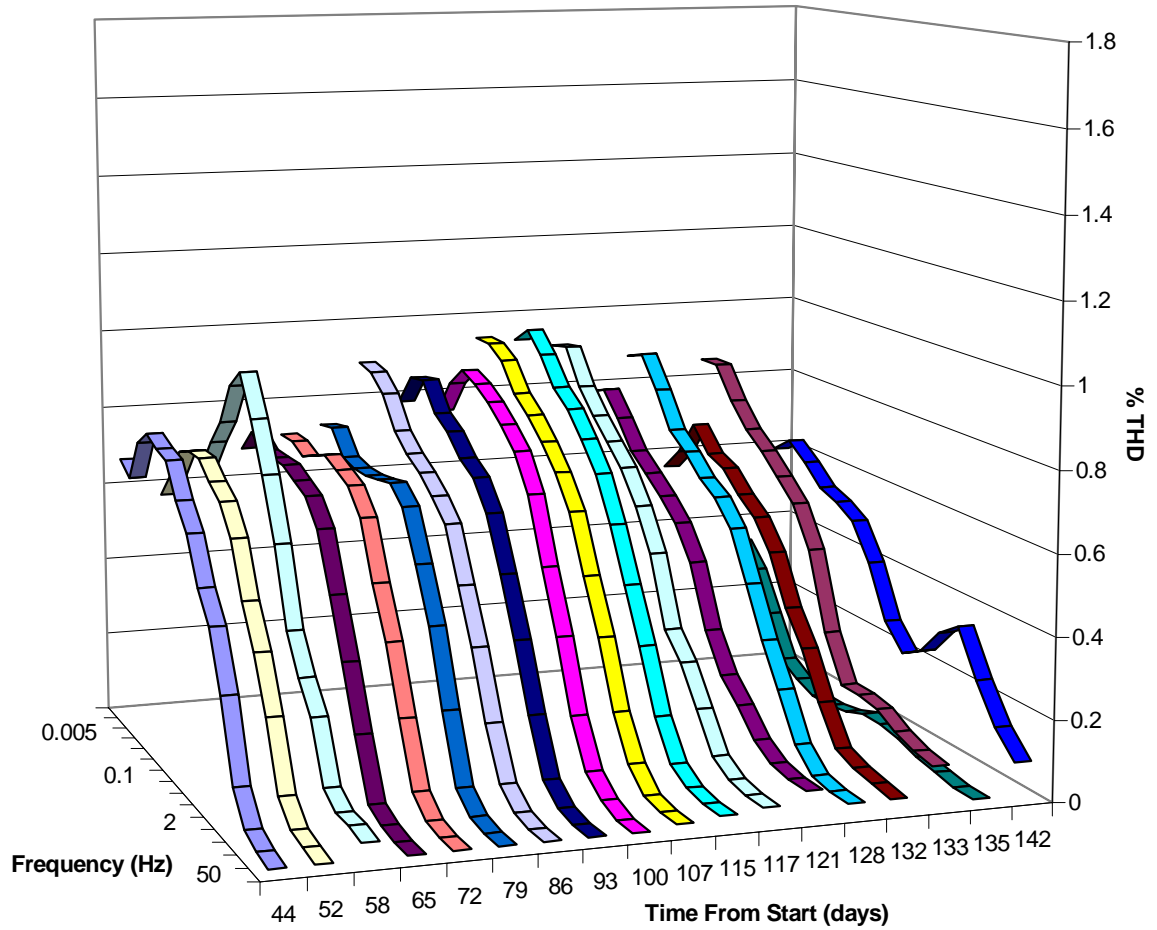


Figure 5.15. CR percent total harmonic distortion (% THD) data for analytical days:
 Column 1, *high-grade ore with biooxidant*.

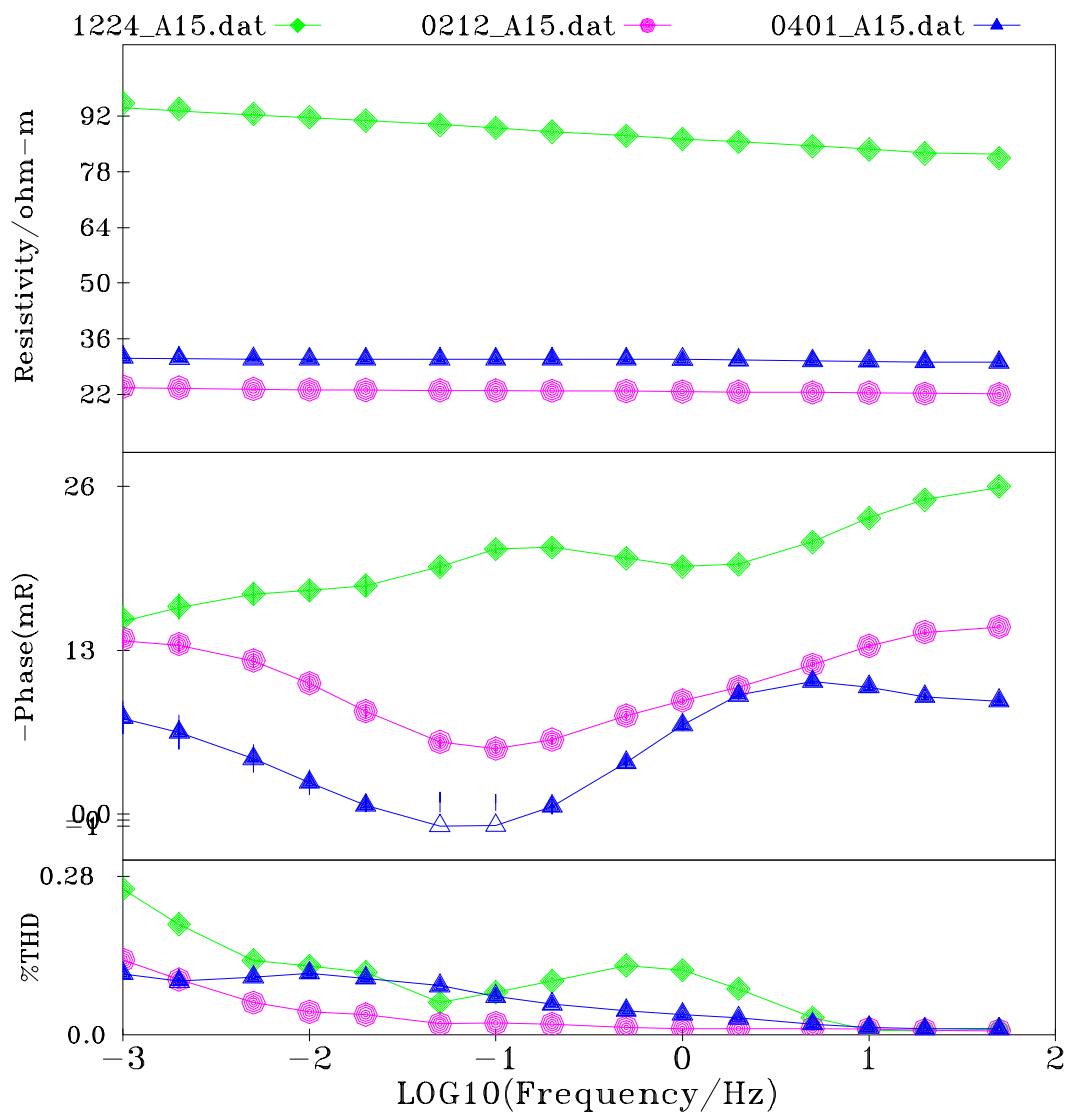


Figure 5.16. Resistivity (top section), negative phase (middle), and %THD (bottom), from 0.001 Hz to 50 Hz, for the *high grade ore with low pH water* at day 14 (diamonds), day 64 (circles), and day 112 (triangles) for a total of 98 days.

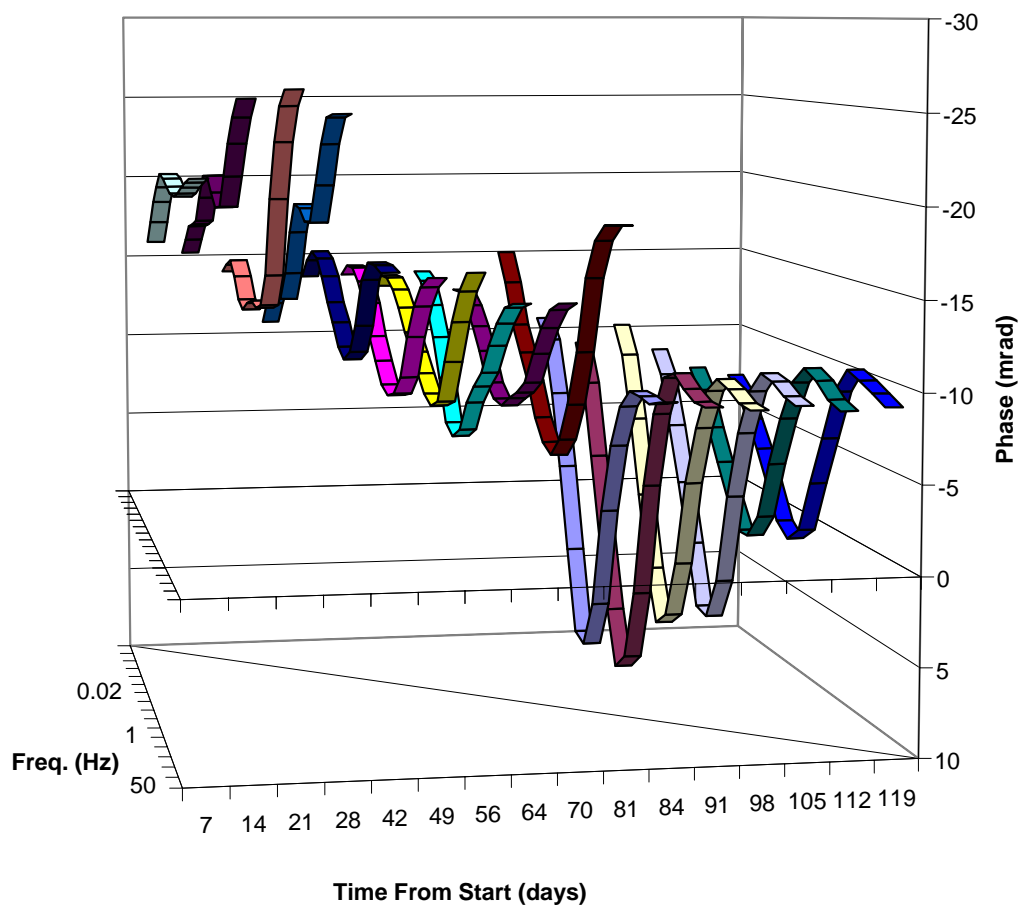


Figure 5.17. CR phase data for analytical days: Column 5, *high-grade ore with low pH water and bacterial inhibitor.*

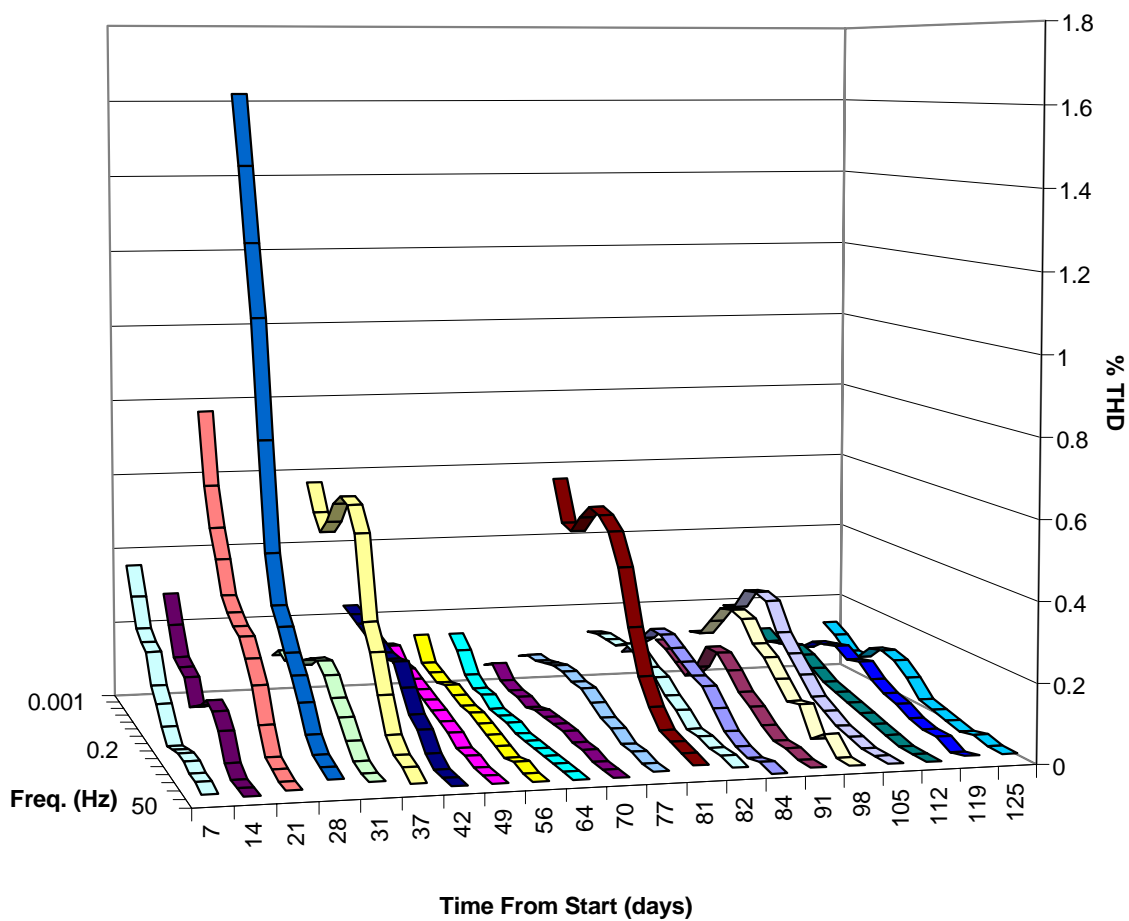


Figure 5.18. CR percent total harmonic distortion (% THD) data for analytical days: Column 5, high-grade ore with low pH water and bacterial inhibitor.

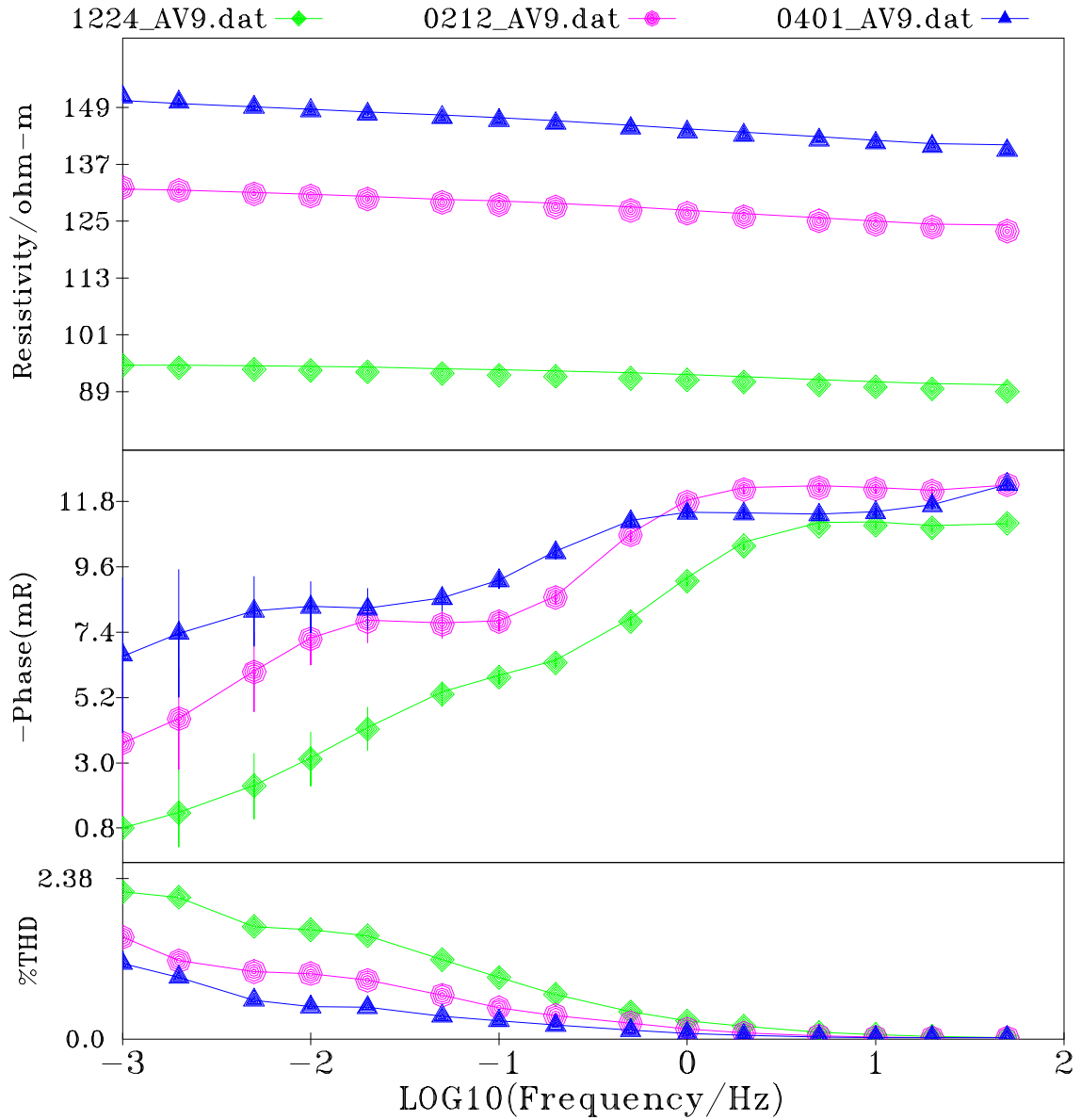


Figure 5.19. Resistivity (top section), negative phase (middle), and %THD (bottom), from 0.001 Hz to 50 Hz, for the *control ore with tap water* at day 14 (diamonds), day 84 (circles), and day 112 (triangles) for a total of 98 days.

with pyrite. This may be due to the problem of the column clogging and water ponding on the top of the ore (see Section 4.4). The phase increased over time, had significant errors below 0.05 Hz, and did not resemble the phase character of the siliceous sulfidic refractory (SSR) ores. The phase angles for analytical days are plotted in Figure 5.20 to emphasize the distinctly different phase patterns. The %THD was much higher than the SSR ores and decreased over time, as demonstrated in Figure 5.21.

The results of these complex resistivity measurements indicate that the magnitude and character of the frequency-dependent phase angles are the key to differentiating between active and inactive pyrite oxidation. The phase peak at 1 - 2 Hz is most prominent (up to 30 milliradians) in the high-grade ore with biooxidant (which oxidized 42.4% of the sulfides) and has a lower magnitude (up to 10 milliradians) in the low-grade ore with biooxidant (which only oxidized 27.5% of the sulfides).

5.4 Data Quality

It is useful to examine the quality of the chemistry and complex resistivity data prior to correlating the two. Discrepancies in the chemistry data are discussed with emphasis on the data quality. Factors affecting the quality of the CR data are discussed, with bad data shown as examples of how data quality can be ascertained.

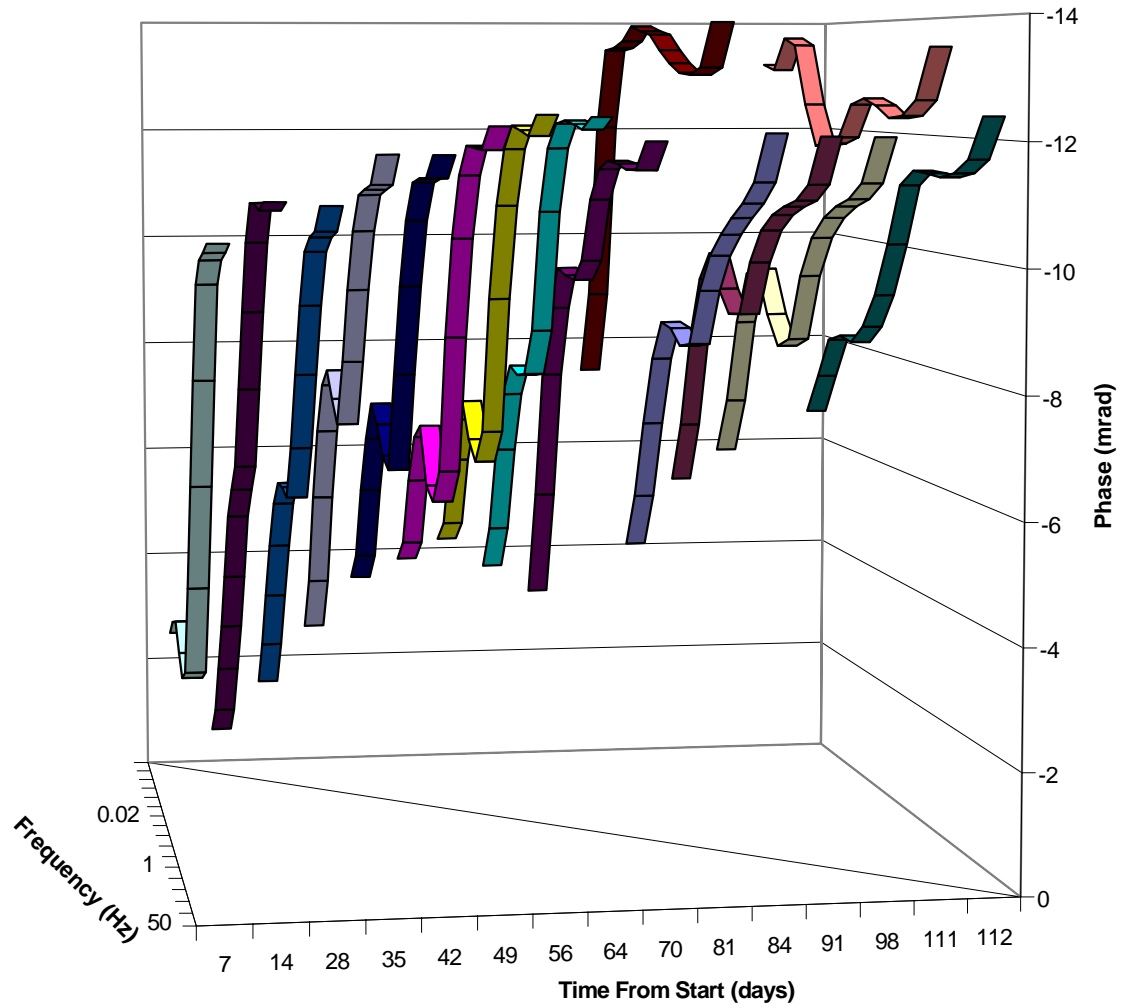


Figure 5.20. CR phase data for analytical days: Column 3, *control ore with tap water*.

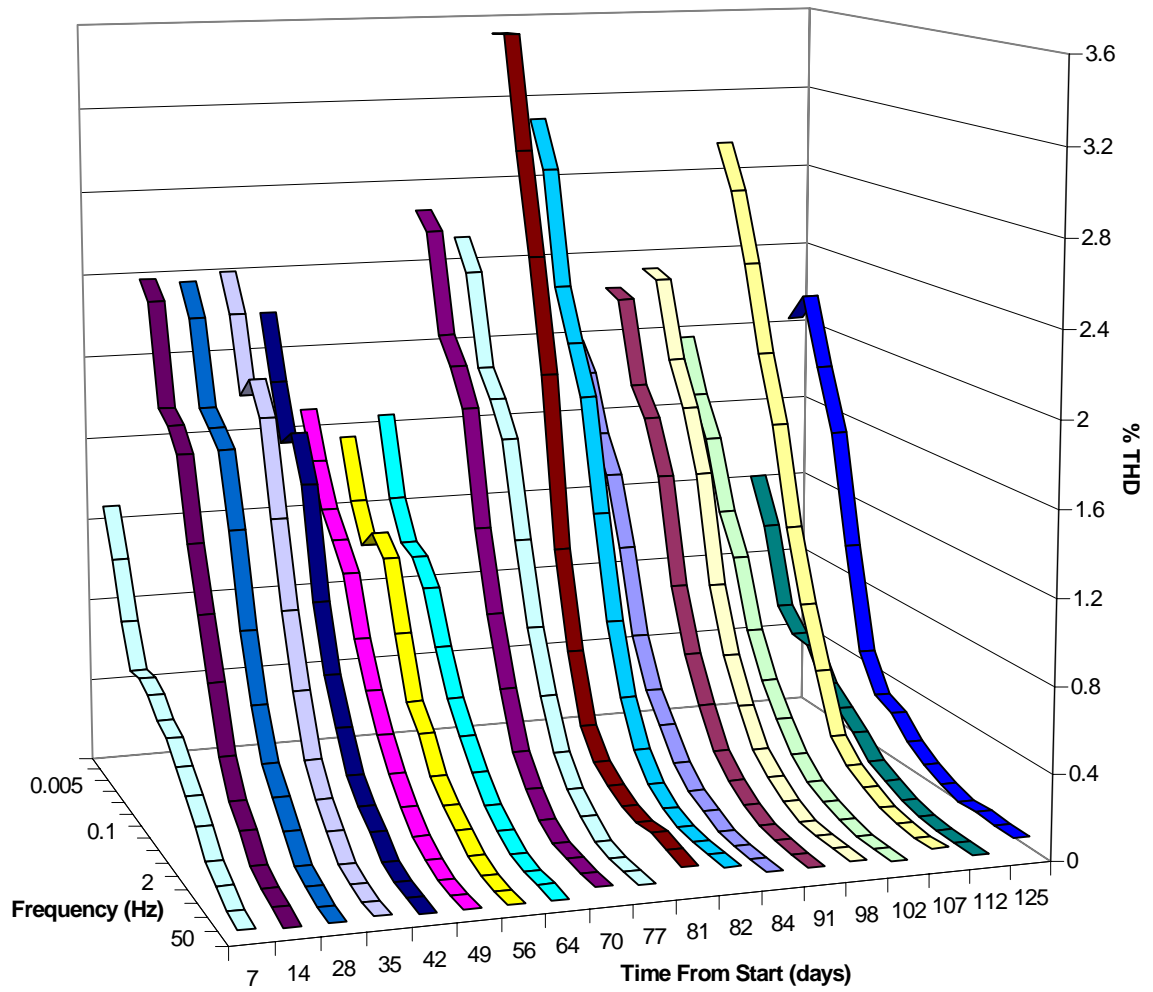


Figure 5.21. CR percent total harmonic distortion (% THD) data for analytical days:
 Column 3, control ore with tap water.

5.4.1 Chemistry Data Quality

The most accurate and useful chemistry data is the weekly pH and iron solution analysis because each measurement was made with exactly the same procedures. The only chemistry data that is known to be of poor quality is the ICP solution analysis data for iron. This was discovered when the more accurate weekly iron titration analysis did not match the pre or post solution ICP analysis for the high-grade or low-grade columns. The change in solution iron content for titration versus ICP analysis is in Table 5.4. Assuming the iron titrations are correct, there is 43 to 97% error in the ICP iron data. However, this problem does not affect the correlation of chemistry and complex resistivity because the more accurate weekly iron titration data is used.

Sample	Pre - Post Total Fe (g/L)			% error
	Titration	ICP	difference	
High-Grade	37.0	7.0	30.0	81%
High-Grade, no bacteria	7.2	4.1	3.1	43%
Low-Grade	37.7	1.2	36.5	97%
Low-Grade, no bacteria	9.2	3.6	5.6	61%

Table 5.4. A comparison of the change total iron content in solution for the accurate titration method versus the questionable inductively coupled plasma (ICP) data.

5.4.2 Complex Resistivity Data Quality

Four ways were used to distinguish between good and bad data in the column studies. The first way was to examine the raw sinusoid current and potential waveforms during data collection. This was used primarily in the initial system setup to verify that each channel had signal input, the polarity was correct, and there was low noise. The full waveforms are not shown here and can be viewed with the program *nocr_nm.c* (see *readme.txt* on CD-ROM). The initial data for the high-grade ore with biooxidant were measured prior to completion of the complex resistivity system upgrades and is intermittent, noisy, and unreliable. An example of two bad measurements compared with one good measurement is plotted in Figure 5.22.

The second data quality check was to measure each channel with an R-RC circuit, as described in Section 4.4. This showed that channels 3, 8, 11, and 14 were bad. The third data quality check was to compare measurements for the 2 or 3 potential electrode pairs in each column to test the repeatability of data. Only the two ores with biooxidant had two good electrode pairs for comparison. Finally, the standard deviations of the measurements used to compute average data plots were computed and plotted for all channels in each column.

Figure 5.23 shows the measurements on day 44, 12/3/98, for the three electrode pairs in column 1, the high-grade ore with biooxidant. Channel 3 has high Hilbert distortion (shown by the poor fit of the calculated resistivity and phase Hilbert transform), large phase error bars, and high %THD when compared with the other two

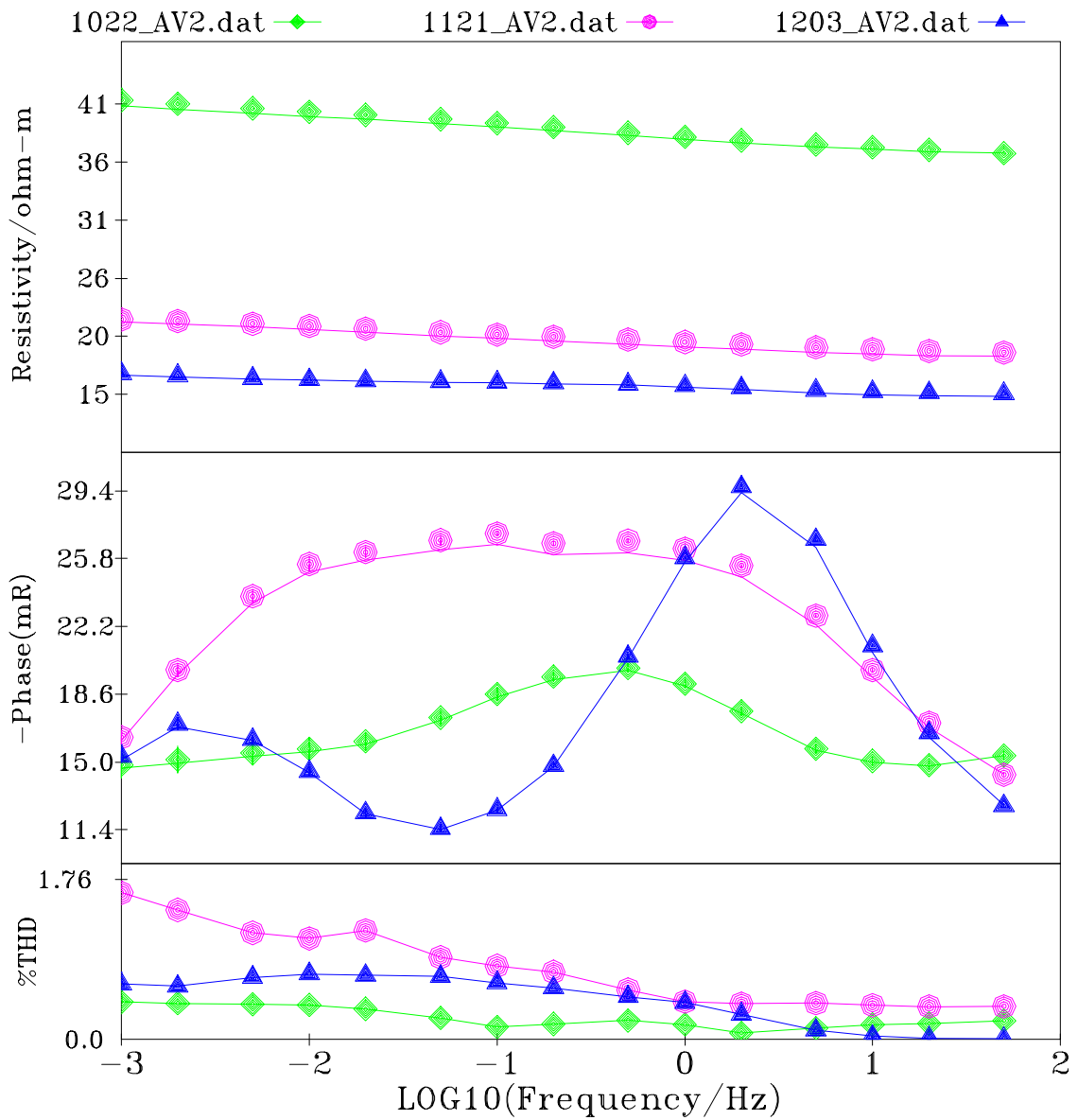


Figure 5.22. Three CR measurements for channel two, the middle electrode pair for the *high-grade ore with biooxidant*. The first two measurements (diamonds and circles) are prior to implementation of the CR updates and the last measurement (triangles) is just after the updates.

electrode pairs in that column. This confirms the fact that channel 3 was bad, as determined with the R-RC test. The standard deviations of the time-averaged spectra in Figure 5.24 are less than 5.3% for resistivity, yet are significant for the phase (17.6 mrad) for channel 3. Because of these results, channel 2 was chosen to represent the high-grade ore with biooxidant. Figure 5.24 also shows the current density to be 0.160 amperes/meter² for column 1 on day 44.

Measurements of the two potential electrode pairs for column 2, the low-grade ore with biooxidant, are shown in Figure 5.25 for 12/24/98. Channel 5 has slightly lower resistivity, a higher phase peak at 1 Hz, and greater total harmonic distortion. The standard deviations of the time-averaged spectra in Figure 5.26 are below 9.2% for the resistivity and 1.5 milliradians for the phase in both potential electrode pairs. The current density is 0.15 A/m² (very close to column 1). Channel 5 was chosen to represent the low-grade ore with biooxidant because the 2 Hz phase peak was more pronounced.

The two potential electrode pairs for column 3, the control ore with tap water, are plotted in Figure 5.27. Channel 8 has higher resistivity, Hilbert distortion, phase, errors, and %THD. The significant resistivity and phase standard deviations in Figure 5.28 for channel 8 on 4/5/99 indicate this channel is bad. Channel 9 was chosen to represent column 3 because it was good according to the R-RC test and has very small phase standard deviation. The current density is 0.031 A/m², less than columns 1 and 2.

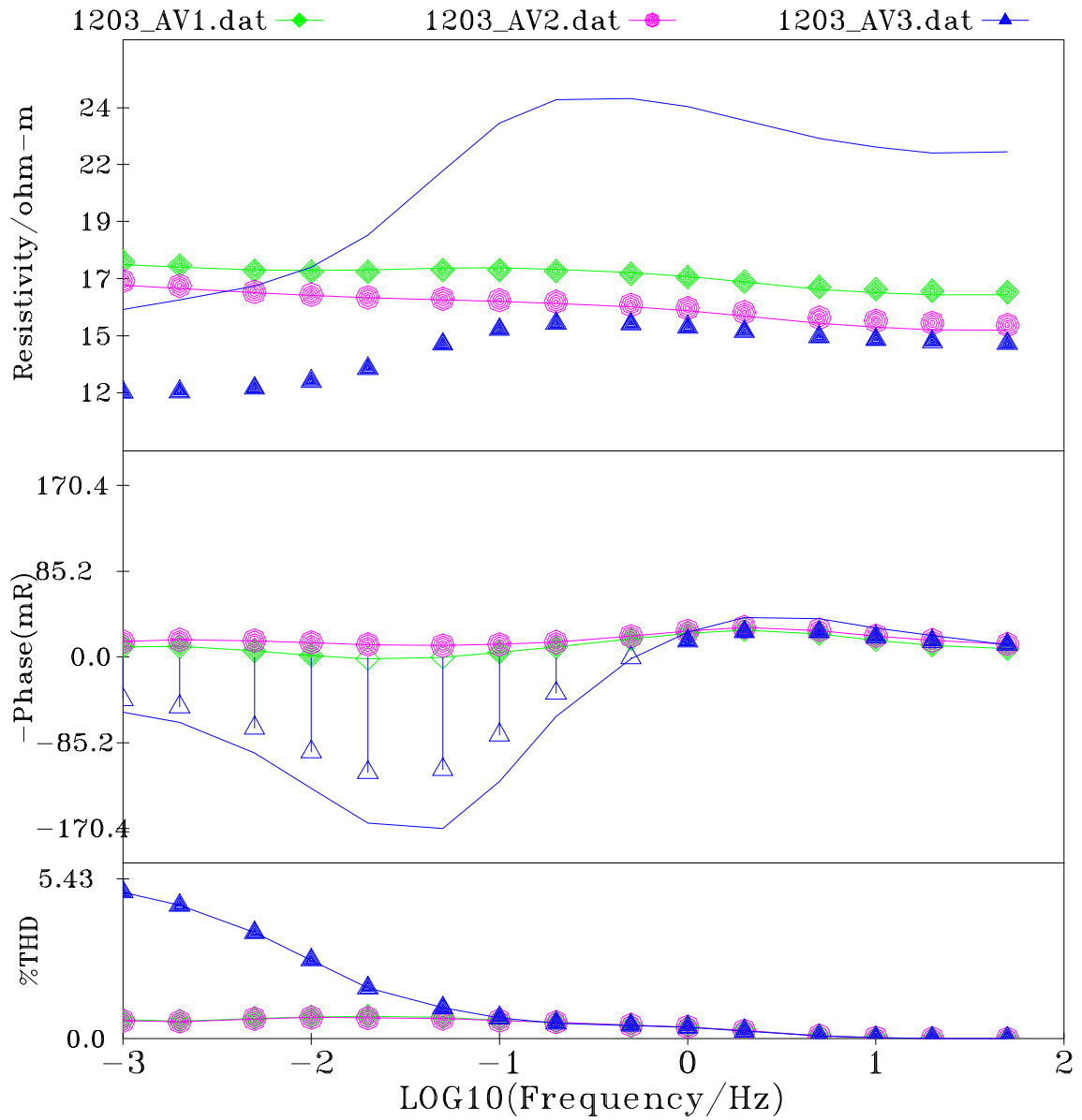


Figure 5.23. CR measurements for all three potential electrode pairs in column 1, *the high-grade ore with biooxidant*. The first two channels (diamonds and circles) are good and channel 3 (triangles) is bad according to the R-RC test.

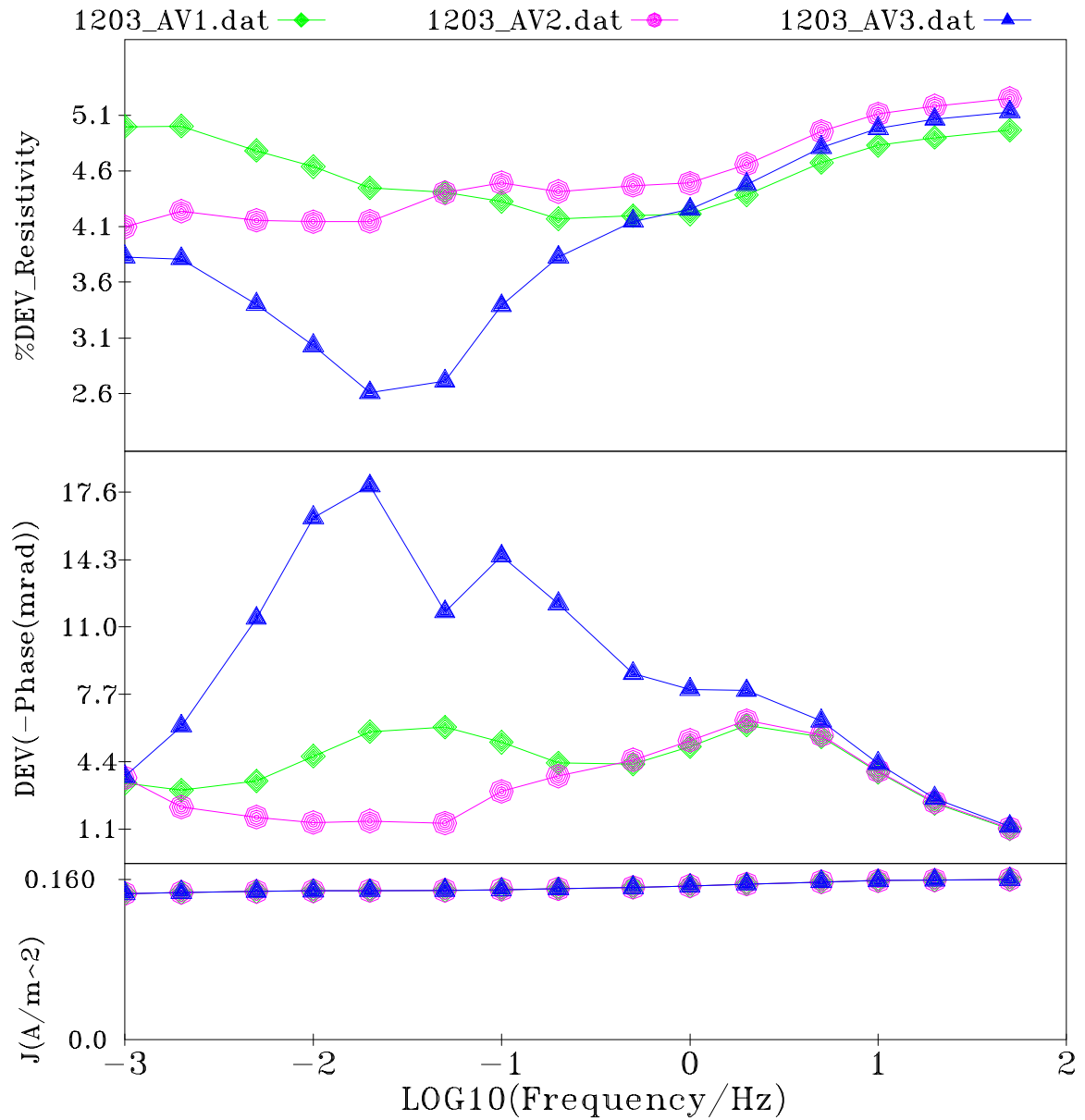


Figure 5.24. Percent resistivity standard deviation (top), phase standard deviation (middle), and current density in amperes/meter² (bottom) for the two good potential electrode pairs in column 1. Channel 2 (circles) is the electrode pair chosen to represent the *high-grade ore with biooxidant*.

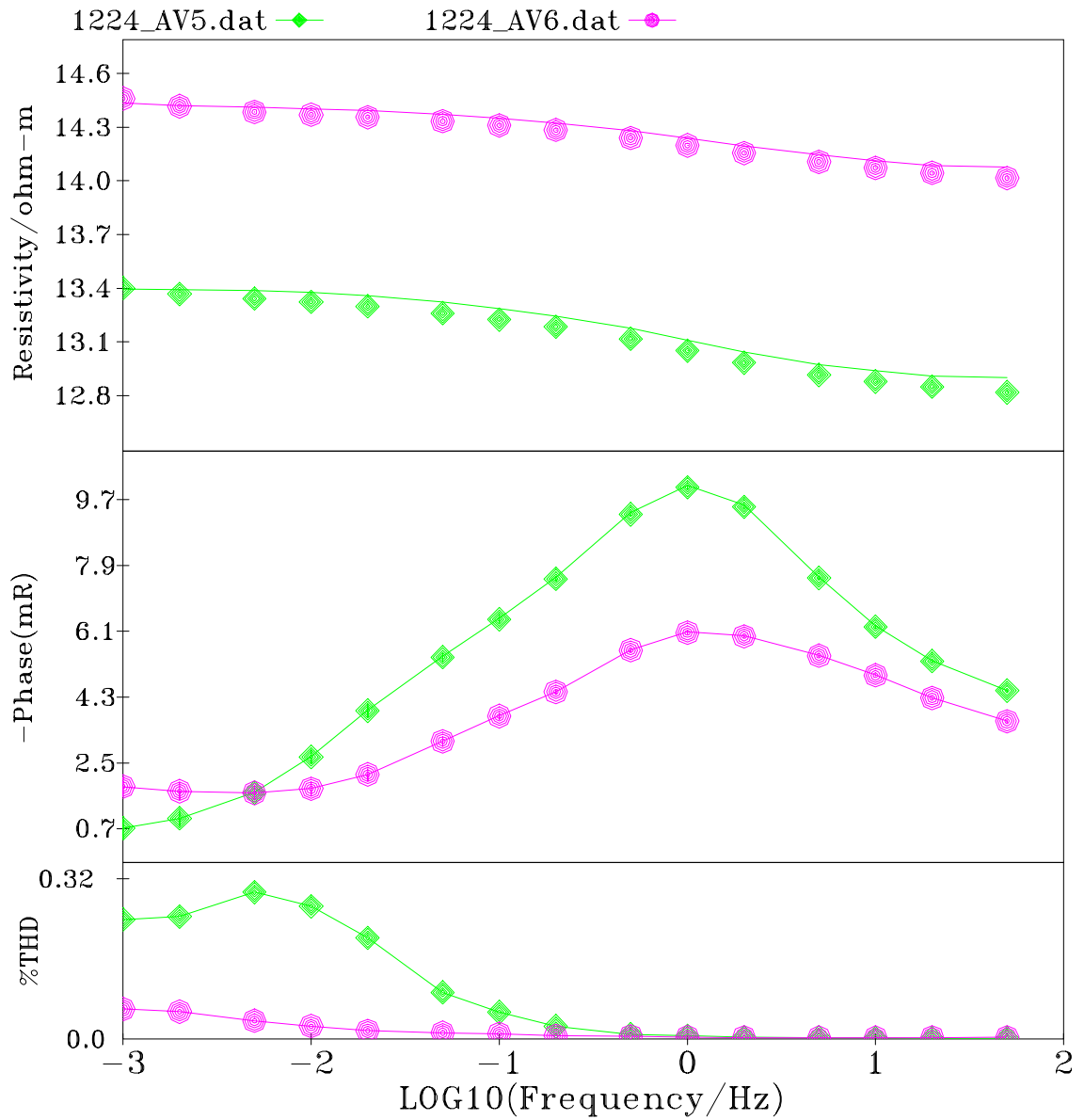


Figure 5.25. CR measurements for the potential electrode pairs in column 2 *the low-grade ore with biooxidant*. Channel 5 (diamonds) and channel 6 (circles) are both good according to the R-RC test. The resistivity is greater, the phase peak is less distinct, and the %THD is lower on channel 6.

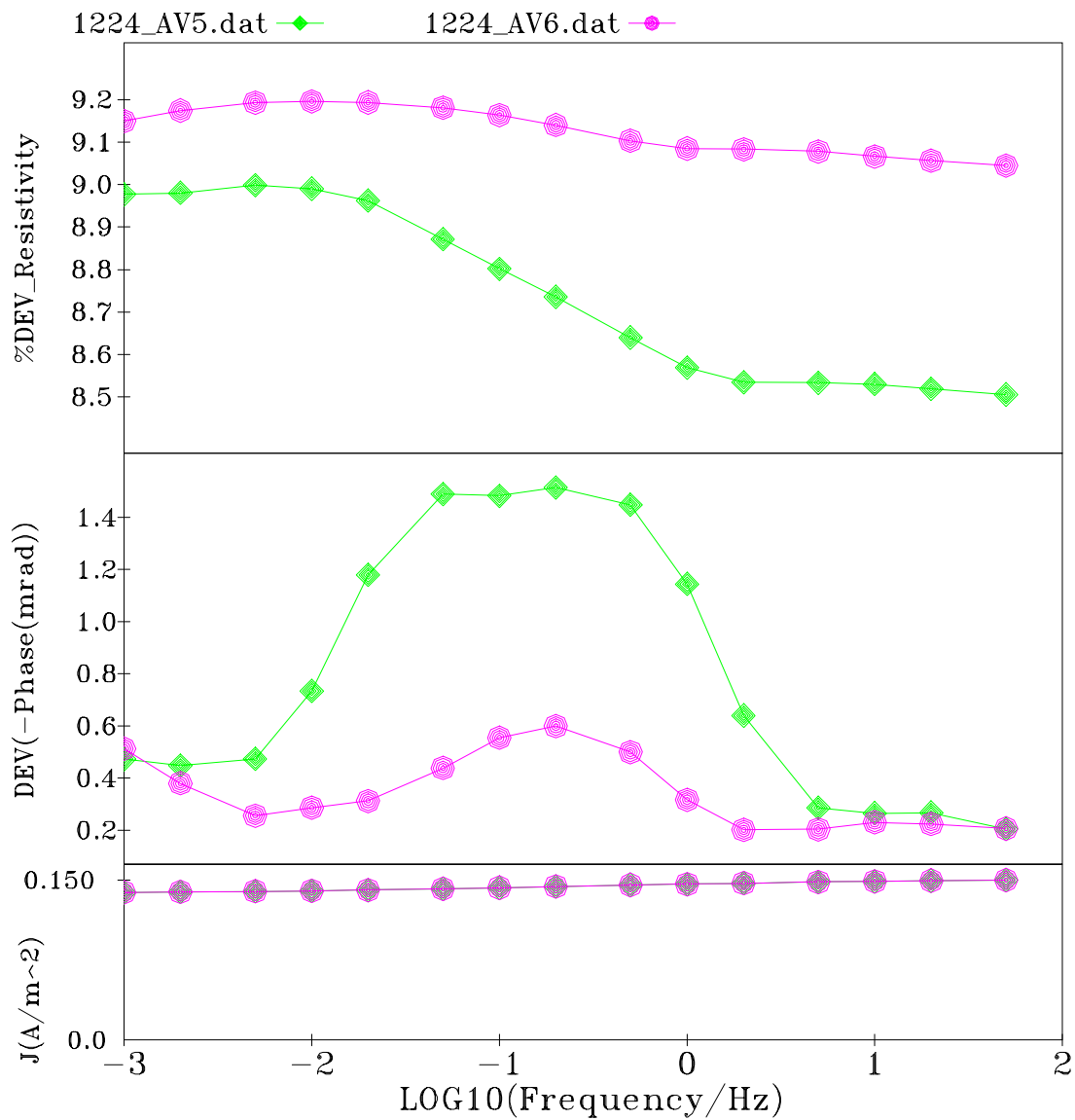


Figure 5.26. Percent resistivity standard deviation (top), phase standard deviation (middle), and current density in amperes/meter² (bottom) for the two good potential electrode pairs in column 2. Channel 5 (triangles) is the electrode pair chosen to represent the *low-grade ore with biooxidant*.

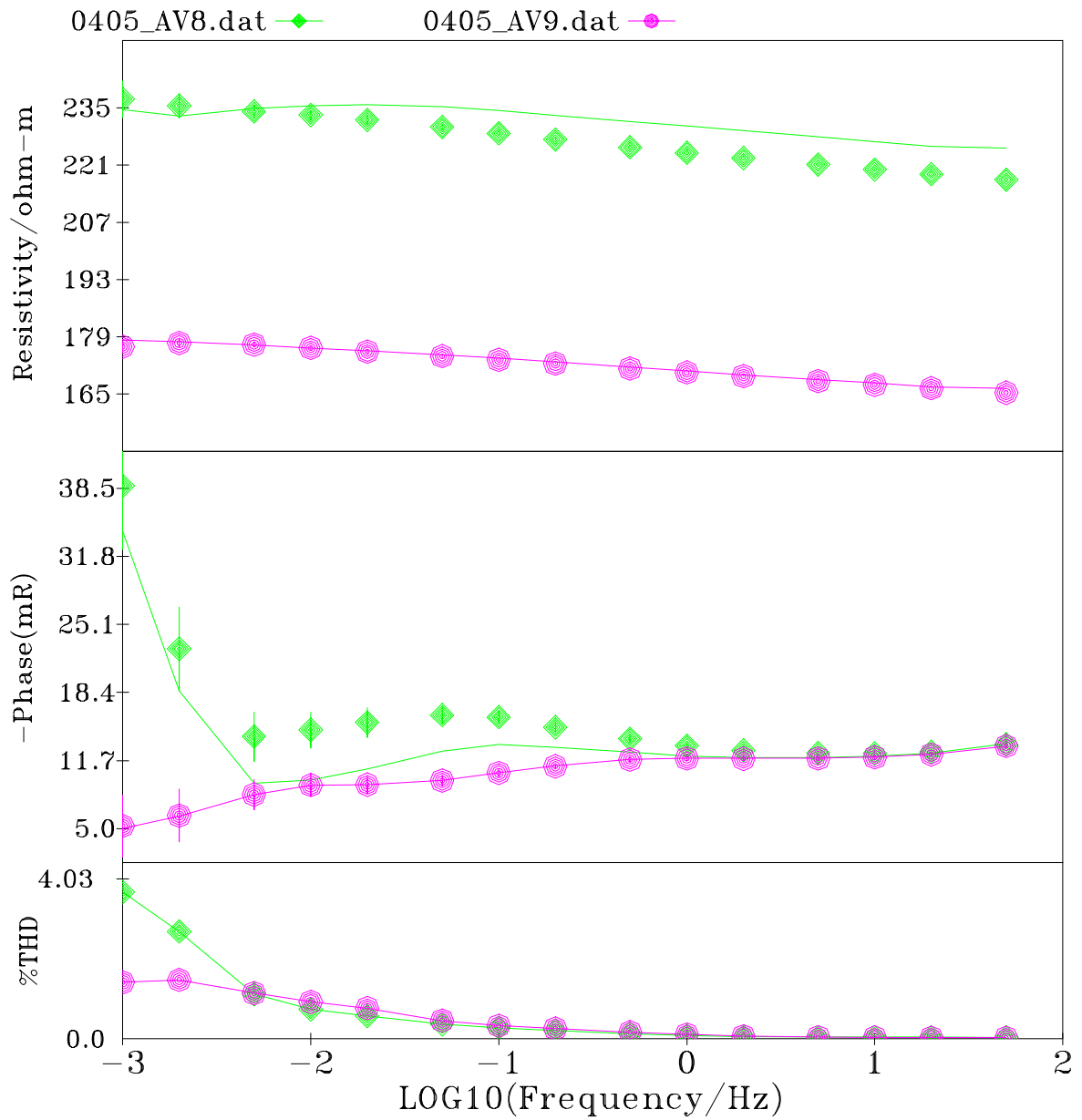


Figure 5.27. CR measurements for the potential electrode pairs in column 3 the *control ore with tap water*. Channel 8 (diamonds) is bad and channel 9 (circles) is good according to the R-RC test.

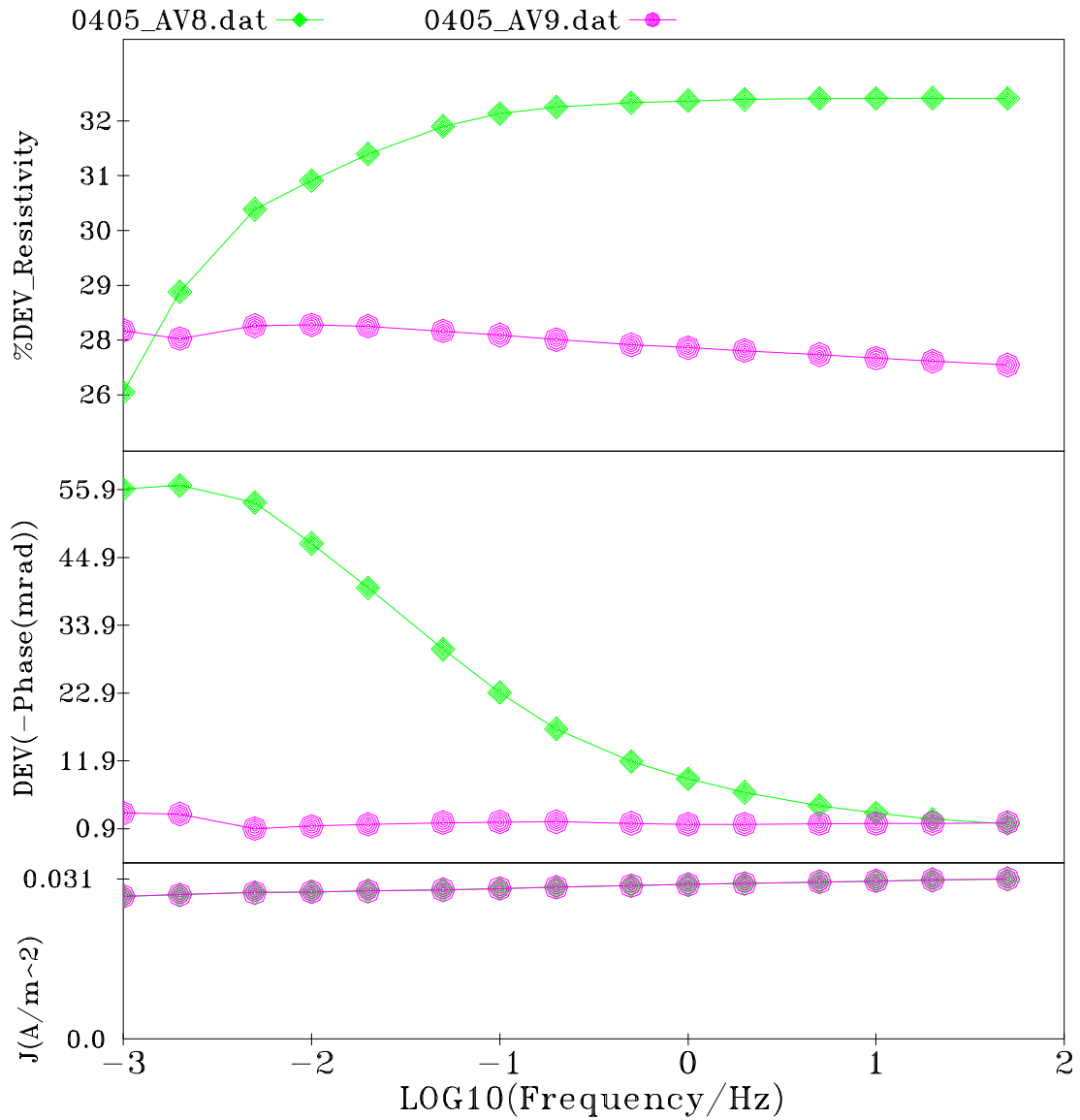


Figure 5.28. Percent resistivity standard deviation (top), phase standard deviation (middle), and current density in amperes/meter² (bottom) for the two potential electrode pairs in column 3. Channel 9 (circles) is the electrode pair chosen to represent the control; *NAL composite ore with tap water*.

Figures 5.29 and 5.30 show the CR measurements, standard deviation, and current density for column 4, the low-grade ore with low pH water and a bacteria inhibitor.

Channel 11 was determined to be bad with the R-RC test, and is verified here with large phase standard deviation. Channel 12 was chosen to represent column 4 and is verified as good with the R-RC test. Figures 5.31 and 5.32 show similar data for column 5, the high-grade ore with low pH water and a bacteria inhibitor, indicating that channel 14 is bad and channel 15 is good. Therefore, channel 15 was chosen to represent column 5. The current density is about 0.09 A/m^2 for column 4 and 0.06 A/m^2 for column 5.

A dramatic change occurred on 3/3/99 and the CR data for all columns remained anomalous for two weeks. This was due to attempts to fill in the air gaps developing beneath the electrodes in columns 2 through 5. The columns were disconnected from the measurement system and tapped with a rubber mallet. Figure 5.33 shows that the resistivity decreased, the phase peak shifted from 1-2 Hz to 0.02-0.05 Hz, and the %THD decreased. If the phase shift was due to compaction of the ore (reduction of pore sizes), a shift to higher frequencies would be expected. The decrease in frequency may be due to changing the geometry between the sample and the electrodes, or altering the pathways for current flow.

These analyses prove that there are multiple ways to assure the quality of the CR data. As a result, channels 2, 5, 9, 12, and 15 are used in Chapter 6 to correlate the chemistry and CR measurements for the five columns. And the data from 3/4/99 and 3/11/99 are omitted from further plots because of the changes due to column disturbance.

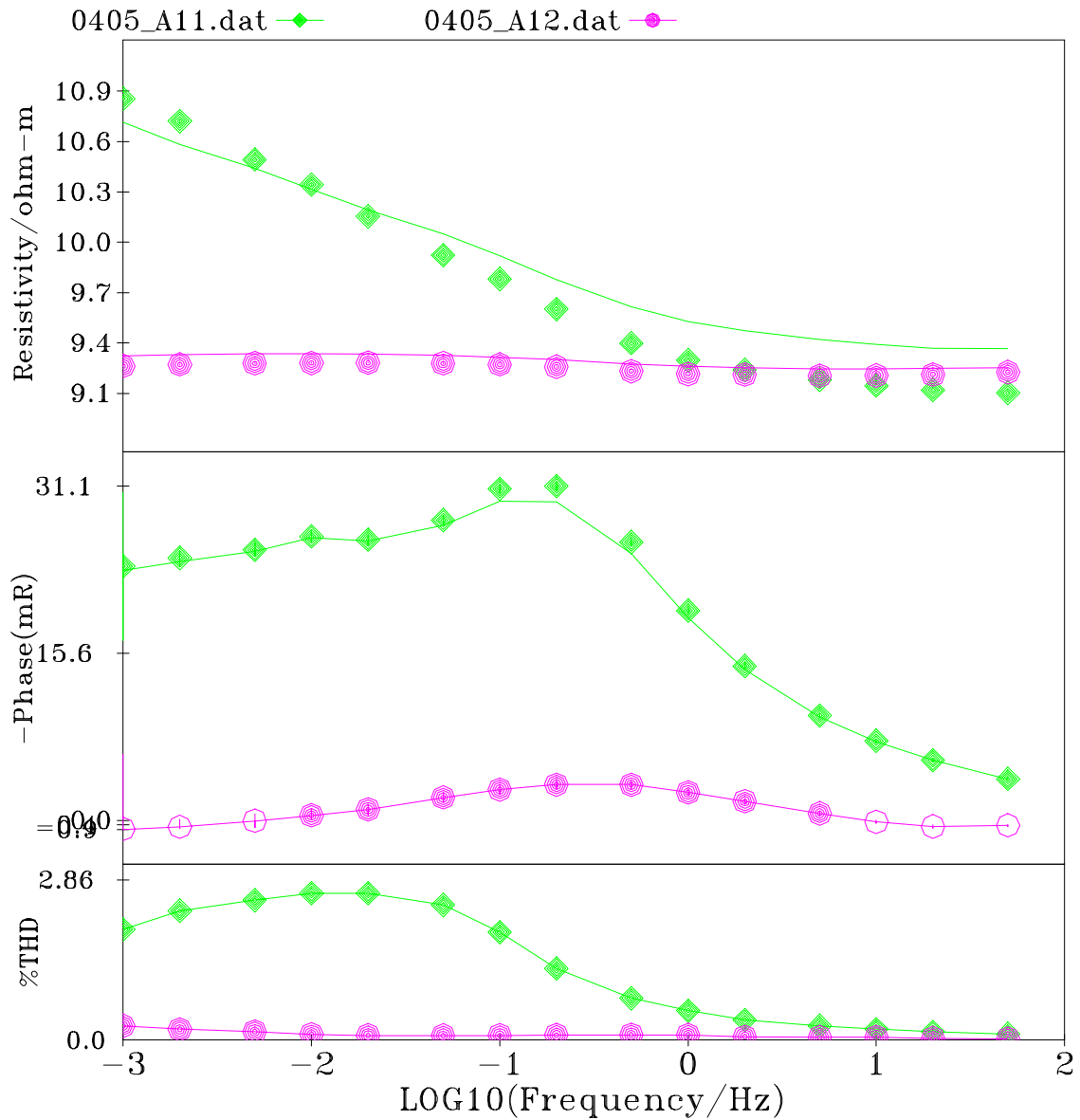


Figure 5.29. CR measurements for the potential electrode pairs in column 4 the *low-grade ore with low pH water and bacteria inhibitor*. Channel 11 (diamonds) is bad and channel 12 (circles) is good according to the R-RC test.

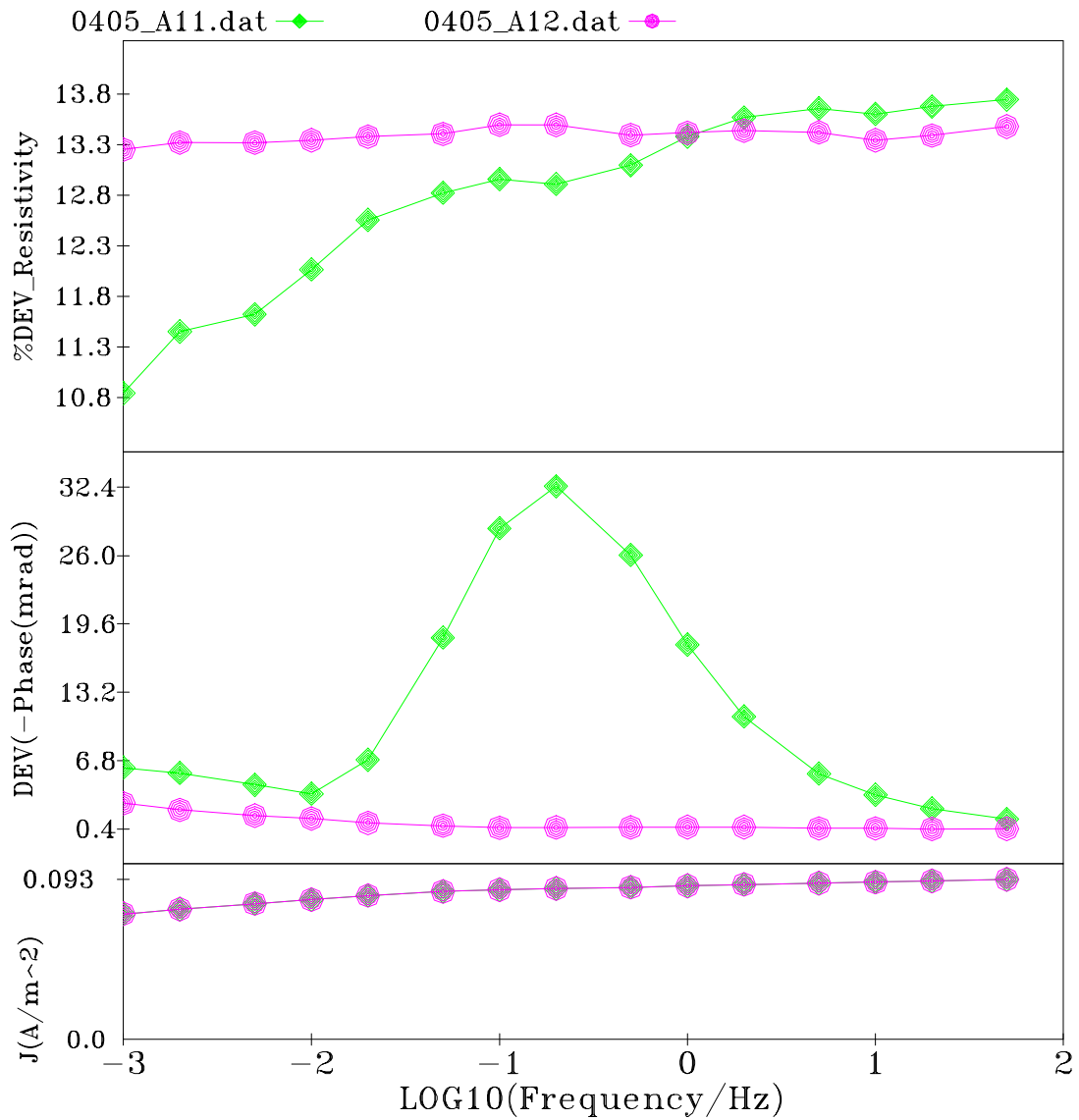


Figure 5.30. Percent resistivity standard deviation (top), phase standard deviation (middle), and current density in amperes/meter² (bottom) for the two potential electrode pairs in column 4. Channel 12 (circles) is the electrode pair chosen to represent the *low-grade ore with low pH water and bacteria inhibitor*.

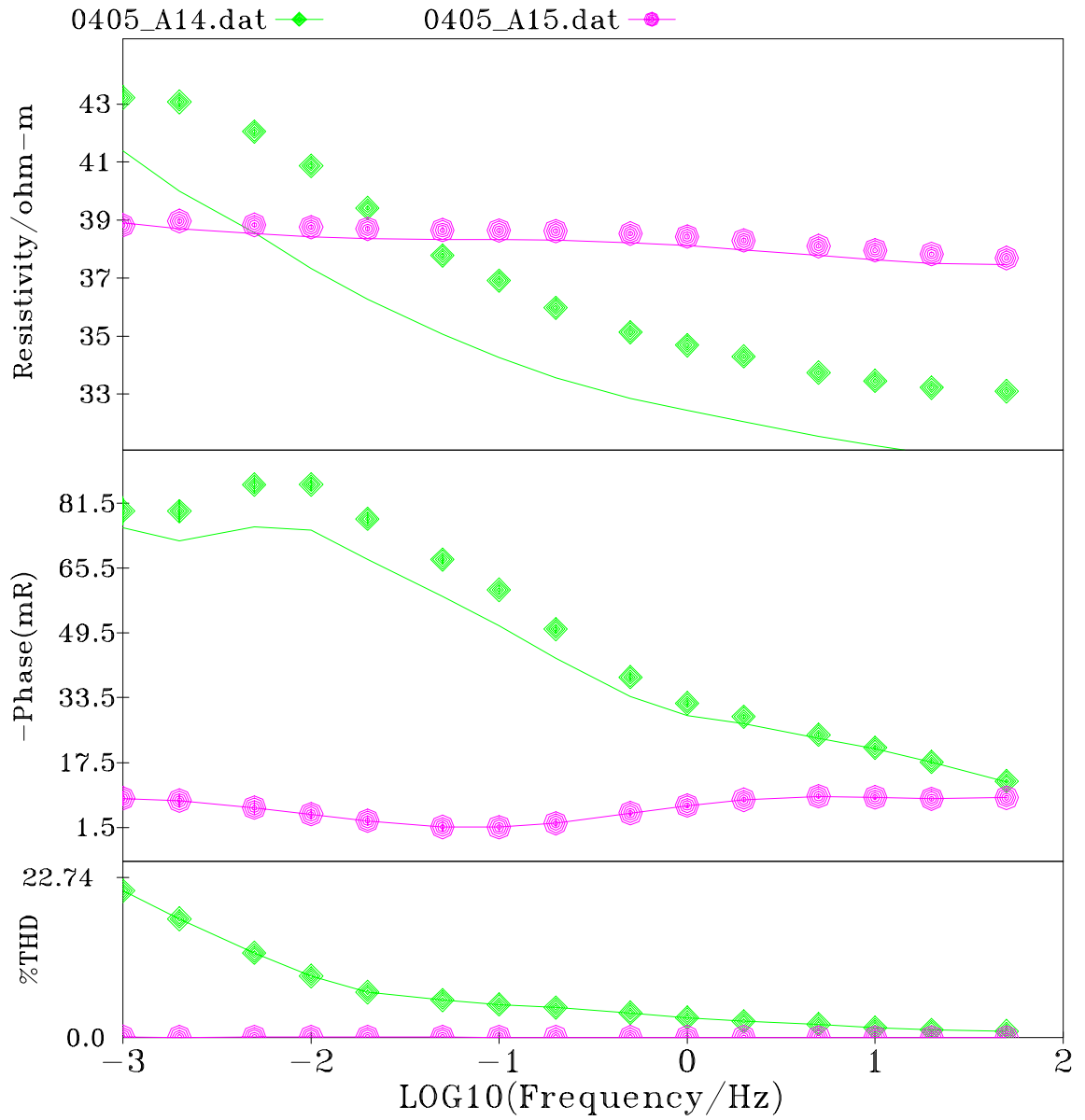


Figure 5.31. CR measurements for the potential electrode pairs in column 4 the *high-grade ore with low pH water and bacteria inhibitor*. Channel 14 (diamonds) is bad and channel 15 (circles) is good according to the R-RC test.

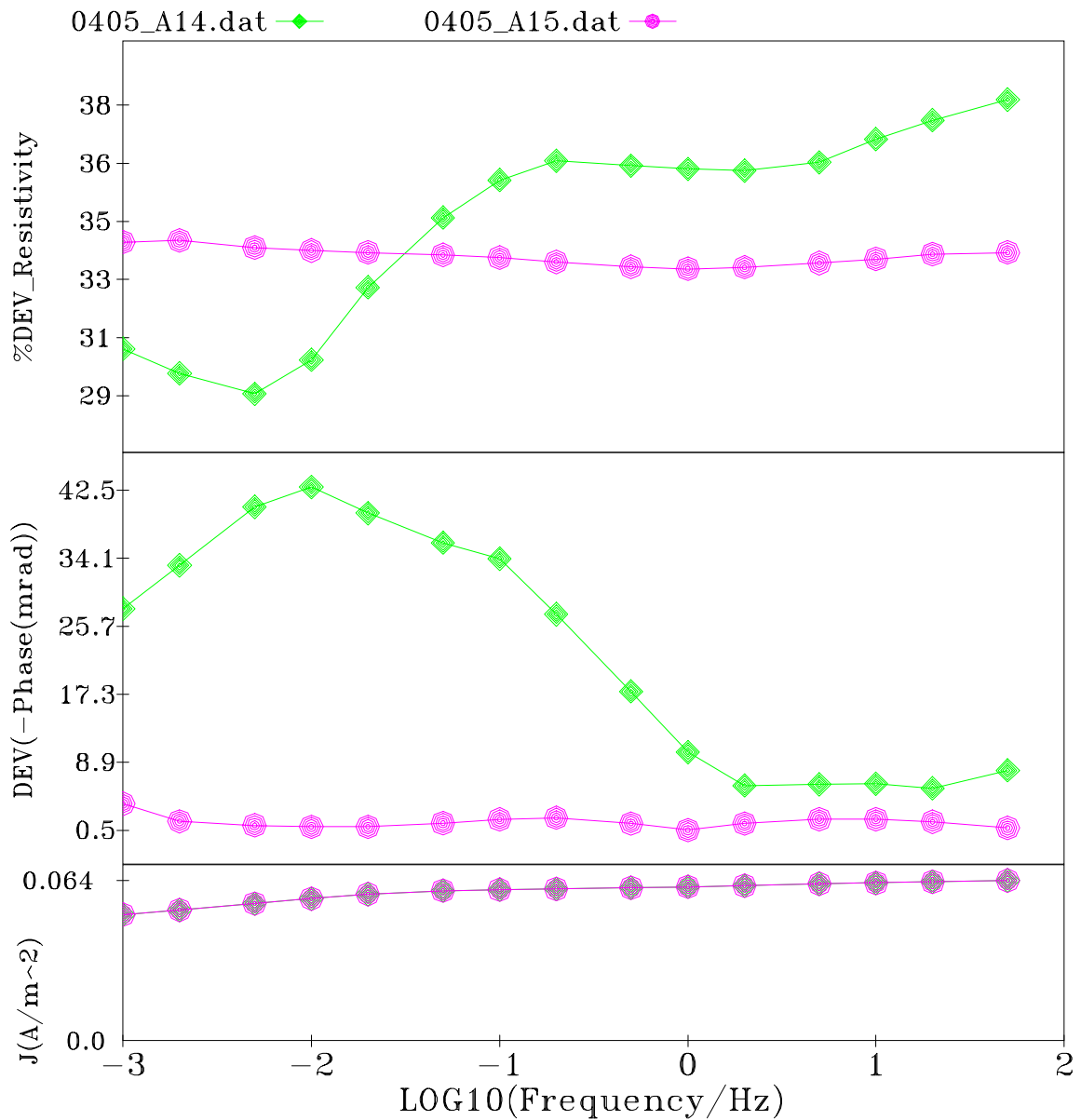


Figure 5.32. Percent resistivity standard deviation (top), phase standard deviation (middle), and current density in amperes/meter² (bottom) for the two potential electrode pairs in column 5. Channel 15 (circles) is the electrode pair chosen to represent the *high-grade ore with low pH water and bacteria inhibitor*.

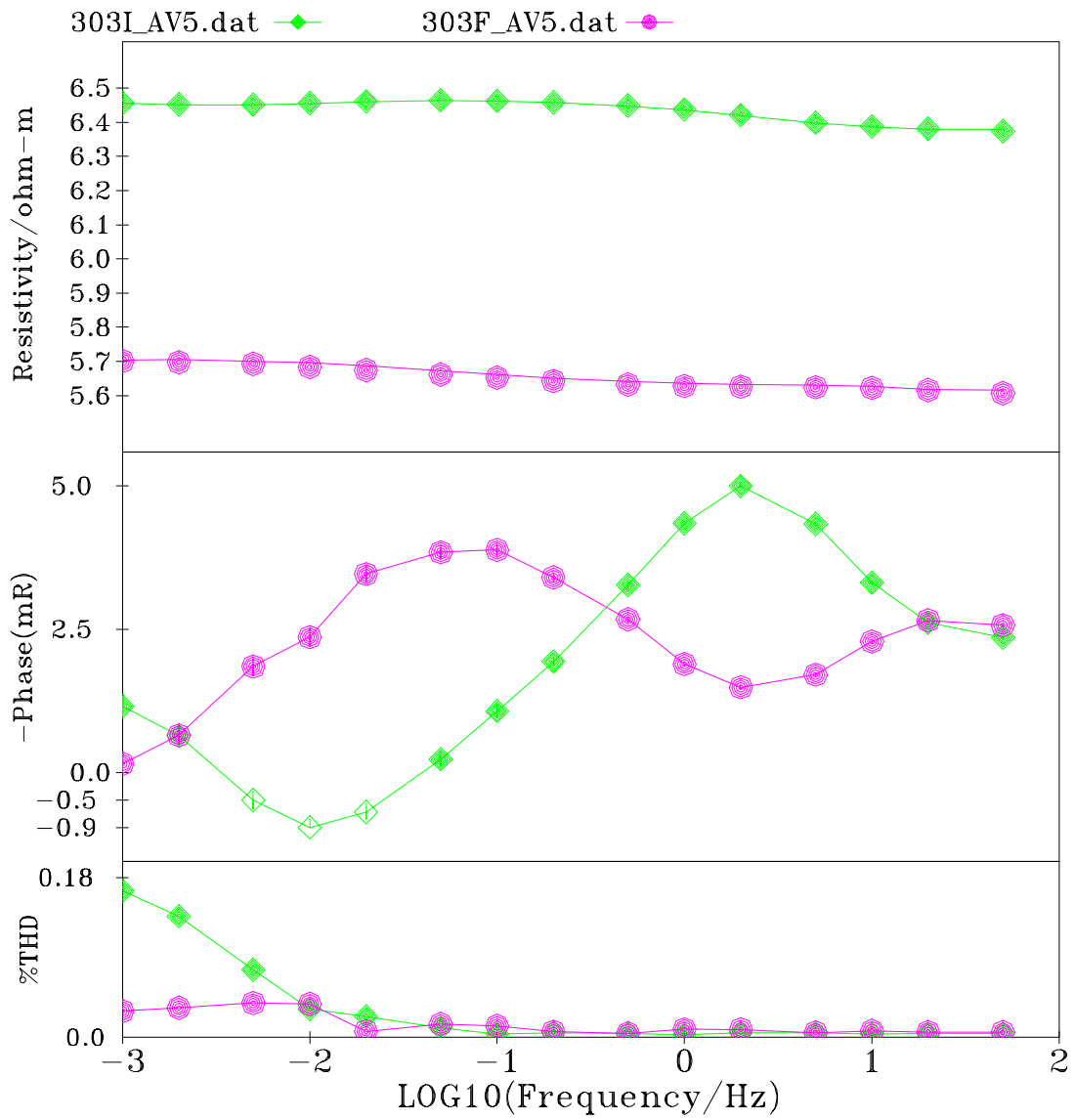


Figure 5.33. CR measurements on 3/3/99, day 90, for the *low-grade ore with biooxidant*. The average of four measurements before disturbing the columns (diamonds) are compared with after moving the ore to fill in gaps under the electrodes (circles).

5.4.3 EM Coupling

Electromagnetic coupling can cause significant errors in induced polarization and complex resistivity data. Capacitive coupling can exist due to displacement currents between wires or from wire to ground and/or leakage currents from electrodes to wires (Sumner, 1976). This effect is not a factor in the column studies because all connections used were in the form of shielded, twisted pair cables. A second form of EM coupling, inductive coupling, is more complicated and difficult to remove. Many articles discuss the problems and removal techniques associated with EM coupling (Madden and Cantwell, 1967; Millet, 1967; Sunde, 1968; Fuller and Wait, 1972; Dey and Morrison, 1973; Hohmann, 1973 and 1975; Hallof, 1974; Wynn and Zonge, 1975; Sumner, 1976; Coggon, 1984).

Inductive coupling occurs when the current electrode loop induces a secondary current in the potential electrode loop due to electromagnetic induction. This can produce phase errors whose sign and magnitude are a function of the electrode geometry, cable layout, frequency, and conductivity of the earth. With a four-inch potential electrode spacing and measurements below 50 Hz minimal inductive coupling is expected. A short cable layout was used to minimize the area of the cable loop, which also minimized coupling. The electrode spacing, frequency, and the conductivity were similar for all columns, indicating that any inductive coupling would not affect comparative results.

5.4.4 Electrode Corrosion

The effects of electrode corrosion were analyzed in column 1 on 3/3/99, day 134, by exchanging the corroded current electrodes for new ones, making four measurements, and then changing the potential electrodes. A photograph of one current and potential electrode removed on 3/3/99 shows the corrosion compared with new MP35N in Figure 5.34. The current electrodes were significantly corroded and the potential electrodes showed no visible signs of corrosion.

Figure 5.35 compares the CR measurements with the original electrodes (oldc_av2.dat), after replacing the current electrodes (newc_av2.dat), and after replacing the potential electrodes (0303_av2.dat). Each measurement is the average of four consecutive measurements. After replacing the current electrodes, the resistivity remained fairly constant and the phase decreased, yet maintained the same frequency dependence. The resistivity increased, the phase flattened, and the %THD decreased when the potential electrodes were replaced.

The original potential electrodes had a slight visible coating, which may have been an iron precipitate, a biofilm, or other coating. Since this coating was not analyzed, its composition and affect are unknown. However, it is possible that the new electrodes were not similarly coated because of chemical changes and a decrease in bacteria activity in the column. The standard deviations (see Figure 5.36) were highest when the current electrodes were replaced, indicating that they may have not yet stabilized in the electrolyte. The current density was the same for these measurements, and is not a factor.



Figure 5.34. One current electrode (left) and one potential electrode (middle) removed from column 1, the *high-grade ore with biooxidant*, on 3/3/99. The raw MP35N (right) looks identical to the potential electrode.

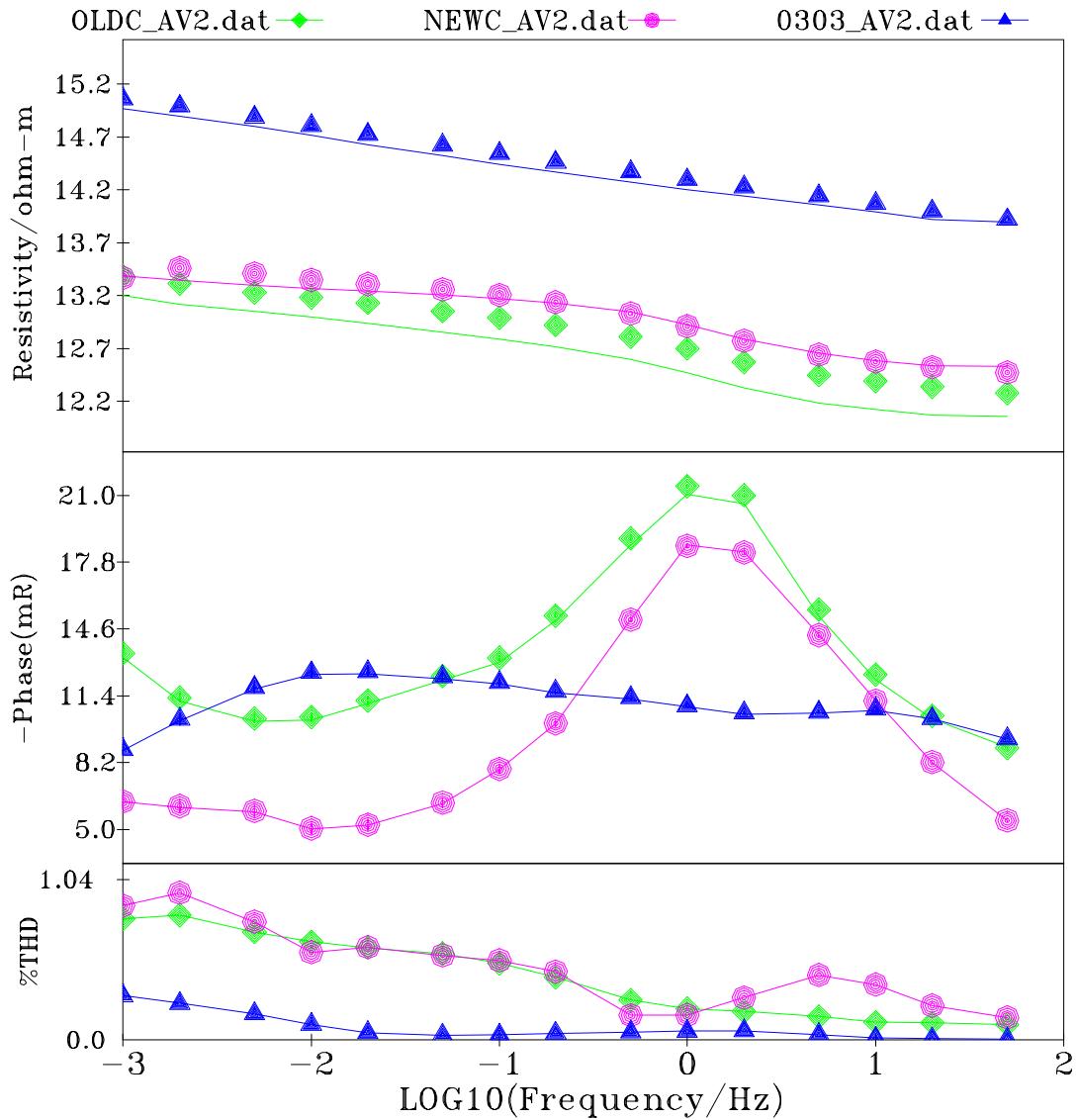


Figure 5.35. CR measurements for column 1, the *high-grade ore with biooxidant*, on 3/3/99, with the original electrodes (diamonds), after replacing the current electrodes (circles), and after replacing the potential electrodes (triangles).

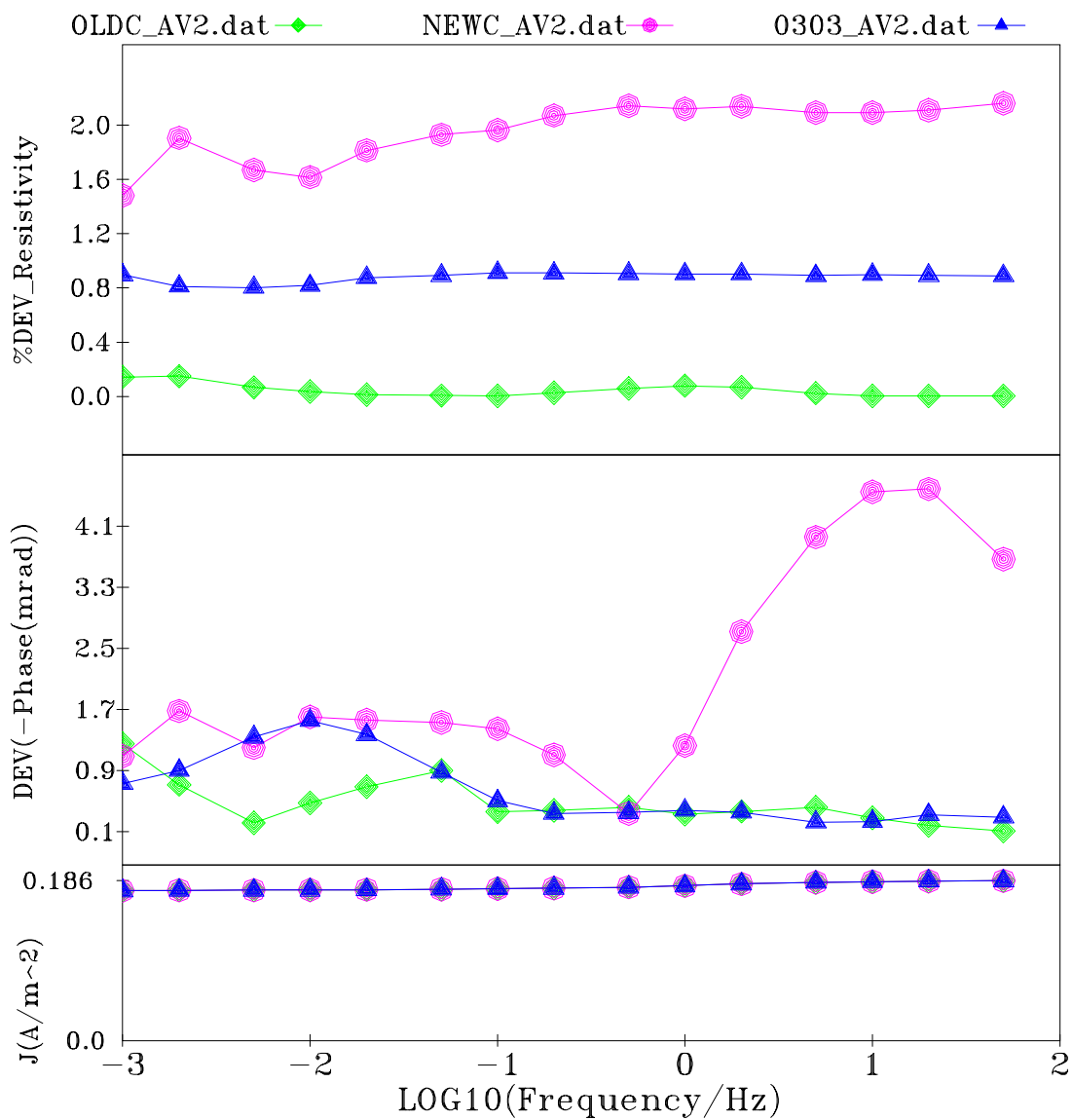


Figure 5.36. Standard deviations and current densities for the CR measurements for column 1, the *high-grade ore with biooxidant*, on 3/3/99, with the original electrodes (diamonds), after replacing the current electrodes (circles), and after replacing the potential electrodes (triangles).

Chapter 6

DISCUSSION AND CONCLUSIONS

6.1 Data Correlation

The objective of this thesis is to determine if there is a correlation between the rate of bacteria-assisted pyrite oxidation and the complex resistivity measurements of two siliceous sulfidic refractory (SSR) ores. The sulfide oxidation rate is related to the rate of change of total iron in solution as described in Section 2.2. Generally, when the slope of the total iron curve flattens a sufficient amount of pyrite has oxidized to release the encapsulated gold. Oxidizing the ore longer will not result in a significant enough increase pyrite oxidation to warrant the extra time and expense. The chemistry and CR data were presented in Section 5.3 and the data quality was discussed in Section 5.4. The phase values at 2 Hz and 0.01 Hz showed the maximum change over time and are used here to compare the CR measurements with the total iron in solution.

6.1.1 High-Grade Ore

The high-grade ore contained 0.188 ounces per ton (opt) of gold and 1.77% sulfide-sulfur (as pyrite) by weight. 42.4% of the sulfide oxidized in 142 days in the column with biooxidant and 18.1% sulfide oxidized in 126 days in the control column with low pH water and a bacteria inhibitor (sodium lauryl sulfate). The initial percent of

recoverable gold was 24.5% for this ore and increased to 61.3% with biooxidant, and 52.1% in the control. The control had significantly improved gold extraction and is likely due to enrichment of gold in only a portion of the total sulfide material. This chemistry data indicates that the biooxidation of the high-grade ore was effective in oxidizing sulfide material and increasing the percentage of recoverable gold.

Figure 6.1 shows the correlation between the solution iron content and the phase values for the high-grade ore with biooxidant, beginning at day 44 (see Section 5.4). The slope of the total iron decreased by day 120, indicating that oxidation was slowing and the ore was ready for removal. The phase values dramatically decrease near the end (31% at 2 Hz and 40% at 0.01 Hz), indicating that the amount of polarization in the sample dramatically decreased. In Figure 6.2, the 2.0 and 0.01 Hz phase difference follows a similar trend to the total iron, and levels off near the end of the experiment.

The iron and phase data for the high-grade ore with low pH water and a bacteria inhibitor is plotted in Figure 6.3. The total iron in solution stayed between 2.2 and 7.6 g/L and is indicative of some bacterial activity. Additional inhibitor was added on days 43 and 99 because the chemistry indicated the start of pyrite oxidation. The first burst of oxidation is evidenced in the 2 Hz phase as a 70% decrease and the second burst of oxidation is evidenced as a 94% decrease in the 0.01 Hz phase. The greatest separation between the two phases occurs when the slope of the iron curve is increasing. Figure 6.4 summarizes the differences between the 2 and 0.01 Hz phase.

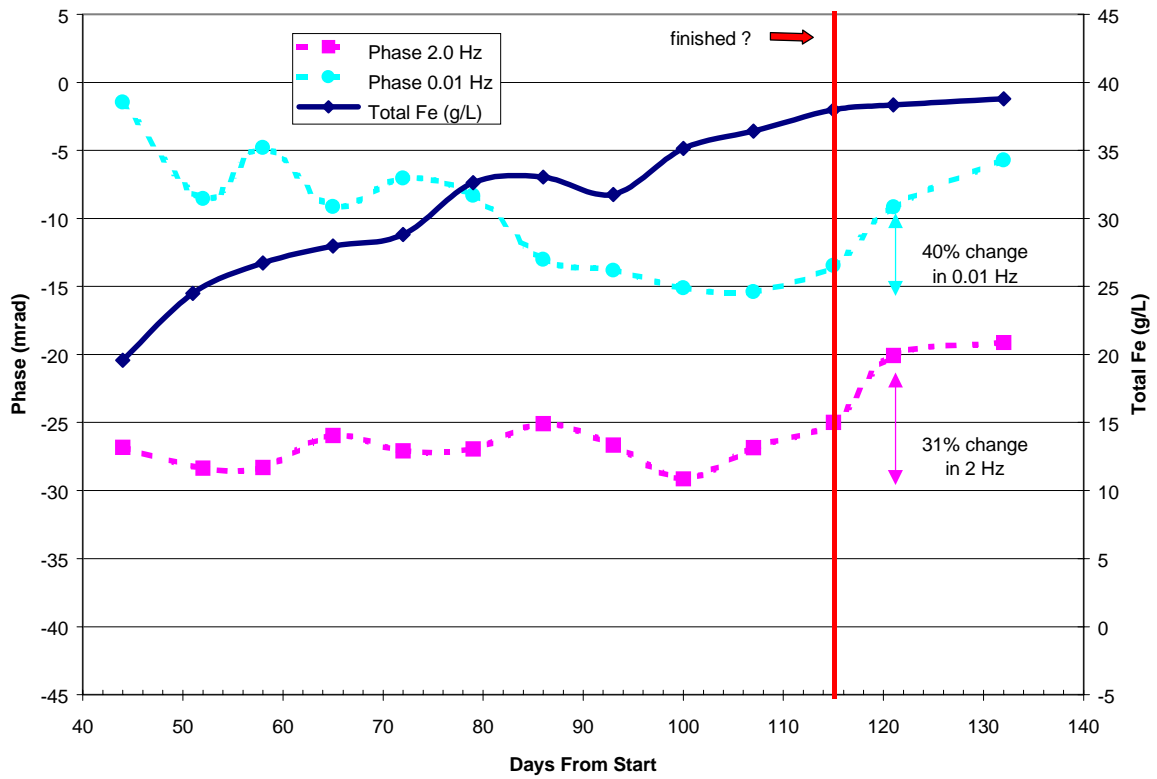


Figure 6.1. Comparison of total iron and phase at 2.0 and 0.01 Hz for the *high-grade ore with biooxidant*. Both the 2.0 and 0.01 Hz phase slopes increased dramatically near at the end of the biooxidation period.

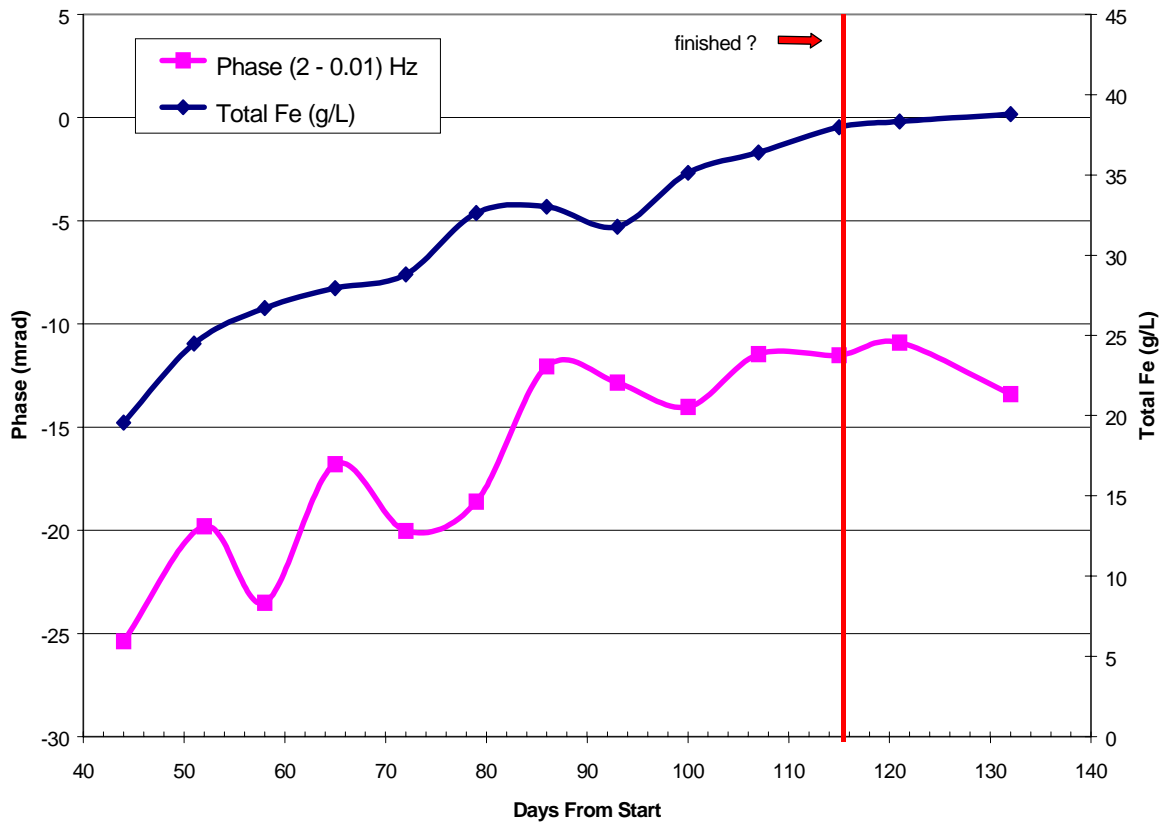


Figure 6.2. The total iron content and the difference between the 2 Hz and 0.01 Hz phase for the *high-grade ore with biooxidant* show similar trends and a leveling off at the end.

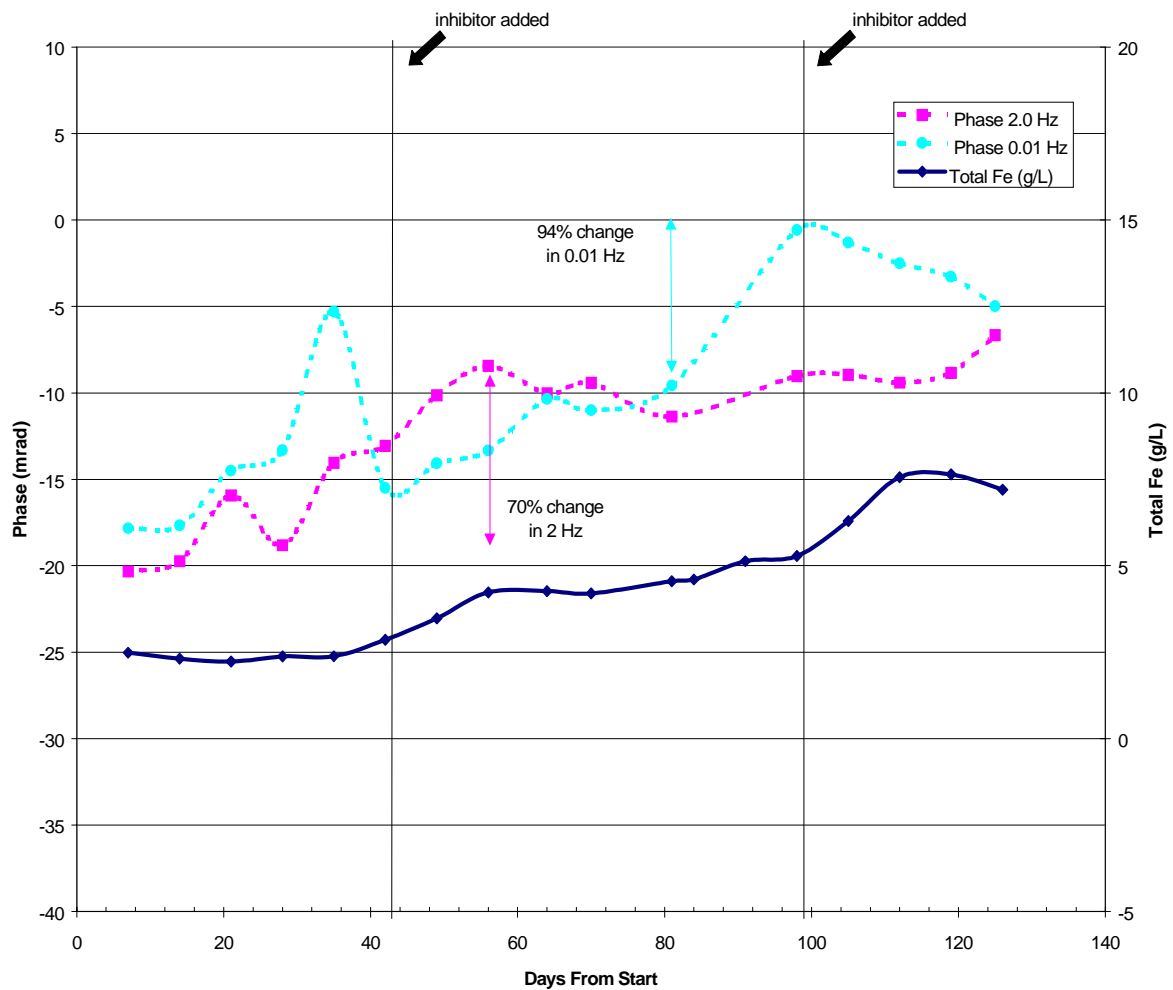


Figure 6.3. Comparison of total iron and phase at 2.0 and 0.01 Hz for the *high-grade ore with low pH water and a bacteria inhibitor*. Additional bacteria inhibitor was added on days 43 and 99. The greatest separation between the two phases occurs when the slope of the iron curve is increasing.

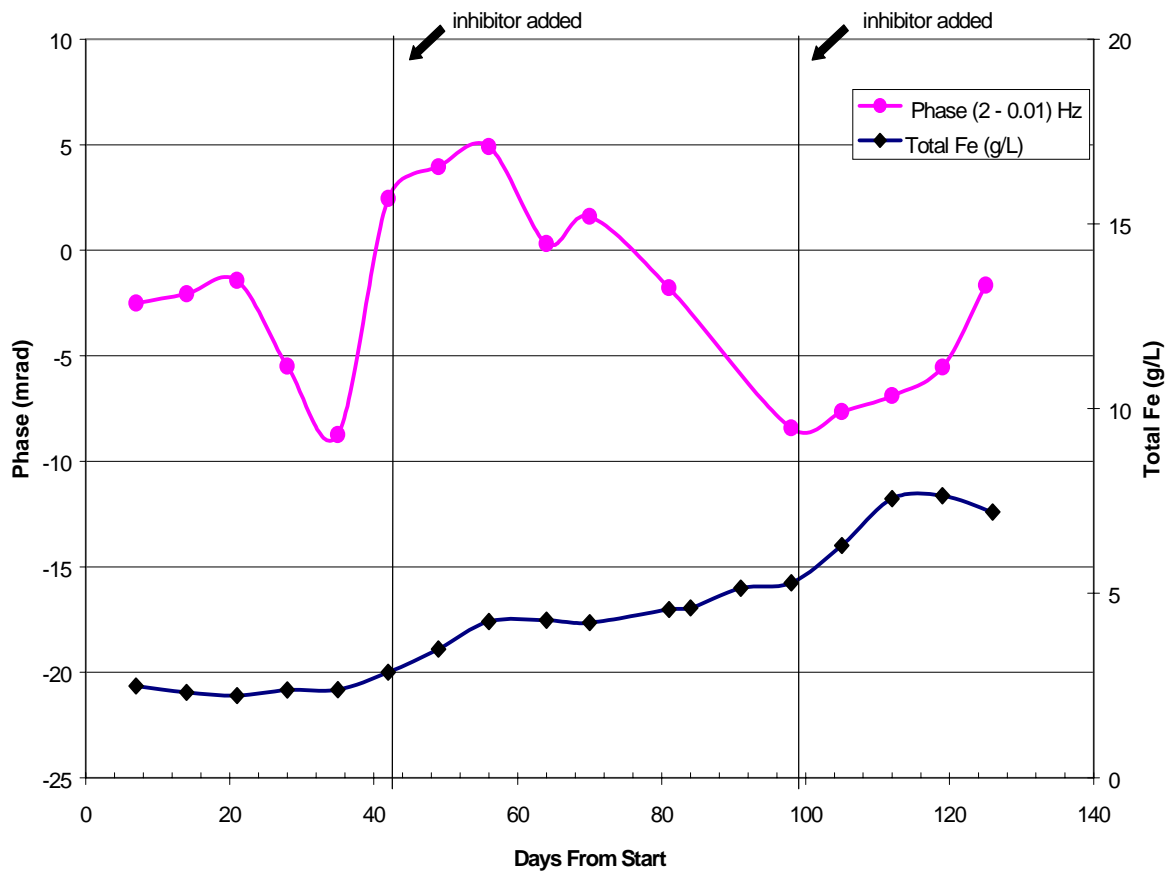


Figure 6.4 Comparison of the total iron and the difference between the 2 Hz and 0.01 Hz phase values for the *high-grade ore with low pH water and a bacteria inhibitor*.

6.1.2 Low-Grade Ore

The low-grade ore initially contained 0.022 opt of gold and 1.60% sulfide-sulfur by weight. The initial percent of recoverable gold was 50% for this ore and decreased to 42% with biooxidant, versus 45% in the control. These negative assay results are most likely due to the minimal gold content and resolution limits of the assay process. It is also possible that pyrite encapsulation may not have been the only cause for initial low gold recovery. Sulfide oxidation was 27.5% in 132 days in the column with biooxidant and 5.6% in 126 days in the column with low pH water and a bacteria inhibitor (sodium lauryl sulfate). Five times more sulfide oxidized in the active sample, indicating that biooxidation was effective in oxidizing sulfide material in the low-grade ore.

Figure 6.5 shows the correlation between the solution iron content and the phase values at 2.0 and 0.01 Hz for the low-grade ore with biooxidant. The solution total iron content increased to 42.3 g/L by day 132. An iron plateau at 33-35 g/L occurred between days 70 and 104, indicating that the ore was ready for removal. During this time, the 2 Hz phase had a drop of 89% and the 0.01 Hz phase had an increase of 55%. The decrease in 2 Hz phase is similar to the decrease in the high-grade ore. Figure 6.6 summarizes the differences between the 2 Hz and 0.01 Hz phase values and correlates well with the iron curve, showing an increase and leveling off when the ore was ready for removal.

The low-grade ore with low pH water and a bacteria inhibitor had much lower iron content and phase values than the active column, which correlates with the lower

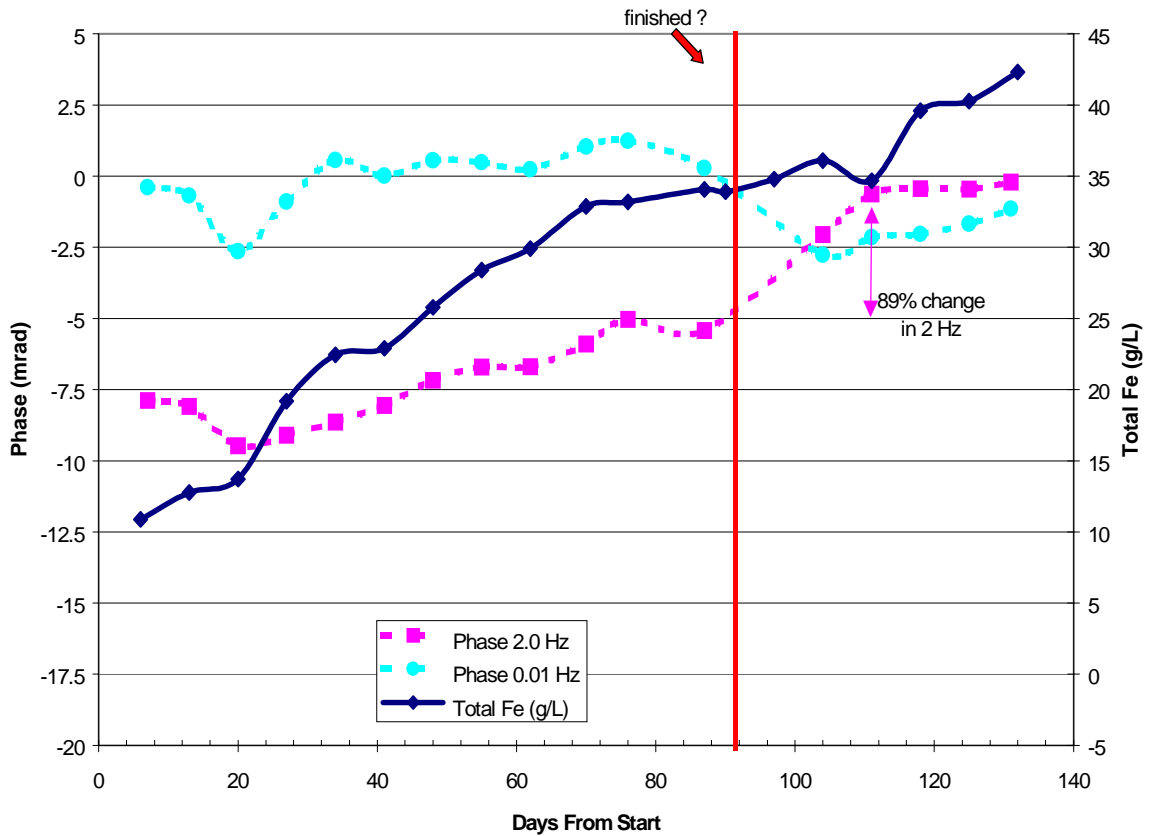


Figure 6.5. Comparison of total iron and phase at 2.0 and 0.01 Hz for the *low-grade ore with biooxidant*. The total iron is plotted on the right scale. The phase values are plotted on the left scale. The 2 Hz values increase and the 0.01 Hz values decrease with a cross-over when the ore was ready for removal.

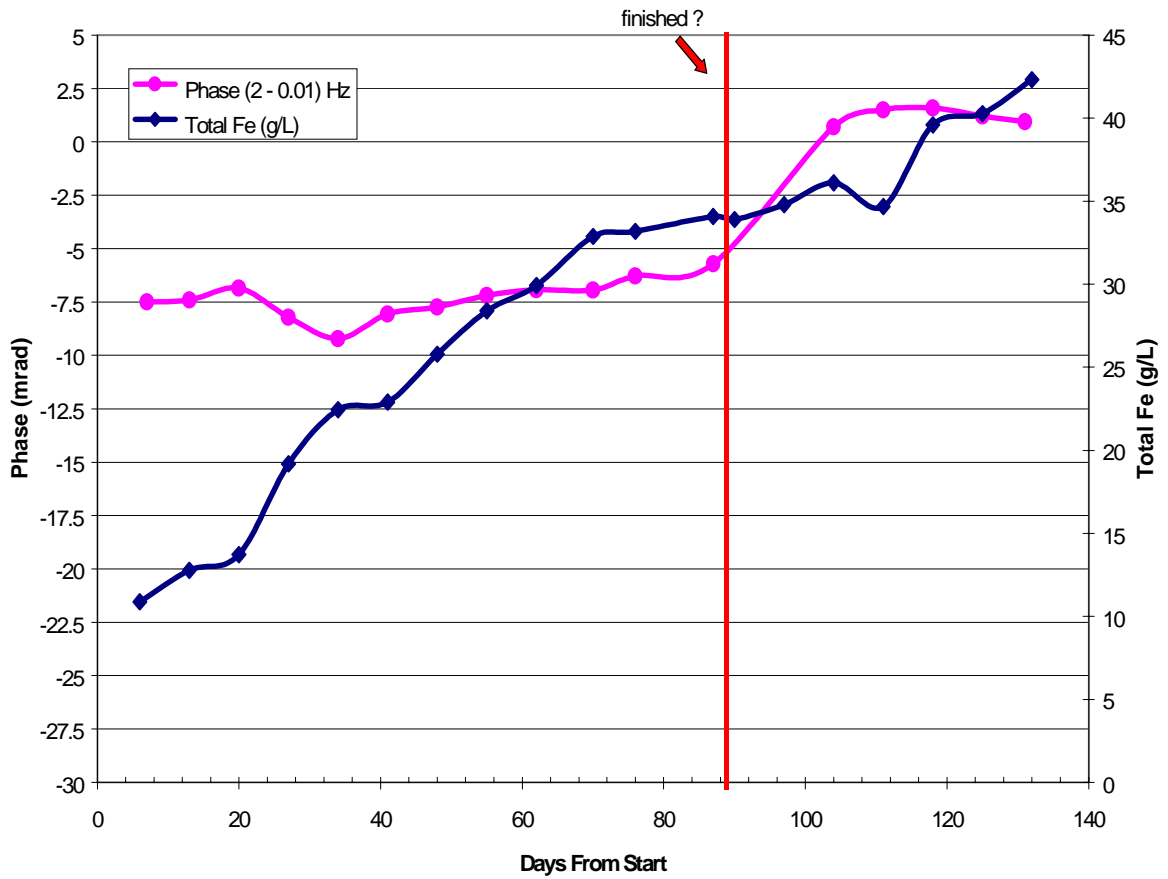


Figure 6.6 Comparison of the total iron and the difference between the 2 Hz and 0.01 Hz phase values *low-grade ore with biooxidant*. The phase curve increases dramatically when the ore was ready for removal.

percentage sulfide oxidation. The data are shown in Figure 6.7. The most significant feature of the plot is the large positive phase values that occurred after the addition of sodium lauryl sulfate on day 64. This is very unusual and is likely due to reactions between the inhibitor and the bacteria and/or the ore. However, the positive phase did not occur on day 112 when more inhibitor was added, nor did it occur in the high-grade ore when inhibitor was added. Otherwise, the phase is very low in magnitude and the values at 2 and 0.02 Hz match for many days, representing the lack of pyrite oxidation. Figure 6.8 summarizes the differences between the 2 Hz and 0.01 Hz phase values and shows the near zero values between days 35 and 65 and between days 95 and 125.

The low-grade ore had less sulfide oxidation and gold recovery than the high-grade ore, despite the similarity in the total iron curves, and also exhibited lower magnitude trends in the complex resistivity 2 Hz phase measurements for the active columns. The differences in the 0.01 Hz data may be due to the onset of new chemical reactions in the low-grade ore as biooxidation ended (perhaps reactions that decreased the percent pyrite oxidation or caused the negligible gold recovery in this ore).

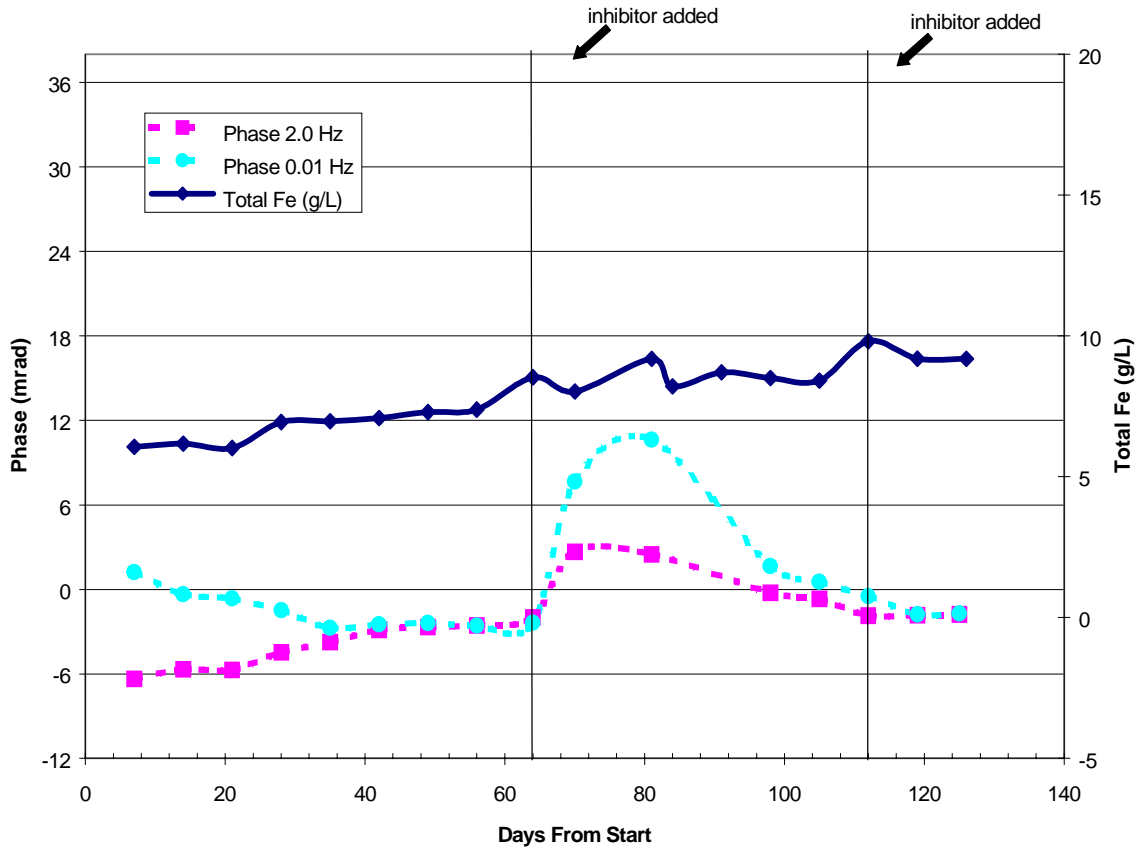


Figure 6.7. Comparison of total iron and phase at 2.0 and 0.01 Hz for the *low-grade ore with low pH water and a bacteria inhibitor*. Additional bacteria inhibitor was added on days 64 and 112. The phase becomes positive with the first addition because of reactions with the bacteria and ore.

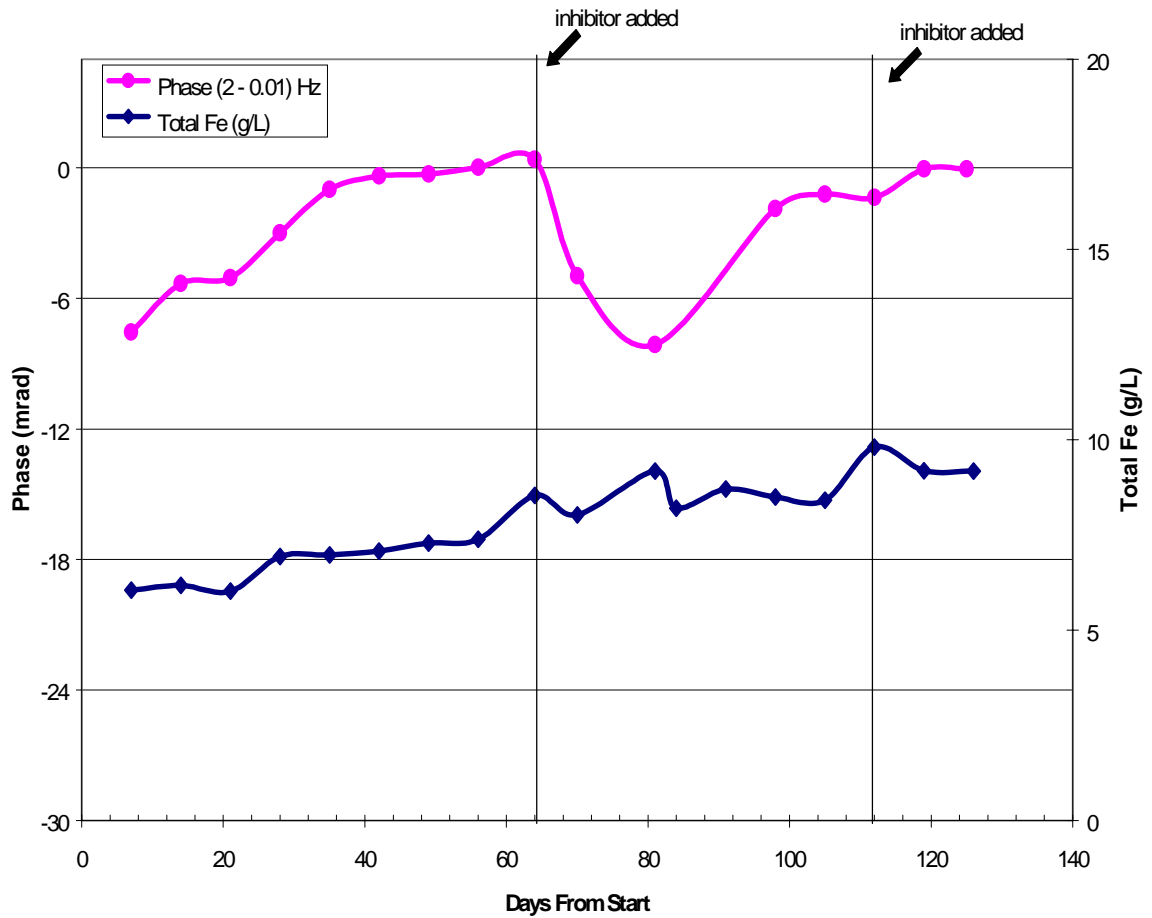


Figure 6.8 Comparison of the total iron and the difference between the 2 Hz and 0.01 Hz phase values for the *low-grade ore with low pH water and a bacteria inhibitor*.

6.1.3 Control Ore

The control ore, NAL composite ore, contained 0.028 opt of gold and minimal sulfide minerals. The control had significantly different mineralogy than the targeted ores and should not have any of the responses associated with sulfide oxidation. The plots in Section 5.3 proved that the chemistry and complex resistivity measurements were much different for this ore. Figure 6.9 shows the total iron and phase measurements for the 126 days this column was in operation. The total iron content was near zero for this column experiment. The 0.01 and 2.0 Hz phase values slowly decreased over the first 80 days and then remained similar. This is evident in Figure 6.10 where the difference between the 2 and 0.01 Hz phases are plotted. These phase measurements are distinctly different from the columns with SSR ore, where differing amounts of sulfide oxidation occurred, and are a good indication that the processes creating the phase values in the other samples are related to biooxidation.

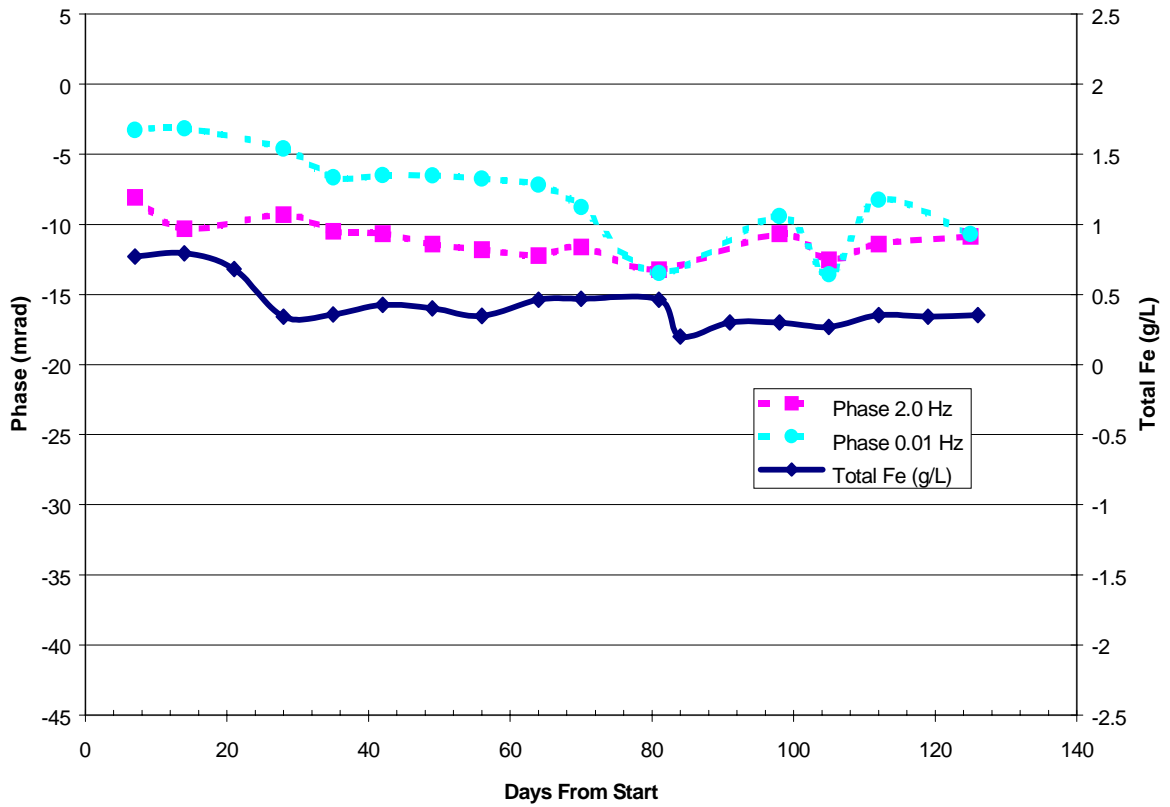


Figure 6.9. Comparison of total iron and phase at 2.0 and 0.01 Hz for the *control ore with tap water*. The total iron is plotted by the scale on the right and the phase according to scale on the left.

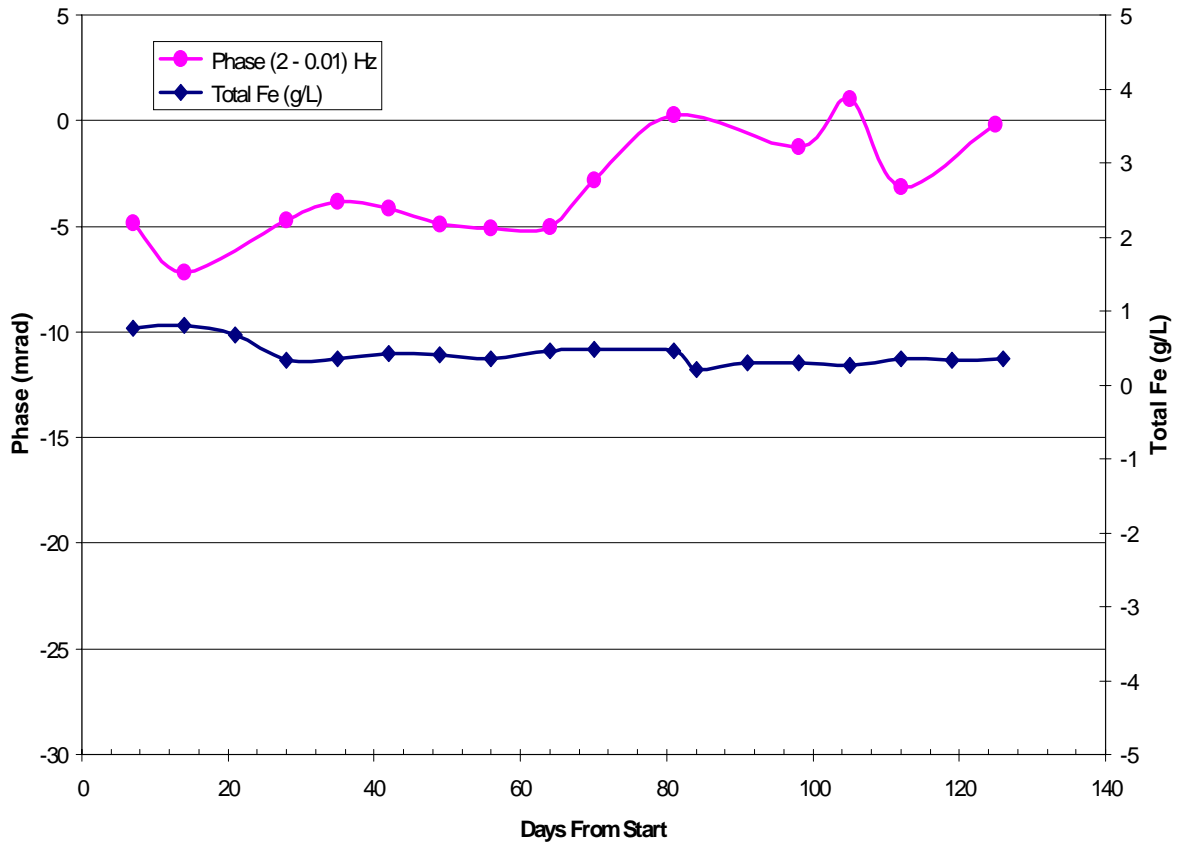


Figure 6.10 Comparison of the total iron and the difference between the 2 Hz and 0.01 Hz phase values for the *control ore with tap water*.

6.2 Recommendations For Future Work

This thesis has been an important first step in determining whether or not complex resistivity is an applicable method for monitoring heap biooxidation. The most important issues with this method relate to the feasibility and practicality of monitoring a heap. Therefore, the next stage in examining the applicability of complex resistivity for monitoring heap biooxidation should be to monitor a small-scale heap. Possible noise sources include electromagnetic coupling, telluric currents, and other ground currents due to mining and/or processing activities. Evaluating a small-scale heap would help to identify important design issues and determine the significance of noise and any other limiting factors.

In addition, the column studies in this thesis should be repeated for different mineralogy suites and at higher temperatures to test repeatability of this data and catalog CR measurements for different ore-types in a controlled laboratory environment. Much work remains to determine how the complex resistivity spectra vary as a function of grain size, temperature, and mineralogy. Grain size is an issue because the gold ores examined in this study contained finely disseminated pyrite, yet some ores targeted for biooxidation contain pyrite and gold in veins. This change in mineral structure and connectivity may effect biooxidation and may show different frequency dependence. In general, smaller metallic mineral grains have a higher frequency of spectral response (Wong, 1979).

The temperature on the exterior of the heap will fluctuate as a function of the daily and annual ambient air temperature changes. Inside the heap, exothermic chemical

reactions greatly increase the temperature (see Section 2.3.3) and will likely correspond with a complex resistivity change. The spectral response will shift to higher frequencies if the speed of chemical reactions increases as temperature increases and may change when thermophilic bacteria begin to dominate the biooxidation process.

The mineralogy of an ore is the primary factor for determining the applicability and effectiveness of biooxidation. The type of sulfide minerals, carbonate content, and clay mineralogy all influence biooxidation. This study evaluated two siliceous refractory ores and had different results that are likely related to mineralogical differences. Carbonaceous refractory ores are also targets of biooxidation and have additional processing problems because acid must be added to maintain the low pH required by the bacteria. Complex resistivity may help identify when more acid must be applied. Another significant mineralogical factor is the presence of clay minerals. Some clay minerals severely inhibit the biooxidation process by coating sulfide minerals and directly interfering with bacteria activity. Complex resistivity is often a good indicator of clay minerals, specifically those of the smectite group (Olhoeft, 1985; Jones, 1997), and may identify problematic sections within the heap due to clay minerals and the reduced sulfide oxidation.

A heap measurement system should have an ample frequency range to sense the frequency dependence of the phase. Results from the column studies indicate this should be at least from 0.01 Hz to 50 Hz for a total of 12 frequencies, with one cycle per frequency taking just over 3 minutes. Even though this study found a relationship

between oxidation and 0.01 the 2.0 Hz spectra, more frequencies should be measured so that the peaks in the data could be identified, especially if they shift frequency due to grain size, temperature, or mineralogy effects. This would also give an adequate frequency range to test the measurement system with an R-RC circuit similar to the one in Figure 4.6. Electrodes could be placed in an array underneath the heap with shielded (or at least twisted pair) wires used to reduce capacitive coupling. A switching box could control which electrode pairs are used for the current and potential to investigate various sample volumes. There are many implementation and logistical constraints for the design and application of complex resistivity to a heap scale.

The most significant problem with measuring over a three-dimensional structure is determining exactly what volume contributed to the response. In many geophysical applications, the target is very small in relation to the sample volume and the spatial resolution must be extremely accurate. However, with heap biooxidation spatial resolution is only required to the level where it is economical to make changes to improve the efficiency or begin removal of the heap. The data processing and interpretation processes need to be automated for ease of interpretation. Fiore (1999) developed a processing program to model various electrode combinations for 3D complex resistivity data, which may prove useful for analyzing heap CR data.

6.3 Conclusions

The correlation between the percentage sulfide oxidation and the complex resistivity phase values for two different grade ores, with and without active biooxidation, indicate that CR is a good indicator of bacteria-assisted sulfide oxidation. These ores and one control ore with minimal sulfide content were examined for 126+ days in column studies at the Newmont Technical Facility in Englewood, CO. Mineralogical and chemical analyses of the sulfide content before and after the column studies and weekly iron titrations showed that a different percent of sulfide oxidized in each column. The control column had no change in the total iron in solution and had distinctly different phase spectra and minimal changes in values near 2 Hz. Increases in the total iron content in solution were associated with decreases in the phase values at 2 Hz for all ores.

Near the end of the active biooxidation process, the drop in the 2 Hz phase magnitude became significant (31% for the high-grade ore and 89% for the low-grade ore). The high-grade ore oxidized 42% of the sulfide and had a 31% decrease in the 2 Hz phase and a 50% decrease in the 0.01 Hz phase. In contrast, the low-grade ore oxidized only 27% sulfide and had an 89% decrease in the 2 Hz phase and a 55% increase in the 0.01 phase. The dramatic difference in the pyrite oxidation and phase data for these two ores may prove to be a diagnostic indicator of the efficiency of biooxidation.

CR data quality was checked by measuring each channel with an R-RC circuit, examining raw data waveforms by eye during acquisition, averaging data sets for a 24 hour period, computing the standard deviations of averaged data sets, and comparing

good potential electrode pairs in each column for repeatability. These methods proved useful in identifying problems with the complex resistivity measurement system and should be incorporated into future efforts.

The next step in analyzing the applicability of complex resistivity as a monitoring technique for the biooxidation of siliceous sulfidic refractory ores is to measure small-scale heaps. Electrodes could be placed under the heap with a switching box to cycle through electrode pairs for various sample volumes. This would determine the spatial resolution attainable and identify noise and practicality issues. Additional laboratory tests need to be performed to determine how the complex resistivity spectra vary as a function of grain size, temperature, and mineralogical composition and texture. In addition to automated data collection, better techniques for automated data analysis must be developed to simplify and expedite the data interpretation process.

REFERENCES CITED

- Anderson, L. A. and Keller, G. V., 1964, A study in induced polarization: *Geophysics*, **29**, 848-864.
- Barrett, J., Hughes, M. N., Karavaiko, G. I., and Spencer, P. A., 1993, *Metal Extraction by Bacterial Oxidation of Minerals*: Ellis Horwood, NY, 191p.
- Bartlett, R. W., 1992, *Solution Mining: Leaching and Fluid Recovery of Materials*: Gordon and Breach Science Publishers, Philadelphia, 276p.
- Bertin, J., and Loeb, J., 1976, *Experimental and Theoretical Aspects of Induced Polarization*, vol. I and II: Berlin, Gebruder Borntraeger.
- Borner, F., Gruhne, M., and Schon, J., 1993, Contamination Indications Derived From Electrochemical Properties in the Low Frequency Range: *Geophysical Prospecting*, **41**, 83-98.
- Braddock, J. F., Luong, H. V., and Brown, E. J., 1984, Growth kinetics of *Thiobacillus Ferrooxidans* isolated from arsenic mine drainage: *Applied and Environmental Microbiology*, **48**, 48-55.
- Brenner, K. C., 1997, Evaluation of the Bioleaching of Gold Ore Using Complex Resistivity: GPGN509 project report, Colorado School of Mines, 61p.
- Brierley, C. L., 1997, Mining Biotechnology: Research to Commercial Development and Beyond, in *Biomining: Theory, Microbes and Industrial Processes*, Rawlings, D.E., ed., Springer-Verlag and Landes Bioscience, 3-17.
- Brierley, J. A., 1999, Personal communication, Newmont Metallurgical Services.
- Brierley, J. A., 1999b, Personal communication, as reported by Jack Tryon and other personnel at the Newmont Technical Facility, Englewood, CO.
- Brierley, J. A., and Hill, D., 1993, Biooxidation process for recovery of gold from heaps of low-grade sulfidic and carbonaceous sulfidic ore materials: U.S. Patent 5,246,486.

- Coggon, J. H., 1984, New three-point formulas for inductive coupling removal in induced polarization: *Geophysics*, **49**, 307-309.
- Colmer, A. R., and Hinkle, M. E., 1947, The Role of Microorganisms in Acid Mine Drainage: A Preliminary Report: *Science*, Sept. 19, 1947, 253-256.
- Crundwell, F. K., 1996, Formation of biofilms of iron-oxidizing bacteria on pyrite: *Minerals Engineering*, **9**, 1081-1089.
- Crundwell, F. K., 1997, Physical Chemistry of Bacterial Leaching, in *Biomining: Theory, Microbes and Industrial Processes*, Rawlings, D.E., ed., Springer-Verlag and Landes Bioscience, 177-200.
- Dey, A., and Morrison, H. F., 1973, Electromagnetic coupling in frequency and time domain induced polarization surveys over a multi-layered earth: *Geophysics*, **38**, 380-405.
- Dutrizac, J. E., 1983, Jarosite-type compounds and their application in the metallurgical industry; in *Hydrometallurgy Research, Development and Plant Practice*: K. Osseo-Assare and J.D. Miller (eds.), The Metallurgical Society of AIME, Warrendale, Pennsylvania, 531-551.
- Evangelou, V. P., 1995, *Pyrite Oxidation and It's Control*: CRC Press, NY, 293p.
- Fiore, R., 1999, 3D numerical forward modeling of complex resistivity field data: MSc thesis, Dept of Geophysics, Colorado School of Mines, Golden, 279p+CD-ROM.
- Fuller, J. A., and Wait, J.R., 1972, High frequency electromagnetic coupling between small coplanar loops over an inhomogeneous ground: *Geophysics*, **37**, 997-1004.
- Grahame, D. C., 1952, Mathematical Theory of the Faradaic Admittance; *Journal of the Electrochemical Society*, **99**, 370c-385c.
- Gray, N. F., 1997, Environmental Impact and remediation of acid mine drainage: a management problem: *Environmental Geology*, **30**, 32-71.
- Hallof, P., 1974, The IP phase measurement and inductive coupling: *Geophysics*, **39**, 650-665.
- Hohmann, G. W., 1973, Electromagnetic coupling between grounded wires at the surface of a two-layer earth: *Geophysics*, **38**, 854-863.

- Hohmann, G. W., 1975, Three-dimensional induced polarization and electromagnetic coupling: *Geophysics*, **40**, 309-324.
- Hustwit, C. C., and Sykes, R. G., 1994, Pipeline treatment of a metal mine drainage containing copper and zinc: *in* Proceedings of the International Land Reclamation and Mine Drainage Conference and the Third International Conference on the Abatement of Acidic Drainage, Pittsburgh, PA, April 24-29, 1994, p.233-240.
- Jones, D. P., 1997, Investigation of Clay-Organic Reactions Using Complex Resistivity: Golden, CO, Colorado School of Mines, Department of Geophysics, Msc. Thesis, 378p.
- Klein, J. D., and Shuey, R. T., 1978, Nonlinear Impedance of Mineral-Electrolyte Interfaces: Part I. Pyrite: *Geophysics*, **43**, 1222-1234.
- Kothoff, M., and Belcher, R., 1957, Volumetric Analysis, 2nd ed.: VIII, Interscience, NY, 123p.
- Macdonald, D. D., and McKubre, M.C.H., 1987, Corrosion of Materials in Impedance Spectroscopy: emphasizing solid materials and systems; J.R. Macdonald, ed, John Wiley & Sons, NY, 260-316.
- Macdonald, D. D., Sikora, E., and Engelhardt, G., 1998, Characterizing electrochemical systems in the frequency domain: *Electrochimica Acta*, **43**, 87-107.
- Macdonald, J. R., ed., 1987, Impedance Spectroscopy: emphasizing solid materials and systems: John Wiley & Sons, NY, 346p.
- Madden, T. R., and Cantwell, T., 1967, Induced polarization, a review; *in* Mining Geophysics, Vol. 2, SEG, Tulsa, 373-400.
- Marshall, D. J., and Madden, T. R., 1959, Induced Polarization, A Study of Its Causes: *Geophysics*, **24**, 790-816.
- Millet, F.B., 1967, Electromagnetic coupling of colinear dipoles on a uniform half-space; *in* Mining Geophysics, Vol. 2, SEG, Tulsa, 401-419.
- Natarajan, K., 1992, Effect of applied potentials on the activity and growth of *Thiobacillus ferrooxidans*: *Biotechnol. Bioeng.*, **39**, 907-913.

- Olhoeft, G. R., 1979a, Electrical Properties, in Initial Report of the Petrophysics Laboratory: U.S. Geological Survey Circular 789, 1-25.
- Olhoeft, G. R., 1979b, Nonlinear Electrical Properties, in Nonlinear Behavior of Molecules, Atoms, and Ions in Electric, Magnetic, or Electromagnetic Fields: Neel, L., ed., Elsevier Sci. Publishing, Amsterdam, 395-410.
- Olhoeft, G. R., 1985, Low Frequency Electrical Properties: *Geophysics*, **50**, 2492-2503.
- Olhoeft, G. R., 1986, Direct detection of hydrocarbon and organic chemicals with ground penetrating radar and complex resistivity in Proc. Of the NWWA/API Conf. On Petroleum Hydrocarbons and Organic Chemicals in Ground Water – Prevention, Detection and Restoration, Nov. 12-14, 1986, Houston: Dublin, Ohio, Natl. Water Well Assoc., 284-305.
- Olhoeft, G. R., and King, T.V.V., 1991, Mapping subsurface organic compounds noninvasively by their reactions with clays: in U.S. Geological Survey Toxic Substance Hydrology Program, Proc. of the technical meeting, Monterey, CA, March 11-15, 1991, U.S.G.S. Water Resources Investigation Report 91-4034, 552-557.
- Pelton, W. H., Ward, S. H., Hallof, P. G., Sill, W. R., and Nelson, P. H., 1978, Mineral Discrimination and Removal of Inductive Coupling with Multifrequency IP: *Geophysics*, **43**, 588-609.
- Ritchie, A.I.M., 1997, Optimization of Biooxidation Heaps; in *Biomining: Theory, Microbes, and Industrial Processes*: D. E. Rawlings, ed., Springer - Verlag and Landes Bioscience, p.201-226.
- Rossi, G., 1990, *Biohydrometallurgy*: McGraw-Hill, Hamburg, NY, 609p.
- Sadowski, R. M., 1989, Clay-organic interactions: Golden, CO, Colorado School of Mines, Department of Geochemistry, Master of Science Thesis, 209p.
- Shutey-McCann, M. L., Sawyer, F. P., Logan, T., Schindler, A. J., and Perry, R. M., 1997, Operation of Newmont's Biooxidation Demonstration Facility in Global Exploitation of Heap Leachable Gold Deposits, D.M. Hausen (ed.), *The Minerals, Metals, & Materials Society*, 75-82.
- Sluyters-Rehback, M. and Sluyters, J.H., 1970, Sine Wave Methods in the Study of Electrode Processes in Electroanalytical Chemistry; A.J. Bard, ed, vol. 4, 1-128.

- Smith, K. S., 1994, Generation and Interactions at the Argo Tunnel: in the Guidebook on the geology, history, and surface-water contamination and remediation in the area from Denver to Idaho Springs, Colorado: U.S. Geological Survey Circular 1097, Stewart, K. C., and Severson, R. C., eds., 39-41.
- Sumner, J. S., 1976, Principles of induced polarization for geophysical exploration: Amsterdam, Elsevier, 277p.
- Sunde, E. D., 1967, Earth conduction effects in transmission systems: NY, Dover Publishing, 370p.
- Van Voorhis, G.D., Nelson, P.H., and Drake, T.L., 1973, Complex resistivity spectra of porphyry copper mineralization: *Geophysics*, **38**, 49-60.
- Wait, J. R., ed., 1959, Overvoltage Research and Geophysical Applications: Pergamon Press, London. 158p.
- Ward, S. H., 1990, Resistivity and induced polarization methods; in *Geotechnical and Environmental Geophysics*: S.H. Ward, ed., Society of Exploration Geophysicists, Tulsa, Oklahoma, 147-189.
- Wong, J., 1979, An Electrochemical Model of the Induced-Polarization Phenomenon in Disseminated Sulfide Ores: *Geophysics*, **44**, 1245-1265.
- Wynn, J.C., and Zonge, K. L., 1975, EM coupling, its intrinsic value, its removal and the cultural coupling problem: *Geophysics*, **40**, 831-850.
- Zonge, K. L., and Wynn, J. C., 1975, Recent Advances and Applications in Complex Resistivity Measurements: *Geophysics*, **40**, 851-864.

APPENDIX OUTLINE

All appendix material is located on the CDROM accompanying this thesis. Each primary directory contains a text file (readme.txt) describing the contents. The outline is as follows:

- A. Chemistry Data.....\chemistry
- B. Laboratory Complex Resistivity Data.....\lab_data
- C. Column Complex Resistivity Data.....\col_data
- D. Processing Programs.....\programs

The CDROM also contains the entire thesis document as a *.pdf file in the thesis directory.